Chair of Reservoir Engineering

Master's Thesis

Numerical Study of Geological Hydrogen Conversion

Wendpanga Jean Donald Minougou

March 2022

Wendpanga Jean Donald Minougou

Master Thesis 2021/2022

Supervisor: Univ.-Prof. Dipl.-Phys. Dr.rer.nat. Holger Ott
Co-supervisor: Dr. Siroos AzizMohammadi

Numerical Study of Geological Hydrogen Conversion

dpe DEPARTMENT PETROLEUM ENGINEERING

MONTAN UNIVERSITÄT

MONTANUNIVERSITÄT LEOBEN
www.unileoben.ac.at

AFFIDAVIT

I declare on oath that I wrote this thesis independently, did not use other than the specified sources and aids, and did not otherwise use any unauthorized aids.

I declare that I have read, understood, and complied with the guidelines of the senate of the Montanuniversität Leoben for "Good Scientific Practice".

Furthermore, I declare that the electronic and printed version of the submitted thesis are identical, both, formally and with regard to content.

Date 19.02.2022

Signature Author
Wendpanga Jean Donald Minougou

To my parents, friends, and everyone who contributed to this paper

Declaration

I hereby declare that except where specific reference is made to the work of others, the contents of this dissertation are original and have not been published elsewhere. This dissertation is the outcome of my own work using only cited literature.

Erklärung

Hiermit erkläre ich, dass der Inhalt dieser Dissertation, sofern nicht ausdrücklich auf die Arbeit Dritter Bezug genommen wird, ursprünglich ist und nicht an anderer Stelle veröffentlicht wurde. Diese Dissertation ist das Ergebnis meiner eigenen Arbeit mit nur zitierter Literatur.

Minougou Wendpanga Jean Donald, 10 March 2022

Acknowledgements

I would like to thank Prof. Holger Ott for supervising my work and providing insightful ideas to improve my knowledge of underground gas storage.

A special thanks to Dr. Siroos Azizmohammadi, who guided me throughout the workflow of this dissertation.

Furthermore, I would like to thank Dipl. Ing. Boris Jammernegg and Dipl. Ing. Denis Nikolaev who provided technical assistance on the software package.

Finally, yet importantly, I would like to thank my family and friends who always supported me throughout my studies.

Abstract

Renewable sources of energy can help mitigate global warming. One of the most significant drawbacks of renewable energy is the disparity between supply and demand. Geological hydrogen storage is a way to overcome this imbalance as it provides a way to store hydrogen as a source of energy and reproduce it during periods of energy shortage. Hydrogen can be then be stored either in depleted gas reservoirs or in deep saline aquifers.

A high concentration of hydrogen in the subsurface can trigger its consumption by in-situ microorganisms. That is why it is essential for us to understand the microbial metabolism of hydrogen. Although microbial consumption of hydrogen is known from the literature, a quantitative assessment that shows the extent to which the consumption takes place is somewhat lacking.

In this study, we investigated in the first place the main influencing parameters of in-situ hydrogen conversion, namely hydrogen conversion into methane (CH_4) when it is co-injected with carbon dioxide or when CO_2 is already present in the medium, a process known as methanation. It is known that methanation and sulfate reduction (a process in which hydrogen is transformed into hydrogen sulfide (H_2S) in the presence of sulfate) are some of the major microbial metabolisms happening during hydrogen subsurface storage.

In the next step, we studied the plume migration of injected gas to investigate the presence of sweet spots for hydrogen, carbon dioxide, and methane. This was followed by an interpretation that estimated the time step at which a steady-state flow for each gas is achieved. After that, we considered different reservoir conditions under which hydrogen can be stored, and we estimated the recovery rates of hydrogen, methane and hydrogen sulfide.

In our last step, we investigated the influence of microbial population growth on rock porosity and permeability by numerical simulations.

Zusammenfassung

Erneuerbare Energiequellen können helfen, die Erderwärmung einzudämmen. Einer der größten Nachteile erneuerbarer Energien ist die Diskrepanz zwischen Angebot und Nachfrage. Die geologische Wasserstoffspeicherung ist eine Möglichkeit, dieses Ungleichgewicht zu überwinden, da sie eine Möglichkeit bietet, ihn als Energiequelle zu speichern und in Zeiten von Energieknappheit zu reproduzieren. Wasserstoff kann dann entweder in erschöpften Gasreservoirs oder in tiefen salzhaltigen Aquiferen gespeichert werden.

Eine hohe Wasserstoffkonzentration im Untergrund kann seinen Verbrauch durch in-situ-Mikroorganismen auslösen. Deshalb ist es uns wichtig, den mikrobiellen Stoffwechsel von Wasserstoff zu verstehen. Obwohl der mikrobielle Verbrauch von Wasserstoff aus der Literatur bekannt ist, fehlt etwas eine quantitative Bewertung, die zeigt, in welchem Umfang der Verbrauch stattfindet.

In dieser Studie haben wir in erster Linie die Haupteinflussparameter der in-situ Wasserstoffumwandlung untersucht, nämlich die Wasserstoffumwandlung in Methan (CH_4) wenn H_2 mit Kohlendioxid co-injiziert wird oder wenn CO_2 bereits im Medium vorhanden ist, ein Prozess bekannt als Methanisierung. Es ist bekannt, dass Methanisierung und Sulfatreduktion (ein Prozess, bei dem Wasserstoff in Anwesenheit von Sulfat in Schwefelwasserstoff (H_2S) umgewandelt wird) einige der wichtigsten mikrobiellen Stoffwechselvorgänge sind, die während der unterirdischen Wasserstoffspeicherung stattfinden.

Im nächsten Schritt unserer Arbeit untersuchten wir die Schwadenwanderung von injiziertem Gas, um das Vorhandensein von Sweet Spots für Wasserstoff, Kohlendioxid und Methan zu untersuchen. Darauf folgte eine Interpretation, die den Zeitschritt abschätzte, bei dem ein stationärer Fluss erreicht wird. Unsere Interpretation soll uns auch bei der Entscheidung über den besten Standort für eine Produktionsbohrung leiten. Danach haben wir verschiedene Reservoirbedingungen betrachtet, unter denen Wasserstoff gespeichert werden kann, und wir haben die Rückgewinnungsraten von Wasserstoff, die Methanisierungsraten sowie die Sulfatreduktionsraten abgeschätzt.

In unserem letzten Schritt untersuchten wir den Einfluss des mikrobiellen Populationswachstums auf die Porosität und Permeabilität des Gesteins durch numerische Simulationen.

Table of Contents

List of Figures

List of Tables

Abbreviations

n_MG: Dimensionless Microbial Density for methane generating bacteria

n_SR: Dimensionless Microbial Density for sulfate generating bacteria

x^CH_4_gas: Gas mole fraction of methane

x^CO_2_gas: Gas mole fraction of carbon dioxide

x^H_2_gas: Gas mole fraction of hydrogen

x^N_2_gas: Gas mole fraction of nitrogen

Chapter 1

Introduction

Renewable energy sources are intermittent as we know. Hydrogen underground storage provides an opportunity to deal with that intermittency. Because geological storage of hydrogen is associated with a lot of uncertainties, research in areas such as reservoir engineering, chemistry, geology, and microbiology is required to implement a commercially viable deployment of this technology.

Our focus in this work is the influence of microbial activities on hydrogen stored in porous media. The main microbial process investigated here is methanogenesis, although we provided some insights into sulfate reduction and hydrogen sulfide generation in the fourth chapter.

In this work, we defined a base case for microbial growth rate and methane production. Using that base case, we varied the initial injection and reservoir parameters from lowest to highest to find out how they affect the conversion rates. The parameters that we investigated ranged from microbes' biological parameters, injection rate, hydrogen fraction in the injected gas, well spacing, and production rate. A tornado plot at the end of this part showed the contribution of each parameter and the most influential ones.

After our investigation on the methanation, we went on to study the hydrogen plume migration to identify the zones of highest gas concentrations, which gives us an indication of the best location of a production well. Next, we estimated the recovery rates of the gas components when 100% of hydrogen is injected under various reservoir conditions. We injected hydrogen in a reservoir using N_2 as cushion gas in the first scenario, CO_2 in the second scenario, and CH_4 in the last scenario. Based on the values of hydrogen recovery in the production well, the methane and hydrogen sulfide production, and considering the amount of gas dissolved in the water phase, we shall know the extent to which initial reservoir conditions could influence hydrogen injection operations. A final investigation was made on the microbial concentration around the injector and the extent to which it could affect the porosity and permeability.

1.1 Background and Context

Microorganisms live mostly as biofilms and are attached to solid surfaces. As previously mentioned, the microbial metabolism of hydrogen must be well understood before geological hydrogen storage can be applied on a large scale. In this thesis, we aim to rely on numerical simulation to investigate the impact of microbial growth on the hydrogen stored underground in terms of in-situ hydrogen conversion, as well as in pore-clogging.

Previous works have been conducted to predict the favorable conditions for microbial growth in potential storage sites (E.M. Thaysen et al., 2021), the physics and chemistry associated with the storage of hydrogen in porous media (Heinemann et al., 2021), the influence of biomass accumulation on hydraulic properties (Neda Hassannayebi et al., 2021) and the gas mixing process hydrogen storage (Felix Feldmann et al., 2016). However, little is known about the quantitative assessment of hydrogen consumption and the methanation rates. This thesis aims to provide more insights into hydrogen conversion rates.

1.2 Scope and Objectives

By varying the injection and reservoir parameters, we are investigating the influence of each parameter on the methane generation, the results are shown on a tornado plot where the most influential parameters can be identified. Microbial hydrogen consumption can cause high conversion rates depending on the growth rate, this can cause significant disturbance in the gas plume migration. We, therefore, performed a sensitivity analysis of the microbial growth rate influence on the gas saturation between the injector and the producer. The saturation profiles for H_2, CH_4, CO_2, and N_2 were investigated.

In this work, we analyzed the role of microbial activity on the stored hydrogen.

Chapter 2

Literature Review

2.1 Hydrogen Storage Hydrodynamics in Porous Media

To store hydrogen in the subsurface, the potential storage sites that were identified are deep saline aquifers or depleted gas reservoirs. However, and as we could imagine, the governing process during the development stage will be different in either case.

2.1.1 Storage in Aquifers

In aquifers, because hydrogen has a lower viscosity and density than water, the displacement process might turn out to be ineffective. It is known that the mobility ratio between hydrogen gas and water is around 2-5. That value is unfavorable as it could induce a viscous fingering and a gravity override of the water phase, as shown in Figure 2-1. Peter O Carden & L. Paterson (1979) based on a study concluded that viscous fingering could cause hydrogen to spread below the caprock and escape. Mathematical derivation of the conditions for stable and unstable displacement was done by (Tek, M. R., 1989). Both (Tek, M. R., 1989) and (Peter O Carden & L. Paterson, 1979) concluded based on their research that the injection rate could be lowered to control viscous fingering and gravity override.

To minimize viscous fingering, we could also employ nitrogen as cushion gas. The advantage here is that nitrogen has a higher density than hydrogen and could therefore be used to displace the water before hydrogen injection starts. That significantly reduces the risk of losing large amounts of the injected gas through viscous fingering.

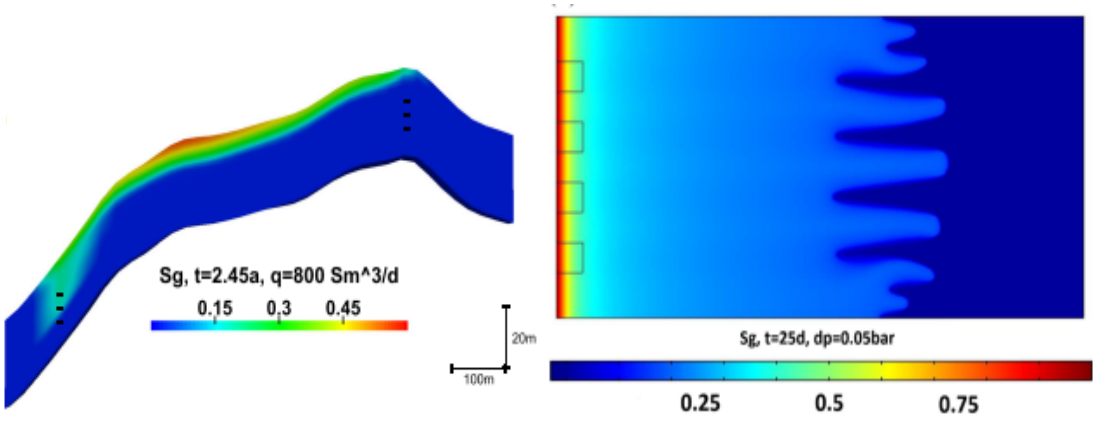

Figure 2-1 Image of water displacement by injected hydrogen. Left: vertical cross-section and Right: horizontal cross-section (Felix Feldmann et al., 2016).

2.1.2 Storage in Depleted Gas Reservoirs

For the case of depleted gas reservoirs, the first question is how could hydrogen displace the residual gas effectively. Again, nitrogen can be used as cushion gas in depleted gas reservoirs even though the residual gas would be the easiest option. In (Curtis M. Oldenburg, 2003), the application of carbon dioxide as a cushion gas was considered. Hydrogen would easily separate from carbon dioxide since the latter is a lot denser. The mixing of gas components must also be considered in the case of depleted gas reservoirs. Among the factors influencing mixing are mobility ratio, density differences, molecular diffusion, and mechanical dispersion.

As far as mobility ratio is concerned, the system H_2-CH_4 has a mobility ratio of about 1.5 while the system H_2-N_2 has a mobility ratio of 4. For this reason, an unstable displacement could therefore occur when hydrogen is used to displace nitrogen. The methane displacement by hydrogen is shown in Figure 2-2 where we can observe a more stable displacement process.

However, it is important to mention that the low density of hydrogen does not only have a negative effect during the injection process as it allows to establish clear segregation between hydrogen and other gases (Felix Feldmann et al., 2016). That is especially of interest in a cyclic injection-production scenario.

The contribution of molecular diffusion depends on the concentration gradient of hydrogen. That means that at the beginning of the injection process, the diffusion will be fast since the gradient is high. But over time, as the concentration gradient decreases, it decreases as well.

Mechanical dispersion arises from variations in the velocity that occur on different scales. The mechanical dispersion coefficient in the case of hydrogen storage was estimated by laboratory measurements (Tek, M. R., 1989) and is in the order of 5×10^2 m/s.

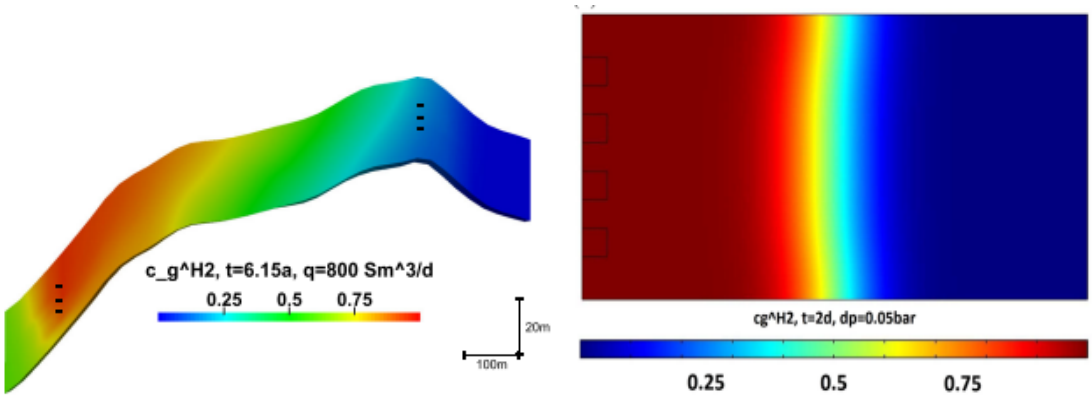

Figure 2-2 Image of gas displacement by injected hydrogen. Left: vertical cross-section and Right: horizontal cross-section (Felix Feldmann et al., 2016).

2.2 Microbiology in Underground Gas Storage

During methanogenesis, a microorganism needs a source of energy and a source of carbon. When hydrogen is stored underground, it will act as an electron donor for microorganisms, and the source of carbon would be CO_2 (Birger Hagemann, 2017).

Waltraud Dilling & Heribet Cypionka (1990) showed that microbial population growth begins with a lag phase during which no growth occurs since microorganisms need a certain time to adjust themselves to the new external conditions.

The next phase is the phase where the microbial population grows exponentially. It is called the log phase (Figure 2-3). The differential equation that describes that phase is expressed as:

$$\frac{dn}{dt} = \mu n \qquad (2\text{-}1)$$

n: number of microbial cells

μ: maximum growth rate in $[\frac{1}{s}]$

After the exponential growth phase, a balance between microbial growth and decay is established. The differential equation for this phase is expressed as:

$$\frac{dn}{dt} = 0 \qquad (2\text{-}2)$$

The last phase is a decay phase, where the number of active cells declines exponentially (Maier, Raina M., 2009). However, individual cells can still duplicate. Mathematically the decay phase can be described as:

$$\frac{dn}{dt} = -bn \qquad (2\text{-}3)$$

b refers to the decay rate in $[\frac{1}{s}]$.

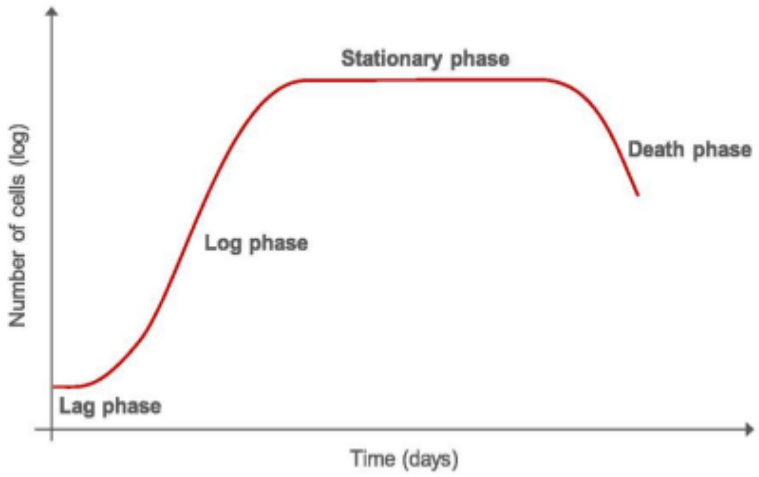

Figure 2-3 Illustration of the microbial population growth curve (C. Müller & T. Straube , 2016).

By assuming that the relative number of microorganisms in a neuston structure is the same as the gas saturation, (Birger Hagemann, 2017) modelled the microbial dynamics as follow:

$$\frac{\partial n}{\partial t} = \underbrace{\frac{\eta_{ns} c_g^{CO_2}(1-S)n}{t_{e,ns}}}_{\text{Growth in neuston}} + \underbrace{\frac{\eta_w c_w^{H_2} c_w^{CO_2} S n^2}{t_{e,w}}}_{\text{Growth in neuston}} \underbrace{- \frac{n}{t_d}}_{\text{Decay}} \qquad (2\text{-}4)$$

$$\underbrace{-\nabla.(u_w n)}_{\text{Advection}} + \underbrace{\nabla.(D_b \nabla n)}_{\text{Diffusion}} \underbrace{- \nabla.(D_{ch} S n \nabla C^{H_2})}_{\text{Chemotaxis}}$$

η: rendering coefficient relating the growth of biomass to the consumption of substrate [1/mol],
S: the water saturation

t_d: the characteristic time of death in [s],

u: the Darcy velocity in [m/s],

$D_{ch:}$ the chemotaxis rate [m^2/s], g and w denote the gas and water.

C^{H2}: the total mole fraction of hydrogen is expressed as:

$$C^{H_2} = \frac{\rho_w c_w^{H_2} S + \rho_g c_g^{H_2}(1-S)}{c_w^{H_2} S + c_g^{H_2}(1-S)} \qquad (2\text{-}5)$$

The transport of microorganisms occurs through advection, microbial diffusion, and chemotaxis, which describes the movement of microorganisms in the direction towards nutrients.

The transport of substrates happens both in the gas and water phase. The consumption of substrates is used as a sink term (Birger Hagemann, 2017). The overall equation is as follow:

$$\varphi \frac{\partial}{\partial t}\left(\rho_w c_w^k + \rho_g \rho_g^k (1-S)\right) + \underbrace{\nabla.\left(\rho_w c_w^k \mathrm{u}_w + \rho_g c_g^k \mathrm{u}_g\right)}_{\text{Advection}} \qquad (2\text{-}6)$$

$$= \underbrace{-\frac{\varphi \gamma^k (1-S) c_g^{CO_2} n}{t_{e,ns}}}_{\text{Bio-reaction in neuston}} \underbrace{-\frac{\varphi \gamma^k S c_g^{H_2} c_g^{CO_2} n^2}{t_{e,n}}}_{\text{Bio-reaction in water}}$$

$$+ \underbrace{\nabla.\left(\rho_w D_w^k \varphi S \nabla c_w^k + \rho_g D_g^k \varphi (1-S) \nabla c_g^k\right)}_{\text{Diffusion}}$$

φ: porosity,

ρ: the molar density in [mol/m^3]

γ: the stoichiometric coefficient

D: the effective diffusion coefficient [m^2/s].

The concentrations of components in the water phase is given by Henry's equilibrium law:

$$c_w^k = H^k P_w c_g^k, \; k = H_2, CO_2 \qquad (2\text{-}7)$$

H is the Henry coefficient in [1/Pa].

According to (Heinemann et al., 2021), four hydrogenotrophic species are most relevant for hydrogen storage.

Methanogenesis refer to methane generation:

$$CO_2 + 4H_2 \longrightarrow CH_4 + 2H_2O$$

Acetogenesis takes place as follows:

$$2CO_2 + 4H_2 \longrightarrow CH_3COOH + 2H_2O$$

Sulfate-reduction occurs through the reaction:

$$SO_4^{2-} + 5H_2 \longrightarrow H_2S + 4H_2O$$

Iron (III)-reducing bacteria use the reaction:

$$3Fe_2^{III}O_3 + H_2 \longrightarrow 2Fe_3^{II}O_4 + H_2O$$

2.3 Optimum Environmental Conditions for Microbial Growth and Hydrogen Consumption

E.M. Thaysen et al. (2021) described the physical and chemical conditions that promote microbial metabolism of hydrogen in porous media. Their study relied on the data from 42 depleted oil and gas fields in the British and Norwegian North Sea. The data were used to evaluate the number of sites where microbial proliferation can be expected. The fact that hydrogen is an electron donor could have considerable implications for hydrogen in-situ conversion rates.

The microorganisms only have access to H_2(aq) and that is why H_2(g) is highly relevant to hydrogen consumption reactions. According to (E.M. Thaysen et al., 2021), microbial growth rate depends on environmental factors. The most important factors are the availability of nutrients, temperature, salinity, pH, and pressure.

Phosphorous is required for all metabolisms alongside elements like C, N, H, Mg, and S. For example, phosphorous concentrations down to 1.7 µM may suffice for microbial growth. Sulfate reduction may take place under sulfate concentrations in the range of 5-77 µM sulfate. A concentration of 29.6 mM Mg is required by methanogens for optimum growth but growth will cease at 16.5 mM. (E.M. Thaysen et al., 2021).

Concerning temperature, microbes are classified according to their optimum temperature. For example, psychrophiles grow optimally below 20 °C, psychrotrophic grow ideally from 20 °C on, mesophiles grow between 20 and 45°C, thermophiles around 45-50 °C.

The salt concentration range for H_2 storage is 0–5 M NaCl at which various bacteria may be found. Non-halophilic bacteria have a salt concentration tolerance of up to 0.2 M NaCl, moderate halophiles proliferate between 0.5 and 2.5 M NaCl, and extreme halophiles grow ideally in salt concentrations in the range of 2.5-5.2 M NaCl (E.M. Thaysen et al., 2021).

The brine pH also affects growth metabolism. Most bacteria are adapted to a pH of 6.5-7.5. Methanogens and sulfate-reducing microbes shall not grow outside the pH range of 4-9.5 (E.M. Thaysen et al., 2021).

At 30-50 MPa, the growth of microorganisms will be compromised (F. Abe et al., 1999) even though high pressure may promote the growth of hyperthermophiles. Above 100 °C, high pressures are needed to maintain a liquid environment (Holden JF et al., 2009).

Based on the study of the 42 depleted oil and gas fields, E.M. Thaysen et al. (2021) defined the distribution of temperature, pH, and salinity for optimum microbial growth (See Figure 2-4).

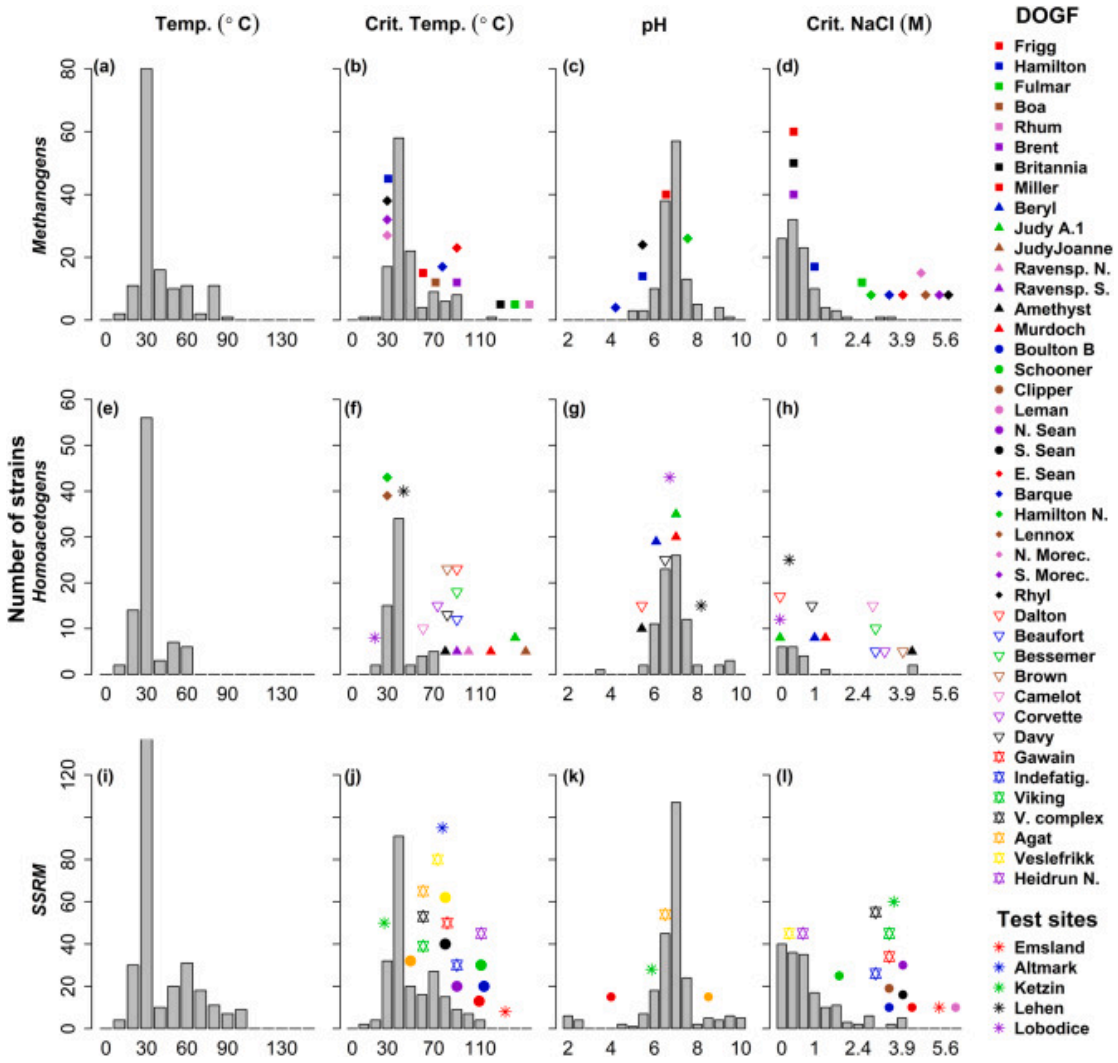

Figure 2-4 Optimum conditions for microbial growth. Shown in this figure are optimum growth temperature, critical growth temperature, optimum pH values, and critical salinity for microorganisms (methanogens, sulfate-reducing bacteria, and homoacetogens) at 42 depleted oil and gas fields (E.M. Thaysen et al., 2021).

2.4 Influence of Microbial Growth on Rock Hydraulic Properties

A biofilm, as shown in (Figure 2-) is an assembly of microorganisms that attaches to a surface by polymeric substances (Sid Becker & Andrey Kuznetsov, 2014). Microorganisms that live in a biofilm are essentially immobile and therefore could influence the hydrodynamic parameters of the porous medium. The result of this could be a reduction of the effective porosity and permeability (T.R.R Pintelon et al, 2012).

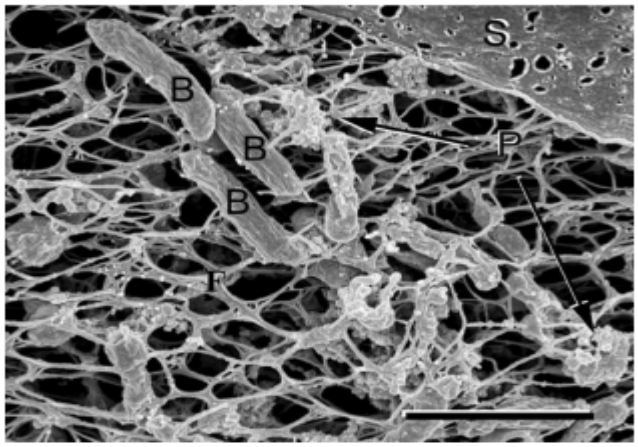

Figure 2-A biofilm from scanning electron microscope (SEM), B: microorganisms, F: EPS, P: particulate matter, S: substrate (Sid Becker & Andrey Kuznetsov, 2014).

Several studies about the reduction in hydrodynamic properties have been conducted. Neda Hassannayebi et al. (2021) investigated biomass accumulation and its influence on the permeability in porous media. The experiments consisted of two experimental stages. In the first stage, a bacterial suspension was flooded to induce an occupation of the pore spaces by microbes. In the second stage, a nutrient solution was injected to induce an exponential growth of the microorganisms. Using optical microscopy, the two phases were visualized as shown in Figure 2-5.

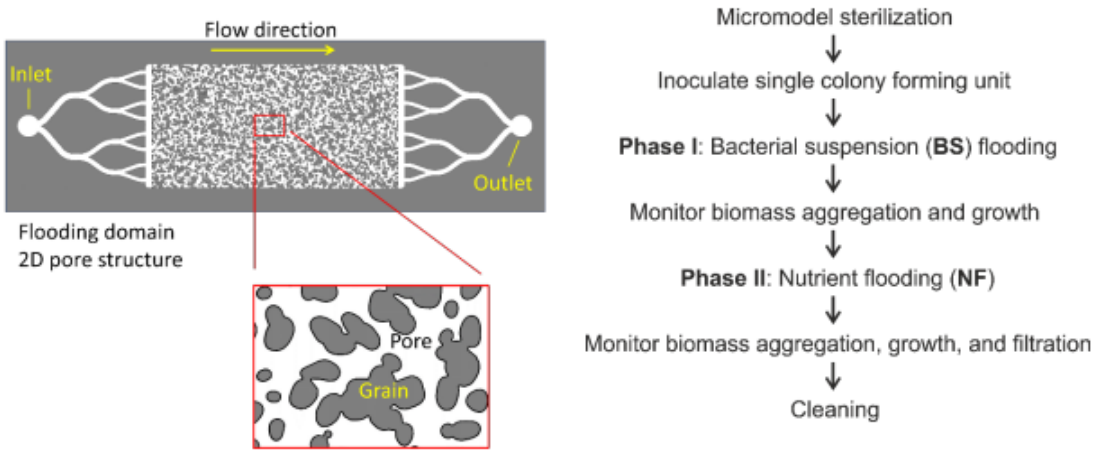

Figure 2-5 Left: pore structure (white) of 2D porous media. Right: schematic workflow (Neda Hassannayebi et al., 2021).

The porosity was 0.5 and the permeability was 2.5D, the total pore volume was 2.3 uL respectively. A constant flow rate of $0.2mLh^{-1}$ was used. Finally, the pressure drop across the micromodel was recorded.

The Lactobacillus casei was the type of bacteria used. The specificity of this bacteria is that it can grow in oxygen-free environments and tolerate a wide range of pH and temperature conditions. The optical density (OD) of the bacterial culture was measured using a spectrophotometer.

Underflow conditions the distribution and evolution of biomass were visualized as shown in Figure 2-6. During the bacterial flooding stage, microbial cells are suspended in the injection water and transported into the porous domain and it can be seen that some cells are deposited in the pore space. The highest microbial density is observed at the inlet of the micromodel and microbes are also heterogeneously scattered along the channel of injection.

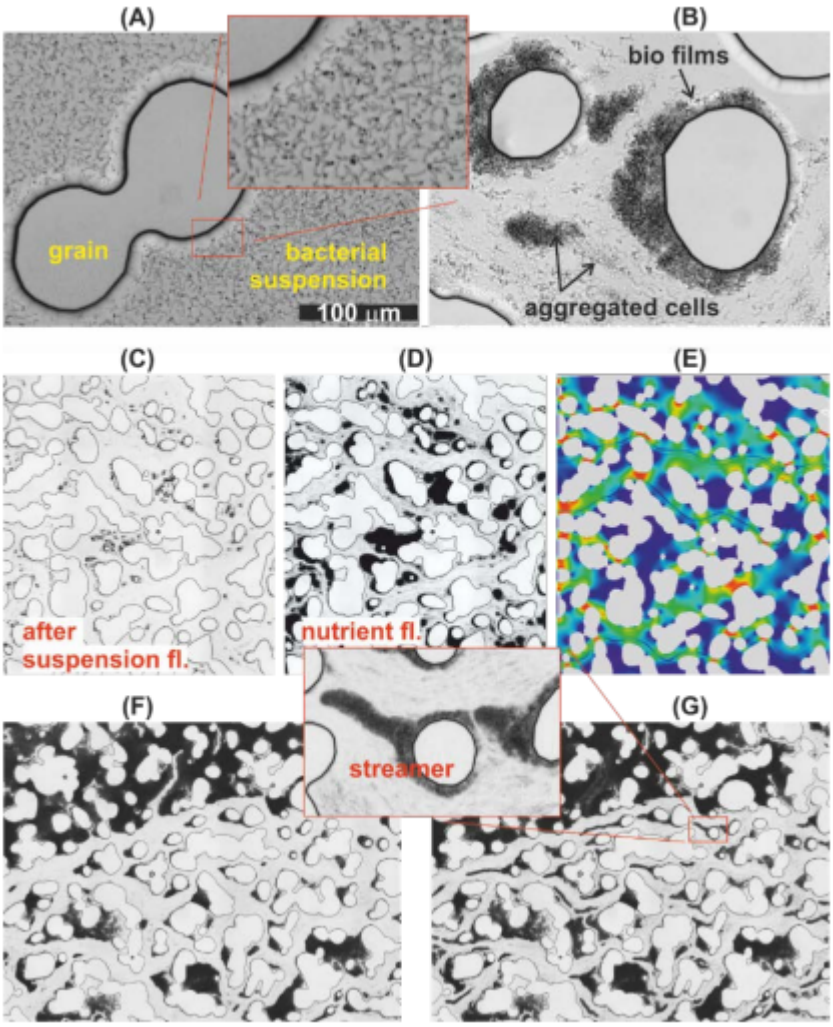

Figure 2-6 A refers to the bacterial suspension phase. B is the suspended microbial cells forming biofilms. C: initially injected bacteria after BS and D: during NF. E refers to the simulated flow velocity. F and G refer to biomass accumulations before and after filtration (Neda Hassannayebi et al., 2021).

The clogging of pore space affects the permeability which is reflected in the experimental pressure drop measure over the flooding domain. When the flooding rate is high, a continuous increase in biomass saturation was observed and the pressure drop increased accordingly (Figure 2-7).

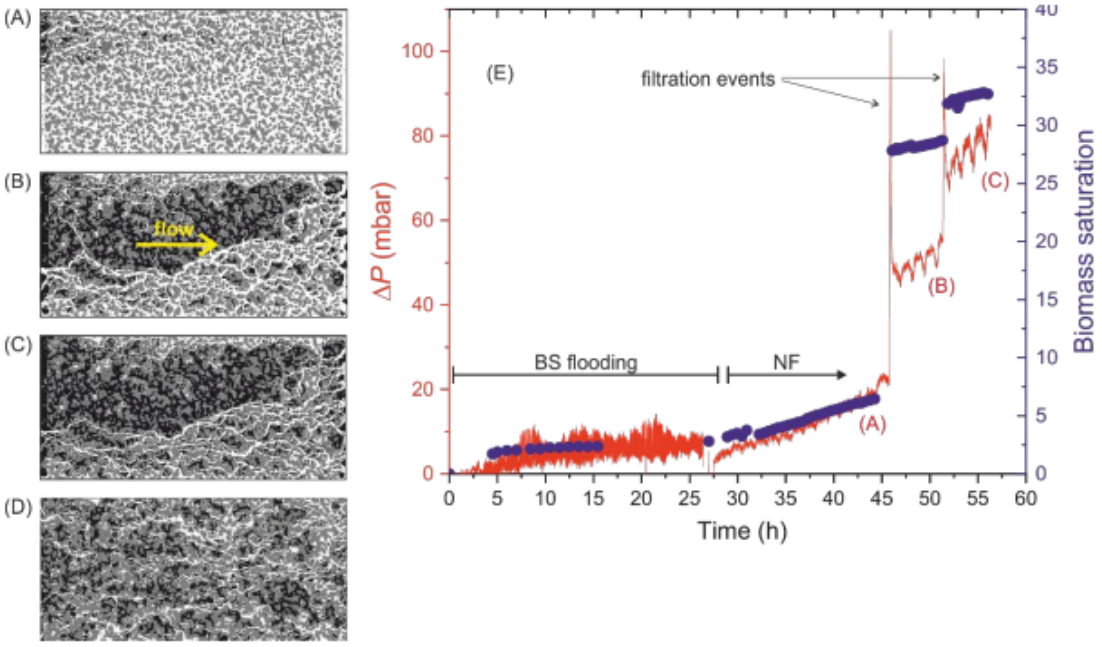

Figure 2-7 A to C show the phase distribution during a nutrient flooding experiment. Images segmentation: white is the open pore space, light is the grains and black is the biomass. C and D are the final states of two different experiments. E shows the relationship between biomass growth and pressure drop (Neda Hassannayebi et al., 2021).

Numerical simulations were performed on homogeneously occupied sub-volumes of the system to estimate the K (φ) relationship. Several cases were simulated on 3D digital twins by considering the biomass as permeable with a single porosity value of 0.5, and permeable with a porosity linearly distributed. When porosity is considered as linearly distributed, the biomass permeability was scaled exponentially to the porosity and expressed as $K_{bm}/K_{bm,0} = (\varphi/\varphi_o)^{\alpha}$ where $K_{bm,0}$ is the maximum possible permeability of 33D and φ_o is the associated maximum porosity. By solving the Navier-Stokes-Brinkman equation on the voxel-based images, the changes in the flow field were computed as a function of biomass accumulation.

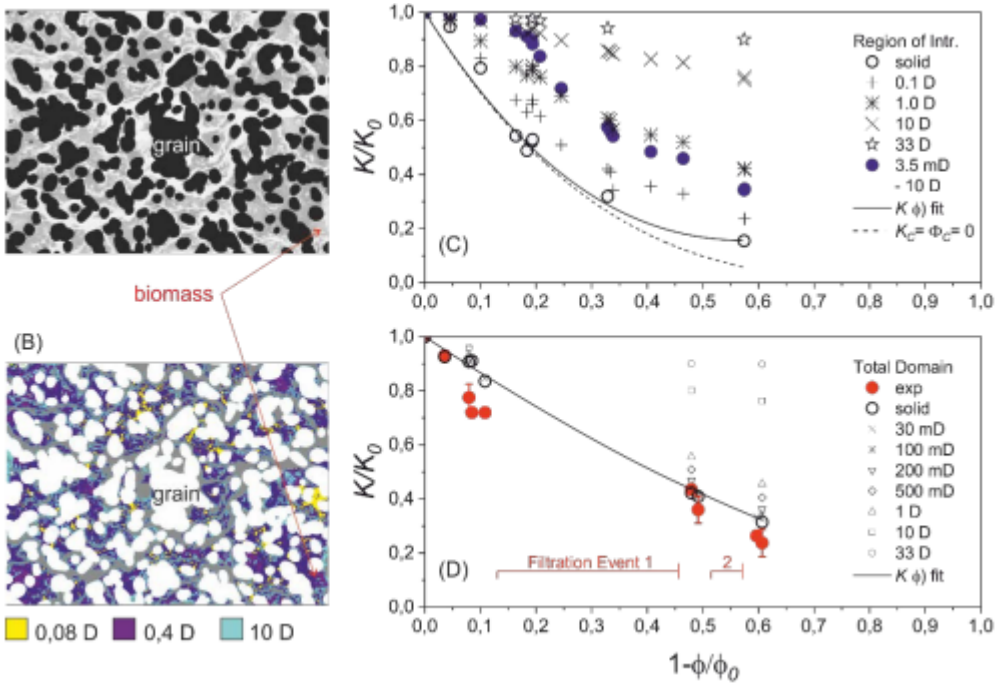

Figure 2-8 A: region of interest where biomass occupies pore space and B: the same image segmented. C: K(φ) relationships simulated for the solid case. The solid symbols refer to the image segmentation of image B considering a permeability distribution. D: K(φ) relationships simulated on the total domain (Neda Hassannayebi et al., 2021).

2.5 Geochemical Reactions and Geomechanical Considerations

For geological hydrogen storage a porous and permeable reservoir formation, a cap rock, and a trapping structure are needed (Figure 2-9). Hydrogen when it is injected will displace the in-situ pore fluids and establish below a low permeable cap rock. The trap ensures that the hydrogen will not migrate.

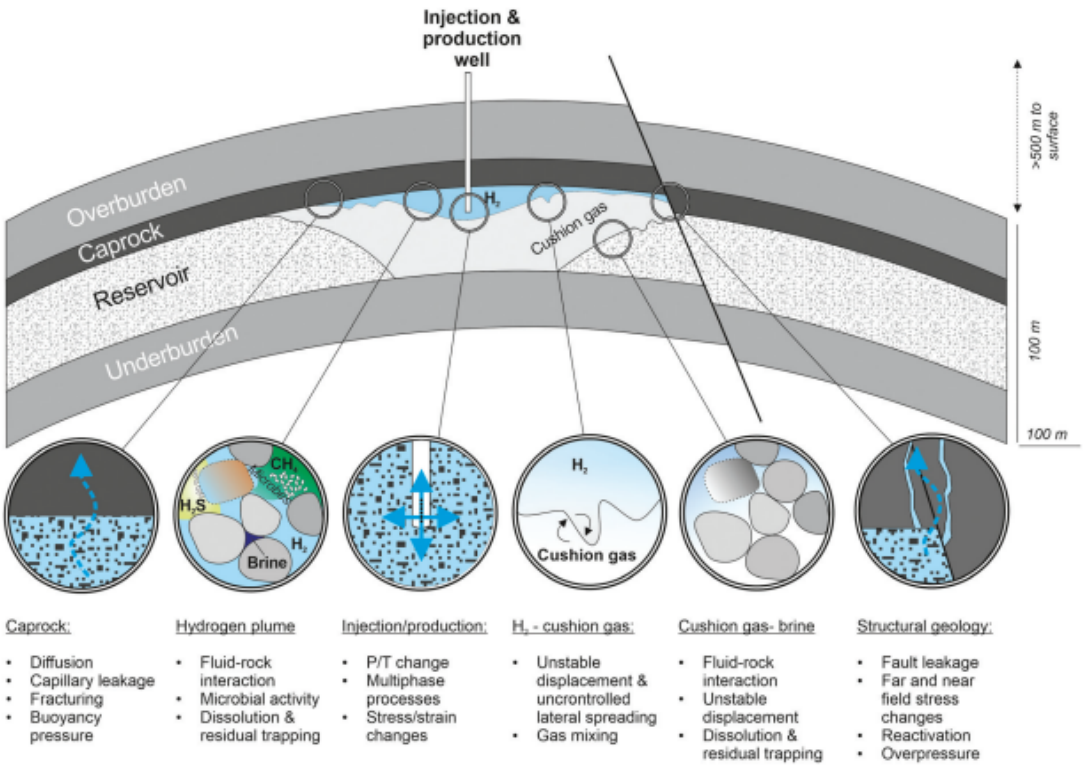

Figure 2-9 Geological uncertainties associated with geological hydrogen storage (Heinemann et al., 2021).

By injecting hydrogen in the subsurface, it will likely react with the rock minerals and the fluids in the pore space. That might be a concern for the storage operation. Furthermore, and as mentioned before, the presence of hydrogen may stimulate the growth of microbial population consuming hydrogen as a substrate. The injection cycles might also induce cyclic stress changes in the field, that may bring concerns over the integrity of the sealing.

2.5.1. Hydrogen, Methane, and CO_2 Fluid Properties

When pressure increases, the density of hydrogen increases as well (Figure 2-10), which promotes an increased storage efficiency with depth. The viscosity of hydrogen is low and shows little variation under gas storage conditions.

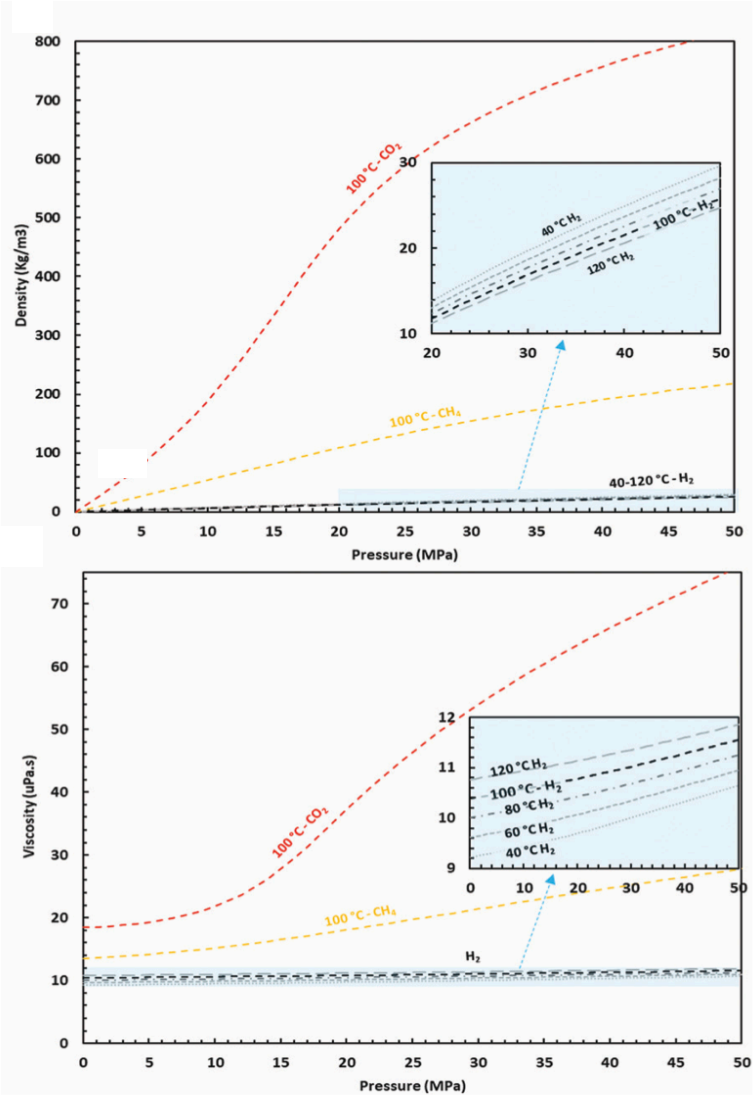

Figure 2-10 Density and viscosity of H_2, CO_2, and CH_4 as a function of pressure and temperature (Heinemann et al., 2021).

2.5.2 Geochemical and Geomechanical Aspects

When Hydrogen is injected into a porous medium, the chemical equilibrium between the formation pore water, the dissolved gas, and rock matrix will change. Geochemical reactions could lead to the conversion of the injected hydrogen. It could also induce mineral dissolution leading to enhanced or reduced injectivity. Dissolved hydrogen may react with initially present components in pore water such as dissolved sulfate and affect fluid pH.

Hydrogen injection into the subsurface will induce stress variations, as a result, deformation may occur beyond the area of pressure change. Changes in the effective stress caused by injection-reproduction cycles may cause rock compaction within the reservoir. Consequences

of this could be porosity reduction and reduced fluid flow, subsidence, and fault reactivation. (Heinemann et al., 2021).

Chapter 3

Methodology and input data

3.1 Methodology: The Fundamentals of Dumuxbio

Dumux was coded in C++ and was developed for the simulation of flow and transport processes in porous media. The Dumuxbio is an adaptation of Dumux for bio-reactive modeling in underground hydrogen storage. The physical models in Dumuxbio include microbial growth and decay in addition to the common models such as multi-phase flow, molecular diffusion, mechanical dispersion, chemical reactions, and non-isothermal flow. The special discretization is the finite volume method and time discretization is the backward Euler method.

The overall conservation of moles considers a continuum scale with advective and diffusive transport (Birger Hagemann, 2017):

$$\varphi \frac{\partial(\rho_g c_g^k S_g + \rho_w c_w^k S_w)}{\partial t} + \nabla . \left(\rho_w c_w^k v_w + J_w^k + \rho_g c_g^k v_g + J_g^k\right) = q^k \qquad (3\text{-}1)$$

φ:porosity

ρ: molar density in [mol/m3],

c: mole fraction,

S: saturation

v: advective flux in [m/s]

J: dispersive/diffusive flux in [mol/m^2/s]

q: source or sink term,

g and w refer to the gas and water phase respectively

k refers to the chemical component.

Darcy's law is used to express the volumetric velocity:

$$v_i = -\frac{KK_{ri}}{\mu_i}(\nabla P_i - \hat{\rho}_i g)\,, \quad i = g, w \qquad (3\text{-}2)$$

K: absolute permeability in [m^2],

Kr: relative permeability,

μ: dynamic viscosity in [Pa · s],

P: phase pressure in [Pa],

ρ: phase density in [kg/m3],

g: gravity acceleration in [m/s^2].

The diffusive flux is the sum of molecular diffusion and mechanical dispersion:

$$J_i^k = -\rho_i \left(D_{diff,i}^k + D_{disp,i}^k\right) \nabla c_i^k,\ i = g, w \qquad (3\text{-}3)$$

$D^k_{diff,i}$: effective molecular diffusion coefficient of component k in phase in [m^2/s].

Using the Brooks-Corey correlation, the hydraulic properties were calculated:

$$P_e(S_w) = P_g - P_w = P_e S_{we}^{-\frac{1}{\lambda}} \qquad (3\text{-}4)$$

$$k_{rw}(S_w) = S_{we}^{\frac{2+3\lambda}{\lambda}} \qquad (3\text{-}5)$$

$$k_{rg}(S_w) = (1 - S_{we})^2 \left(1 - S_{we}^{\frac{2+\lambda}{\lambda}}\right) \qquad (3\text{-}6)$$

P_e is the entry pressure in [Pa] and S_{we} is the effective water saturation:

$$S_{we} = \frac{S_w - S_{wr}}{1 - S_{wr} - S_{gr}} \qquad (3\text{-}7)$$

S_{wr}: residual water saturation

S_{gr}: residual gas saturation.

The equality of fugacities defines the thermodynamics equilibrium in this model:

$$f_g^k = f_w^k \ \ or \ \ c_g^k \varphi_g^k P_g = c_w^k \varphi_w^k P_w \qquad (3\text{-}8)$$

f is the fugacity in [Pa] and φ is the fugacity coefficient. The system of equation is closed by the sum of saturations and the sum of concentrations:

$$S_g + S_w = 1 \quad \sum_k c_g^k = 1 \quad \sum_k c_w^k = 1 \qquad (3\text{-}9)$$

The microbial dynamics in Dumuxbio is formulated in Birger Hagemann (2017) as:

$$\frac{\partial n}{\partial t} = \psi^{growth}(c^S, c^A)\,.n - \psi^{decay}.n + \nabla.(D_m \nabla n) \qquad (3\text{-}10)$$

n: microbial density in [1/m^3],

ψ^{growth}: microbial growth function in $[\frac{1}{s}]$ which is a function of the substrate concentration C_w^s and the electron acceptor concentration C_w^A in the water phase,

ψ^{decay}: decay function in $[\frac{1}{s}]$ and D_m is the microbial diffusion coefficient in [m^2/s].

If we assume that CO_2 is the source of carbon; a new term must to be introduced for the rate of CO_2 consumption (Birger Hagemann, 2017):

$$q^k = \varphi \gamma^k \frac{\psi^{growth}}{Y_e} n,\ n = 1, \dots, n \backslash \{CO_2\} \qquad (3\text{-}11)$$

$$q^{CO_2} = \varphi \left(\gamma^{CO_2} \frac{\psi^{growth}}{Y_e} + \frac{\psi^{growth}}{Y_c} - \frac{\psi^{decay}}{Y_P} \right) n \qquad (3\text{-}12)$$

γ: coefficient relating the consumption or production of components to the consumption of H_2.

Y is the yield coefficient relating the rate of energy update (Ye), the rate of carbon consumption (Yc), and the rate of carbon production (Yp) to the rates of microbial growth and decay.

To formulate the final model, a coupling of flow, transport, microbial processes is required. The system of equation applied is as follows (Birger Hagemann, 2017):

For microbial dynamics:

$$\frac{\partial n_m}{\partial t} = \psi_m^{growth}\,.n_m - \psi_m^{decay}\,.n_m + \nabla.(D_m \nabla n_m) \qquad (3\text{-}13)$$

The reactive transport for mobile components except for CO_2:

$$\begin{aligned} &\varphi \frac{\partial \left(\rho_g c_g^k S_g + \rho_w c_w^k S_w \right)}{\partial t} \\ &+ \nabla . \left(-\rho_g c_g^k \frac{K K_{rg}}{\mu_g} . \left(\nabla P_g - \hat{\rho}_g g \right) - \rho_w c_w^k \frac{K K_{rw}}{\mu_w} . \left(\nabla P_w - \hat{\rho}_w g \right) \right) \\ &+ \nabla . \left(-\rho_g \left(D_{diff,g}^k + D_{disp,g}^k \right) \nabla c_w^k - \rho_w \left(D_{diff,w}^k + D_{disp,w}^k \right) \nabla c_w^k \right) \\ &= \varphi po \sum_m \gamma_m^k \frac{\psi_m^{growth}}{Y_{m,e}} n_m \end{aligned} \qquad (3\text{-}14)$$

k = H_2, CH_4, H_2O, H_2O, H_2S, CH_3COOH, SO_4^{2-}

The reactive transport for CO2 is given by:

$$\varphi \frac{\partial\left(\rho_g c_g^k S_g + \rho_w c_w^k S_w\right)}{\partial t} + \nabla .\left(-\rho_g c_g^k \frac{KK_{rg}}{\mu_g} .\left(\nabla P_g - \hat{\rho}_g g\right) - \rho_w c_w^k \frac{KK_{rw}}{\mu_w} .\left(\nabla P_w - \hat{\rho}_w g\right)\right) + \nabla .\left(-\rho_g \left(D_{diff,g}^k + D_{disp,g}^k\right) \nabla c_w^k - \rho_w \left(D_{diff,w}^k + D_{disp,w}^k\right) \nabla c_w^k\right) = \varphi \sum_m (\gamma_m^{CO_2} \frac{\psi_m^{growth}}{Y_{m,e}} + \frac{\psi_m^{growth}}{Y_{m,e}} - \frac{\psi_m^{decay}}{Y_{m,p}}) n_{m,} \quad (3\text{-}15)$$

For the heterogeneous reaction:

$$(1-\varphi) \frac{\partial(\rho_s c_s^k)}{\partial t} = \varphi \gamma_I^k \frac{\psi_m^{growth}}{Y_I} n_I, \; k = Fe_2^{III} O_3, Fe_3^{II} O_4 \quad (3\text{-}16)$$

m relates the four microbial species: methanogenic archaea, acetogenic archaea, sulfate-reducing bacteria, and iron-reducing bacteria.

s, w, and g: solid, water, and gas-phase respectively.

k refers to the components of the system: H_2, CO_2, CH_4, H_2O, H_2S, CH_3COOH, SO_2^{-4}, $Fe_2^{III}O_3$, $Fe_3^{II}O_4$.

For microbial growth ψ^{growth} a method called the double Monod model was used to define the microbial growth function (Birger Hagemann, 2017).

For methanogenic archaea:

$$\psi_M^{growth} = \psi_{M,max}^{growth} \left(\frac{c_w^{H_2}}{\alpha_{M,1} + c_w^{H_2}}\right)\left(\frac{c_w^{CO_2}}{\alpha_{M,2} + c_w^{CO_2}}\right) \quad (3\text{-}17)$$

For acetogenic archaea:

$$\psi_A^{growth} = \psi_{A,max}^{growth} \left(\frac{c_w^{H_2}}{\alpha_{A,1} + c_w^{H_2}}\right)\left(\frac{c_w^{CO_2}}{\alpha_{A,2} + c_w^{CO_2}}\right) \quad (3\text{-}18)$$

For sulfate-reducing bacteria:

$$\psi_S^{growth} = \psi_{S,max}^{growth} \left(\frac{c_w^{H_2}}{\alpha_{S,1} + c_w^{H_2}}\right)\left(\frac{c_w^{SO_4^{2-}}}{\alpha_{S,2} + c_w^{SO_4^{2-}}}\right) \quad (3\text{-}19)$$

For iron-reducing bacteria:

$$\psi_I^{growth} = \psi_{I,max}^{growth}\left(\frac{c_w^{H_2}}{\alpha_{I,1}+c_w^{H_2}}\right)\left(\frac{c_s^{Fe_2^{III}O_3}}{\alpha_{I,2}+c_s^{Fe_2^{III}O_3}}\right) \qquad (3\text{-}20)$$

M stands for methanogenic bacteria, A means acetogenic bacteria, S means sulfate-reducing bacteria, and I stand for iron-reducing bacteria.

3.2 Input Data

The model that we used in this study has a grid cell size of 50×50×3 m with 2350 grids cells and has a thickness of 15 m.

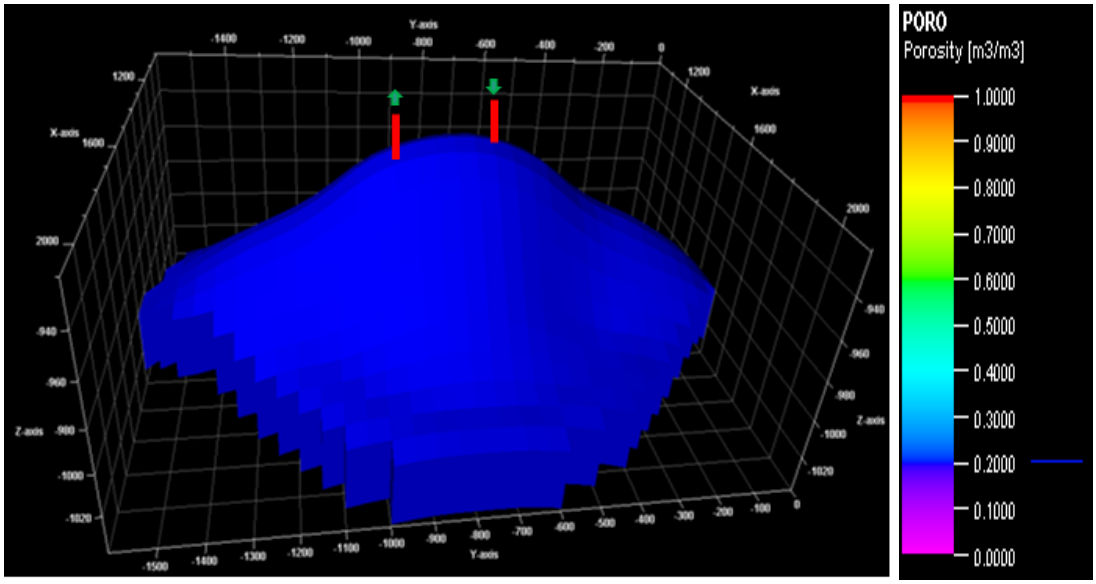

Figure 3-1 Geometry of the homogeneous model

The parameters are shown in table 3-1

Table 3-1. Initial parameters of the homogeneous model

Parameter	Value	Unit
GWC	1050	m
Pressure@GWC	90	bar
Temperature	300	K
Kxx, Kyy, Kzz	200	mD
Porosity	20	%
GIIP	6.03×10^{6}	m^3
Number of grid cells	2350	-
Grids dimensions	50×50×3	m

The rock fluids parameters are also known:

- Residual water saturation: 0.1
- Residual gas saturation: 0.1
- Capillary entry pressure Pe: 100000 Pa
- Lambda λ: 2

Initial composition:

- Nitrogen as a cushion gas, in this case, is used to displace the initial gas in the reservoir.
- A little amount of sulfate (SO_4) is dissolved in the water phase: 0.0003375% in mole fraction.

Using the Brooks-Corey method we obtain the relative permeability and capillary pressure curves as shown in Figure 3-2.

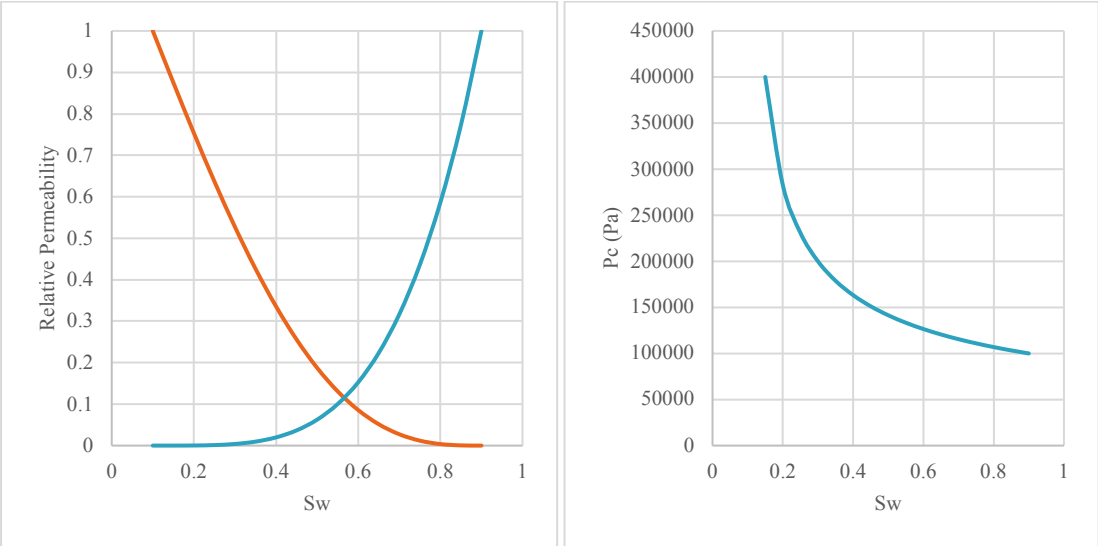

Figure 3-2 Relative permeability (Left) and capillary pressure (right) for the model

In our study, we have established a base case, which we used to perform a sensitivity analysis for several parameters. We assume that hydrostatic equilibrium exists in the reservoir. The values of the pressure in the gas, transition, and water zones and the values of saturations are calculated using the pressure gradients and the capillary pressure curve.

The goal in the first part of this study is to find out the parameters influencing bio-methanation the most. The numerical parameters that were used in our base case are as follows:

- Distance between wells: 350 m
- Total injection rate: 15 moles/s
- Injection gas composition: 50% N_2, 40% H_2, 10% CO_2
- Total production rate: 13 moles/s
- Simulation period: 30 years

Based on a sensitivity analysis we have chosen a base case in which the rate of methanation is high enough to enable us to distinguish that rate from different ones. The injected gas is a mimic of the so-called "town gas" which is composed mainly of H_2, CO_2, and Hydrogen and which is usually obtained by coal combustion. The injection scenario in the first part of the study is solely intended to investigate the underground bio-methanation, which is the reason why such special conditions were chosen. Other scenarios with only hydrogen injection are studied in subsequent parts.

The microbial parameters used for the case are shown in table 3-2:

Table 3-2. Base case microbial kinetic parameters

Parameter	Value	Unit
Microbial growth rate	3×10^{-5}	$\frac{1}{s}$
Microbial decay rate	2×10^{-6}	$\frac{1}{s}$
Microbial yield	2.5×10^{11}	/mol
Hydrogen half velocity constant	1.1×10^{-7}	mol/mol
CO2 half velocity constant	3.2×10^{-4}	mol/mol
Microbial number density n^*	6×10^{10}	-

3.2.1 Base Case without Microbial Activity

In the first step, a simulation of the base case without microbial activity was performed to have a view of the hydrogen plume propagation throughout the top of the gas zone.

In the absence of no or very little microbial activity, the hydrogen plume is almost entirely observed in the gas cap.

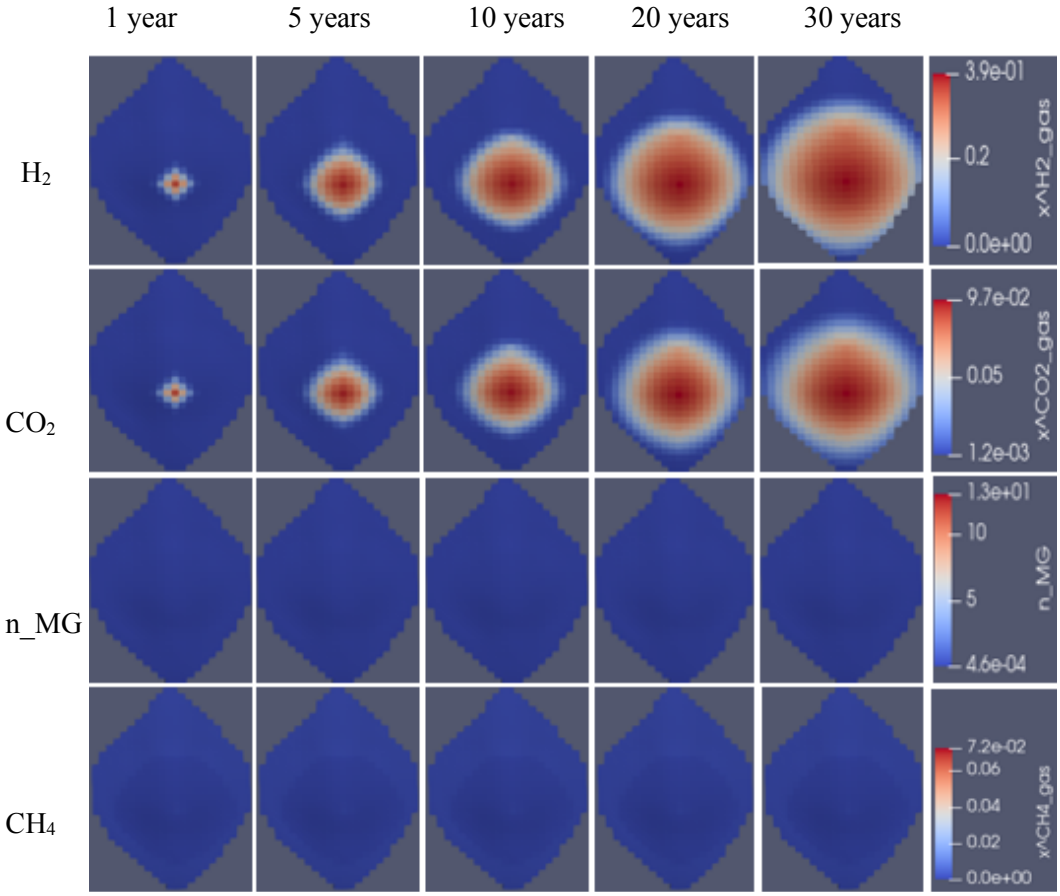

Figure 3-3 Temporal evolution of gas concentration in the base case without microbial activity

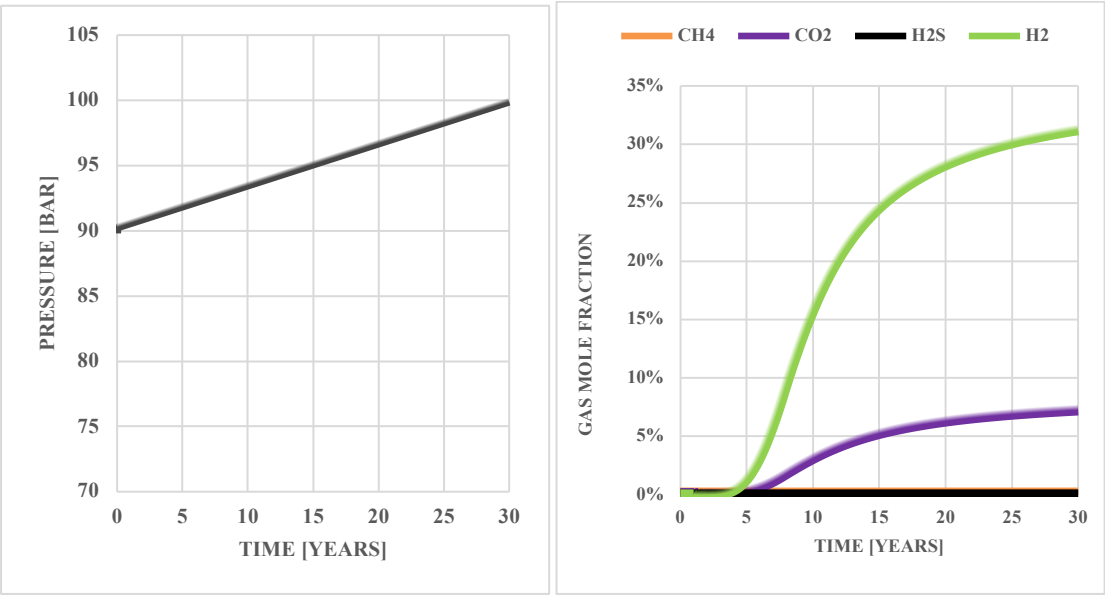

Figure 3-4 Pressure (Left) and temporal evolution of gas concentration for the base case without microbial activity

Most of the gas recovered from the production well is composed of around 32 % H_2 and about 7% of CO_2. No methane recovery is recorded. As we know the initial gas, the composition is 50% N_2, 40% H_2, and 10% CO_2. It means that part of the H_2 and CO_2 injected is accumulated in the reservoir either as a trapped gas or dissolved in the liquid phase. It also means that a large amount of gas recovered after 30 years is composed of cushion gas (N_2). In the following chapters, we studied the recovered concentrations in detail as we are only dealing with the methanation process in this chapter. The gradually increasing pressure over time indicates that the accumulation term (see equation (3-1)) in the reservoir is quite considerable.

3.2.2 Base Case with Microbial Activity

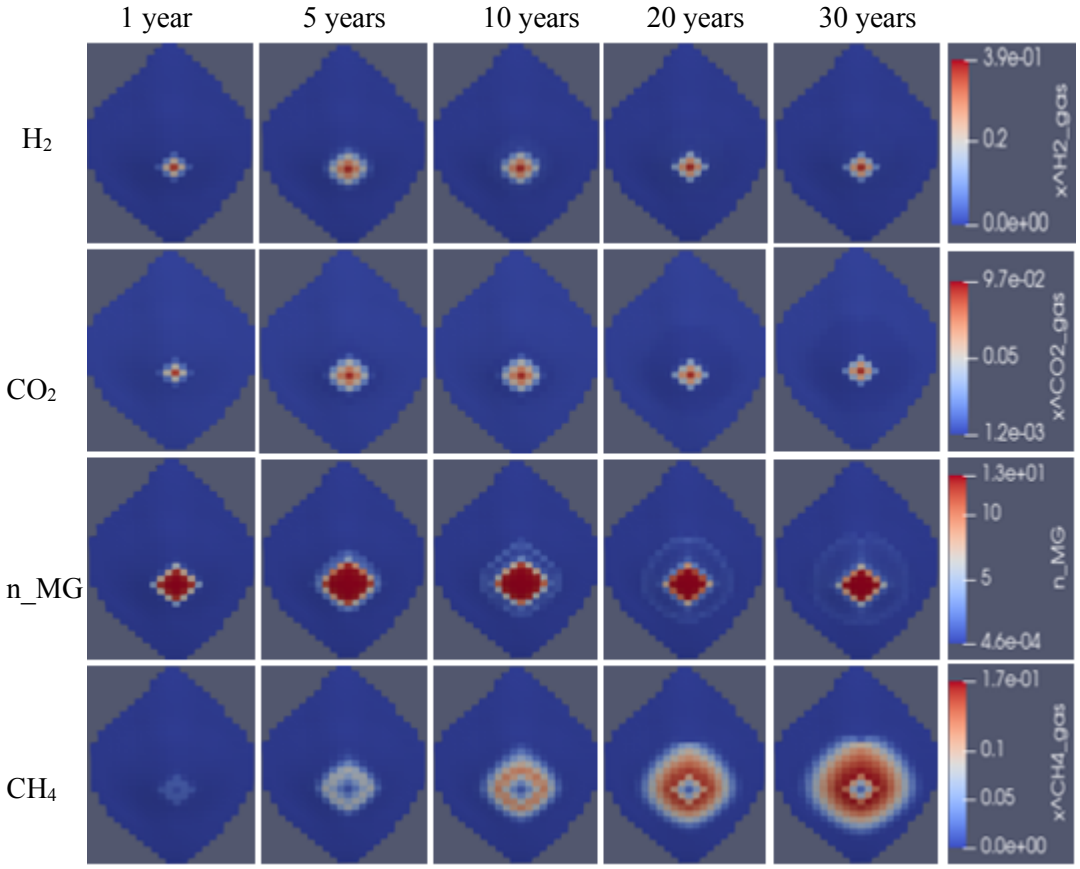

Figure 3-5 Temporal evolution of the gas concentration of the base case with microbial activity

The results of the gas propagation in the reservoir show that our base is characterized by very strong microbial and methanation processes. The gradual increase in methane production is an indication of a high conversion rate as most of the hydrogen initially injected was consumed by microorganisms. A strong microbial density is indeed observed around the injector where the concentration of nutrients such as H_2 and CO_2 are the highest. We investigated microbial dynamics in detail in chapter 4.

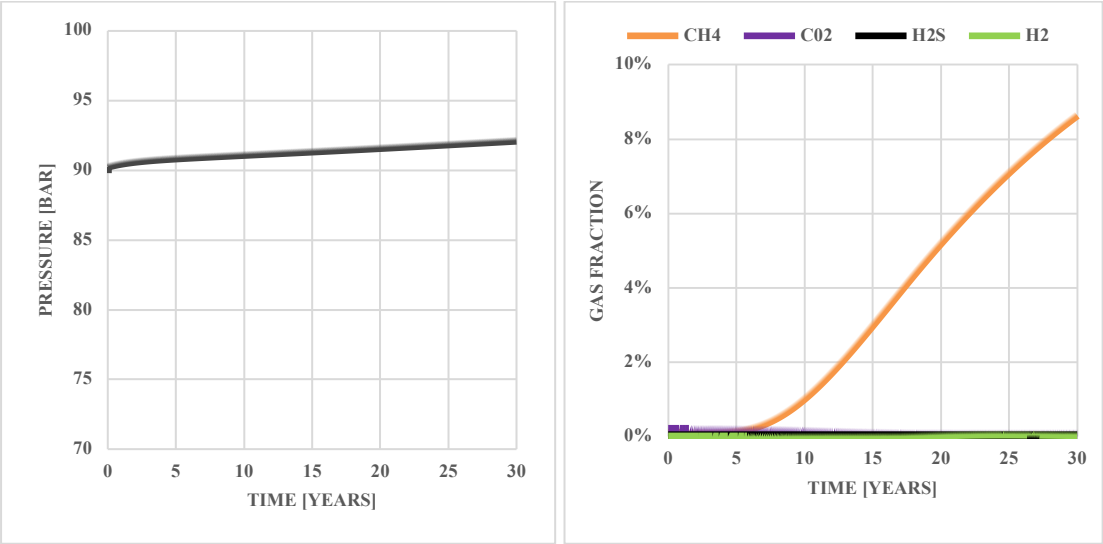

Figure 3-6 Pressure (Left) and gas concentration (Right) with microbial activity

The pressure increase in the case where microbial activity is present is less pronounced. This might be explained by the fact that more gas is being dissolved in the liquid phase as methane has a solubility greater than that of hydrogen. Furthermore, we should keep in mind that in terms of stoichiometry, four moles of hydrogen are needed to create a single mole of methane; therefore, the volumetric might be negatively impacted. In addition, methane is a heavier component than hydrogen and less mobile, the result is a smaller gas expansion, which leads to a minimal pressure increase. Nonetheless, hydrogen is injected in combination with heavier components such as CO_2 (10%) and nitrogen (50%) and that could explain why the overall pressure trend is increasing.

We know that 15 moles per second is injected and hydrogen accounts for 40% of the injected gas. That means that we can calculate the cumulative amount of hydrogen injected after 30 years and based on the cumulative methane generated across the entire reservoir, we can derive the consumption rate as shown in Figure 3-7.

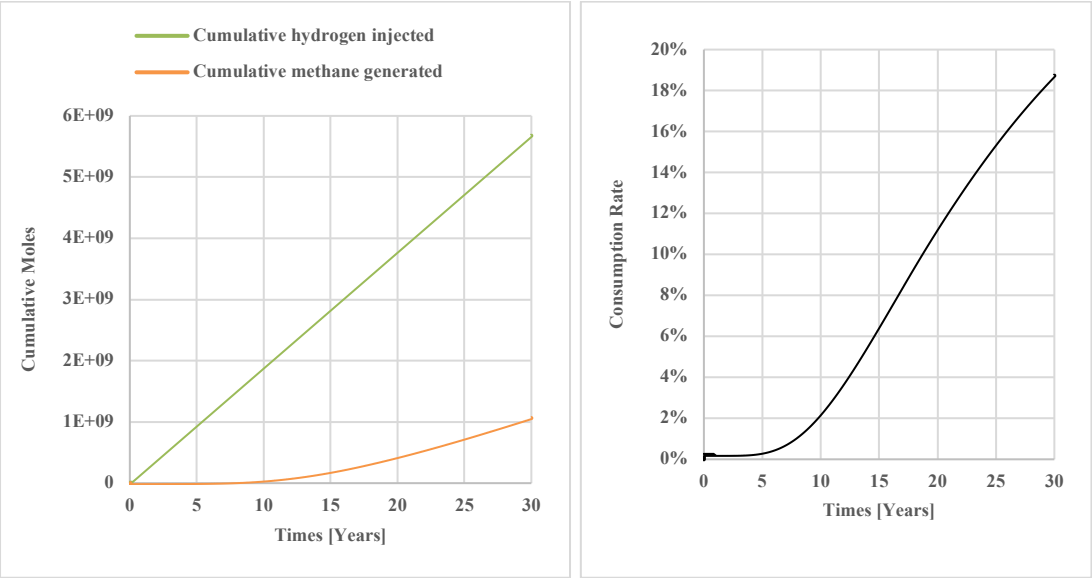

Figure 3-7 Cumulative moles of hydrogen and methane generated in the entire field (Left) and the resulting consumption rate over time (Right)

Our base case is taking place with a high microbial growth rate and we could observe a maximum consumption rate of around 11%. However, as we are looking forward to knowing the parameters that influence methane generation, we performed a sensitivity analysis of the most important parameters in the next chapter to figure that out.

Chapter 4

Results and Discussion

4.1 Parameters Influencing Methanation

4.1.1 Microbial Growth Rate

The first parameter that we investigated is microbial growth. This term in this case refers to the rate at which the cells reproduce themselves. Our base case has a microbial growth rate of 3×10^{-5}/s. Our sensitivity analysis includes the results obtained with lower and higher growth rates than the base case.

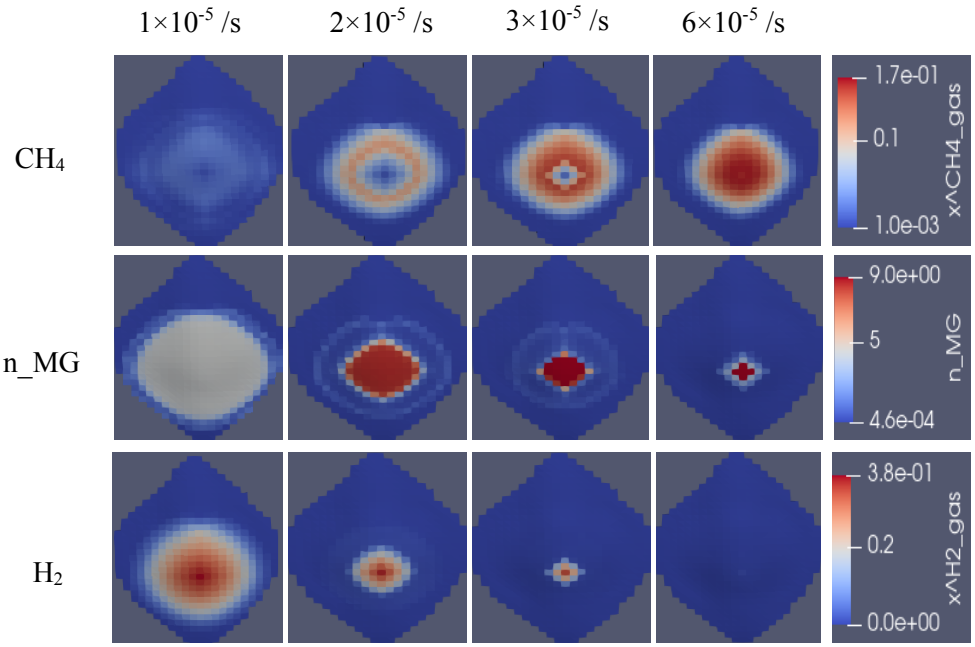

Figure 4-1 Concentration of generated gas as a function of microbial growth rate

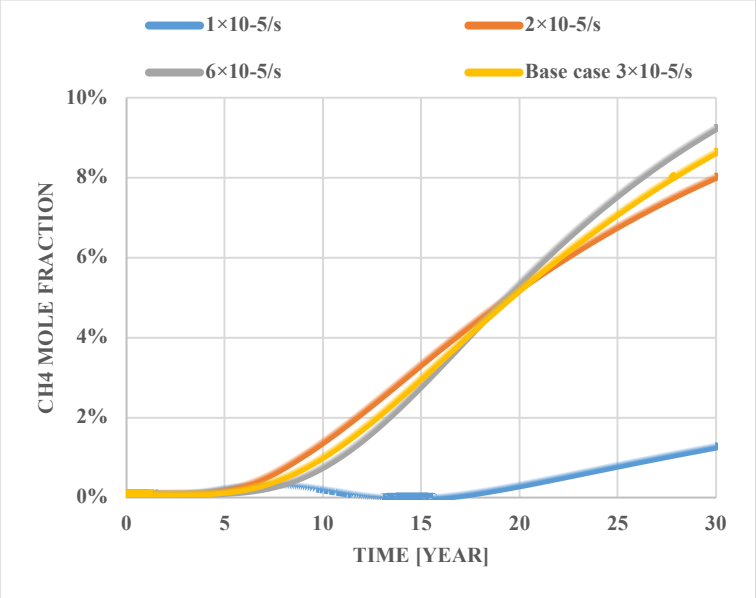

Figure 4-2 Temporal evolution of generated methane concentration as a function of microbial growth rate

Based on these results we can see that the minimum conversion rate is achieved with a microbial growth rate of 1×10^{-5}/s. The conversation rate achieved with the other values of growth rate is close to each other although the maximum conversion rate of 9% is achieved at a growth rate of 6×10^{-5}/s. We can observe from the figure that a high methanation rate is correlated with the high consumption of hydrogen. Indeed, the lowest growth rate of 1×10^{-5}/s leaves most hydrogen untouched while the highest value of 6×10^{-5}/s consumes most of the hydrogen.

One particular observation that we make is the evolution of microbial density. The closer the microbes are to the injector the highest the methanation rate. This is because when microorganisms are distributed across the entire reservoir, access to nutrients is limited. However, when they are clustered around the injector large access to nutrients leads to a large conversion rate. That could explain why an increased microbial growth rate (an increasing hydrogen consumption rate) is associated with a microbial movement towards the injector.

4.1.2 Microbial Yield

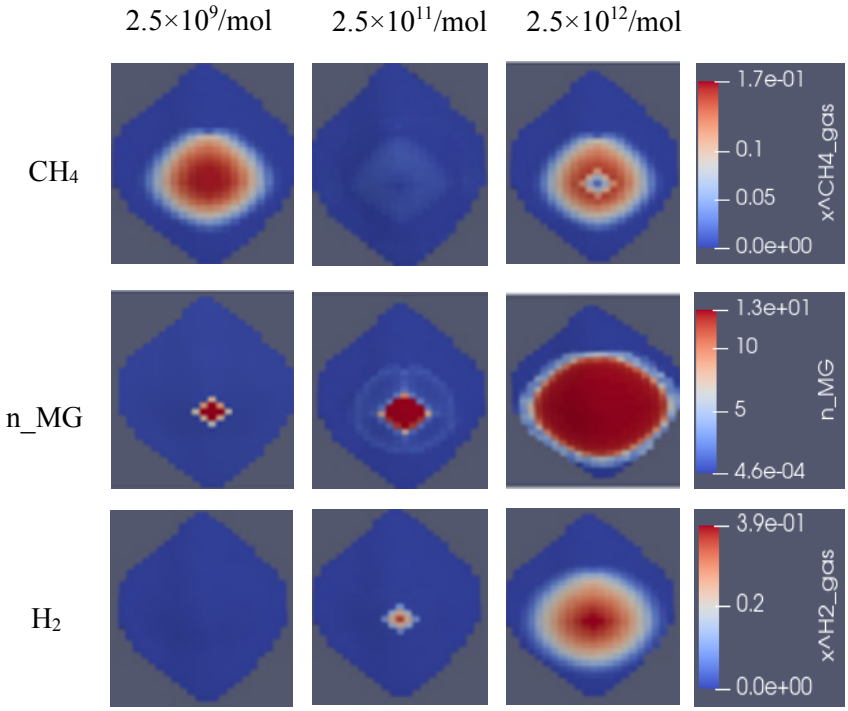

Figure 4-3 Concentration of generated gas a function of microbial yield

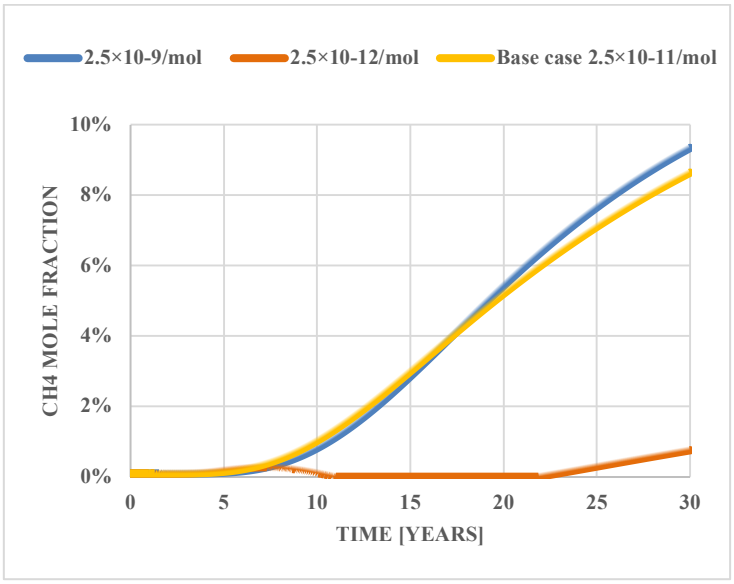

Figure 4-4 Concentration of generated methane over time as a function of microbial yield

The microbial yield can be defined as the number of bacteria formed per mol of substrate consumed. Contrary to the growth rate, the yield could harm the methanation process. The highest yield of 2.5×10^{12} /mol leads to the lowest methanation rate (1%) after 30 years of injection while the lowest yield leads to the highest conversion rate (around 10%). One possible explanation is that when the microbial yield is high, due to the intense competition for nutrient access, the majority of the cells are left without access to hydrogen and carbon sources and eventually decay. Another observation that reinforces our interpretation in the previous section is that a large conversion rate is correlated with a large clustering of microbes around the injector as can be seen in Figure 4-3.

4.1.3 Hydrogen half Velocity Constant

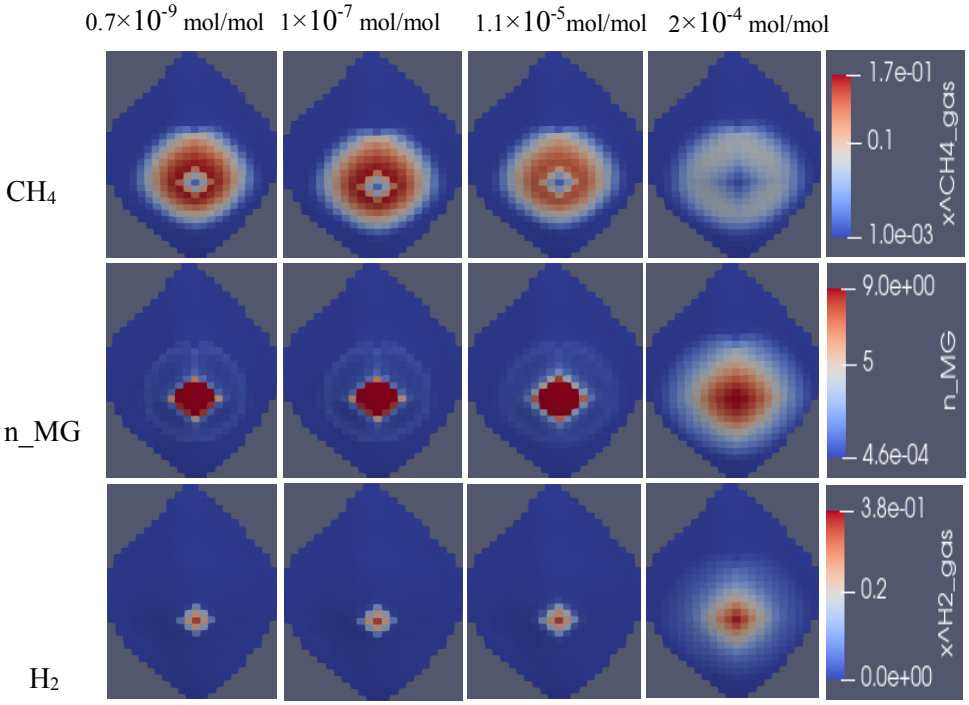

Figure 4-5 Concentration of generated gas as a function of hydrogen half velocity constant

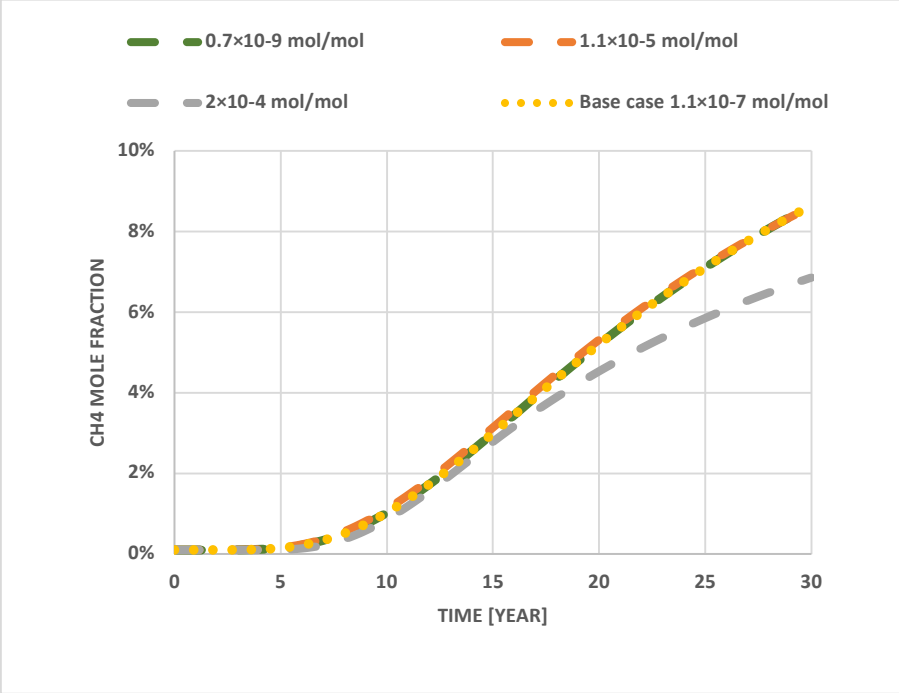

Figure 4-6 Concentration of generated methane over time as a function of hydrogen half velocity constant

The hydrogen half velocity constant is defined in the Monod's equation as the concentration of the limiting substrate (hydrogen in this case) when the actual growth rate is half the maximum growth rate (Birger Hagemann, 2017). The half-velocity constants are provided in [µM] or [mM]. The unit M refers to the molar concentration in [mol/L] . If we consider the components to be dissolved in 1L of water, the conversion into [mol/mol] requires the molar concentration of water which is 55.55 mol/L. In such case:

$$1\mu M = 1 \times 10^{-3}\ mM = \ 10^{-6} \times \frac{1}{55.555}\ \frac{mol}{mol} \qquad \textit{(Birger Hagemann, 2017)} \quad \textit{(4-1)}$$

It looks like the methanation rate does not exceed 9% after 30 years of injection when the Half velocity constant is equal to or below 0.7×10^{-9} mol/mol and the lowest methanation rate is reached when its value is at a maximum of 2×10^{-4} mol/mol. Although the sensitivity of the half velocity constant to the methanation rate is not strong, we can see that an increased value negatively affects hydrogen conversion.

4.1.4 CO2 half Velocity Constant

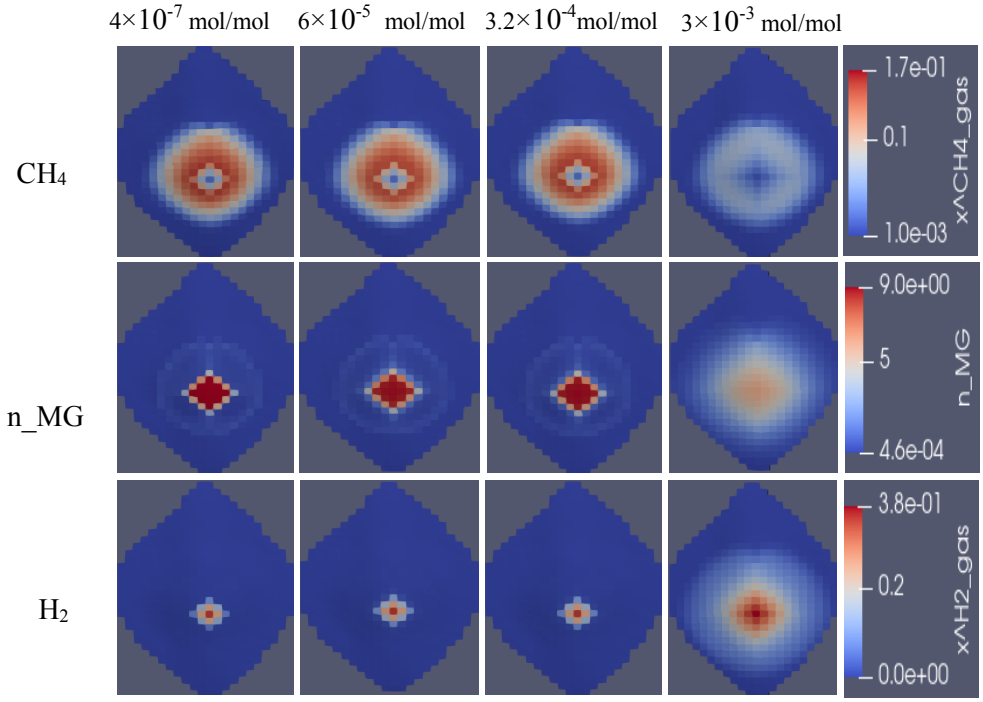

Figure 4-7 Concentration of generated gas as a function of CO2 half velocity constant

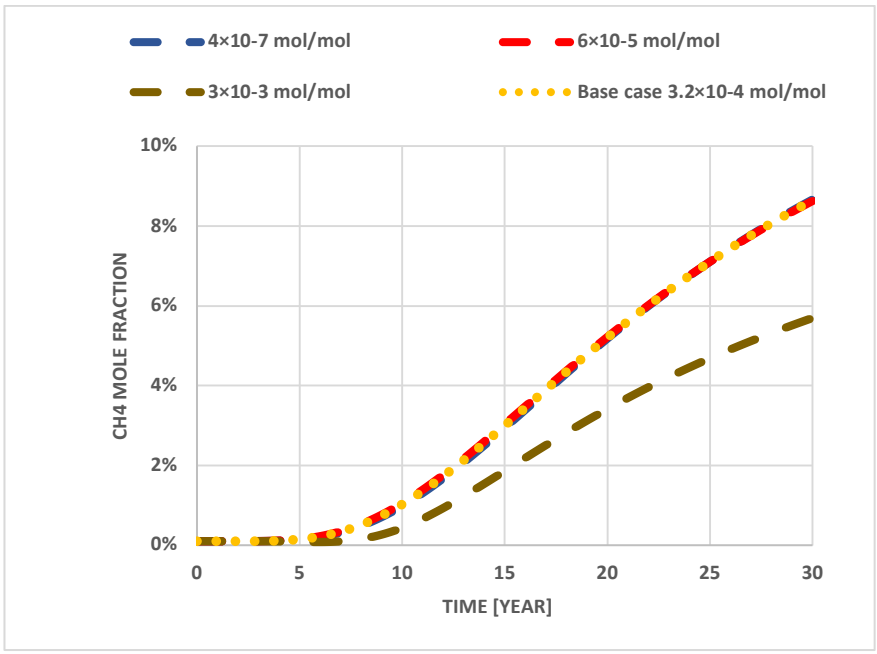

Figure 4-8 Concentration of generated methane over time as a function of CO_2 half velocity constant

The CO_2 half velocity constant is the concentration below which it is no longer consumed. The same observation as with the hydrogen half velocity constant can be made. The sensitivity is not strong either in this case but we can observe that a maximum of 9% conversion rate is

reached when the CO_2 half velocity constant falls to 3.2×10^{-4} mol/mol (base case) or below. As we could expect, the minimum conversion rate is reached when the value of the half velocity constant is the highest.

4.1.5 Injection Rate

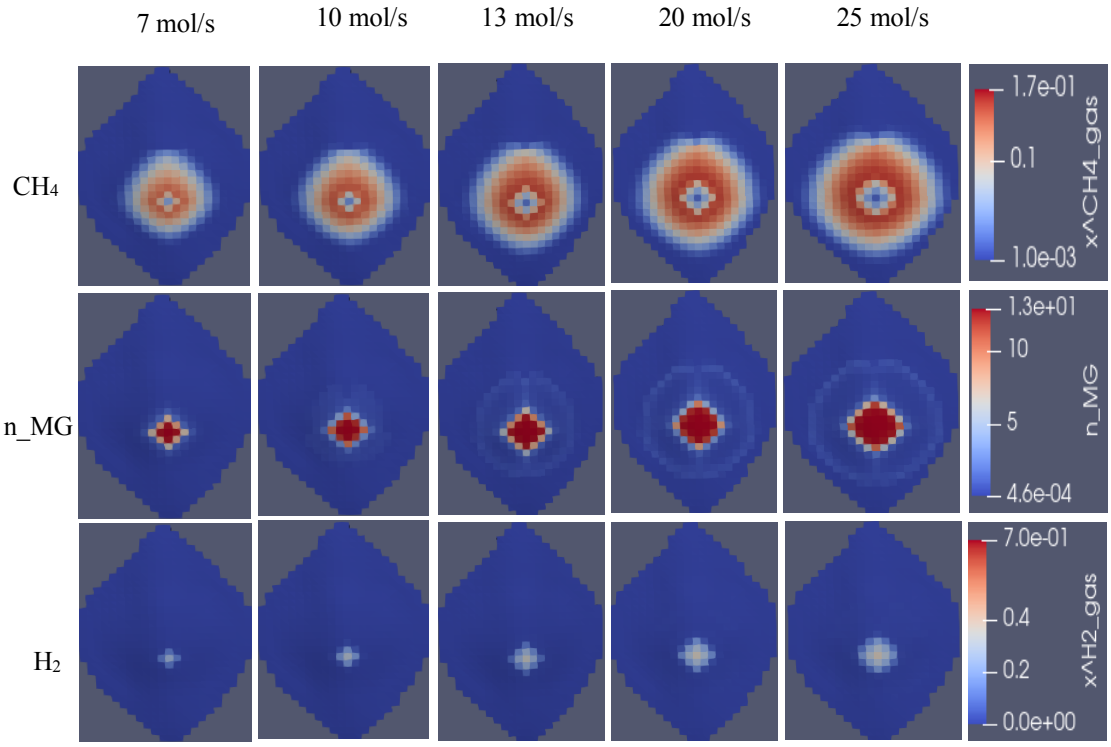

Figure 4-9 Concentration of generated gas as a function of injection rate

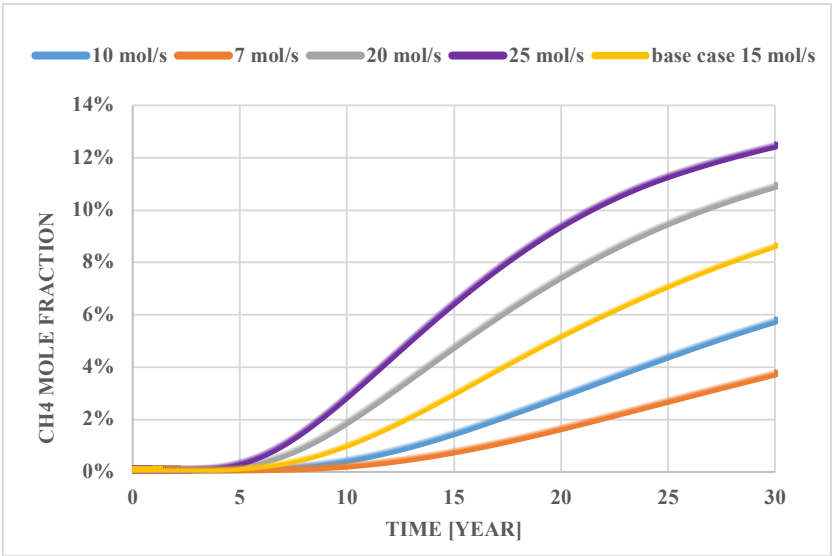

Figure 4-10 Concentration of generated methane over time as a function of injection rate

It looks like there is a positive correlation between injection rate and conversion rate. The 8% of methanation produced in our base case seems to be an average between the minimum

production of 4% and the maximum of 12% obtained respectively with injection rates of 7 moles/s and 25 moles/s. To optimize hydrogen production and consumption rates, it would then be advisable in this case to use an injection rate between 7 moles/s and 15 moles/s although the requirements may vary depending on the reservoir conditions.

4.1.6 Hydrogen Concentration in the Injected Gas

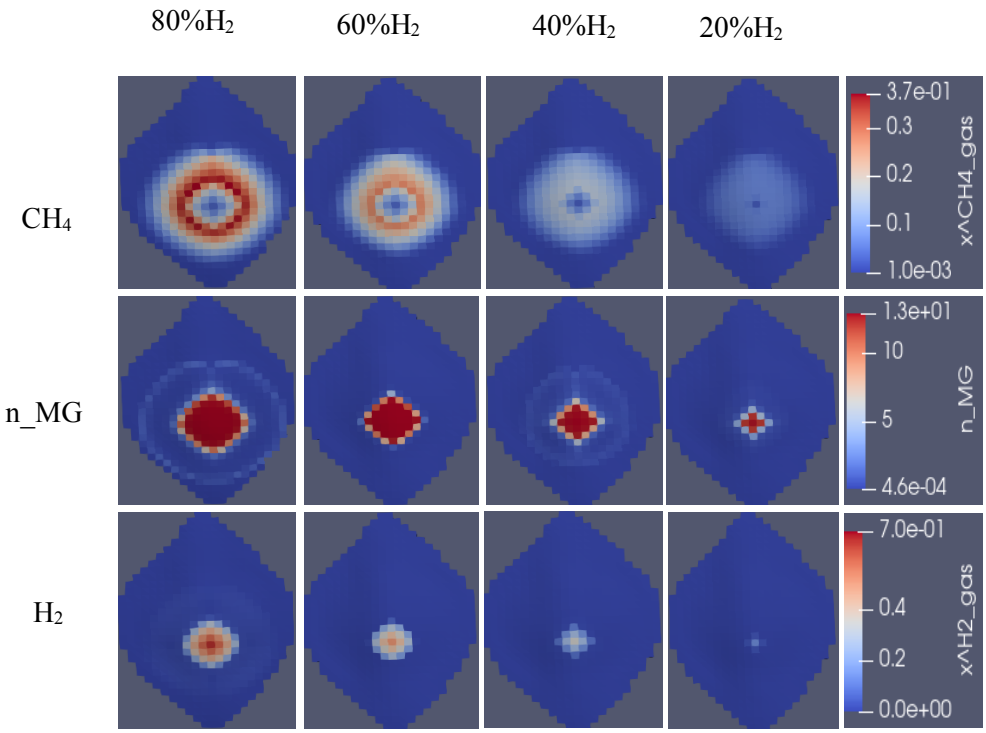

Figure 4-11 Concentration of generated gas as a function of H2 concentration in the injected gas

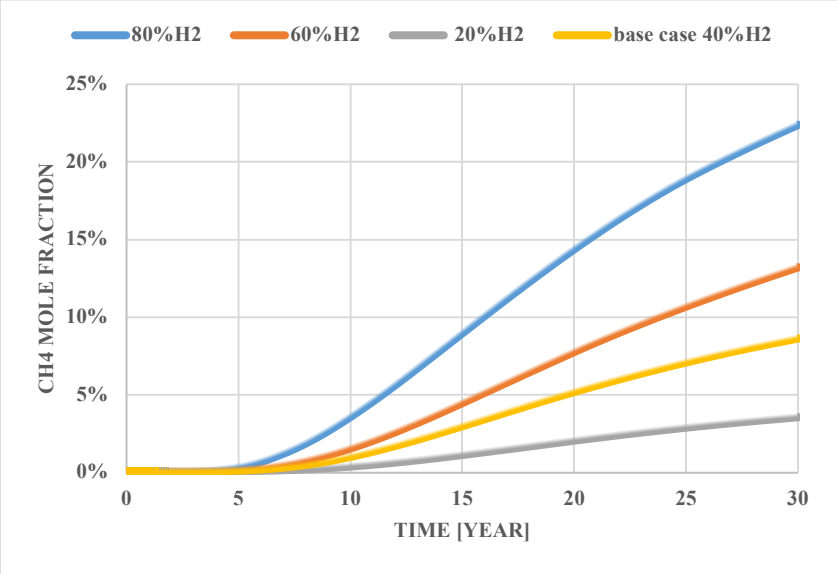

Figure 4-12 Concentration of generated methane over time as a function H_2 concentration in the injected gas

In this section, we are investigating the influence of the H_2 concentrations on the conversion rate. As we know, H_2 is the main substrate for microorganisms and we know that based on stoichiometry, 4 moles of H_2 and 1 mole of CO_2 are needed to produce 1 mole of methane. Under such conditions, we would expect the highest conversion rate when the percentage of hydrogen is the highest. The maximum production of methane of 24% is indeed recorded when we have an H_2 proportion of 80%. Then we observe that as we are reducing the H_2 concentration in the injected gas, less methanation is recorded. The influence of the H_2/CO_2 ratio of the recovery was studied in detail in the next chapter.

4.1.7 Well Spacing

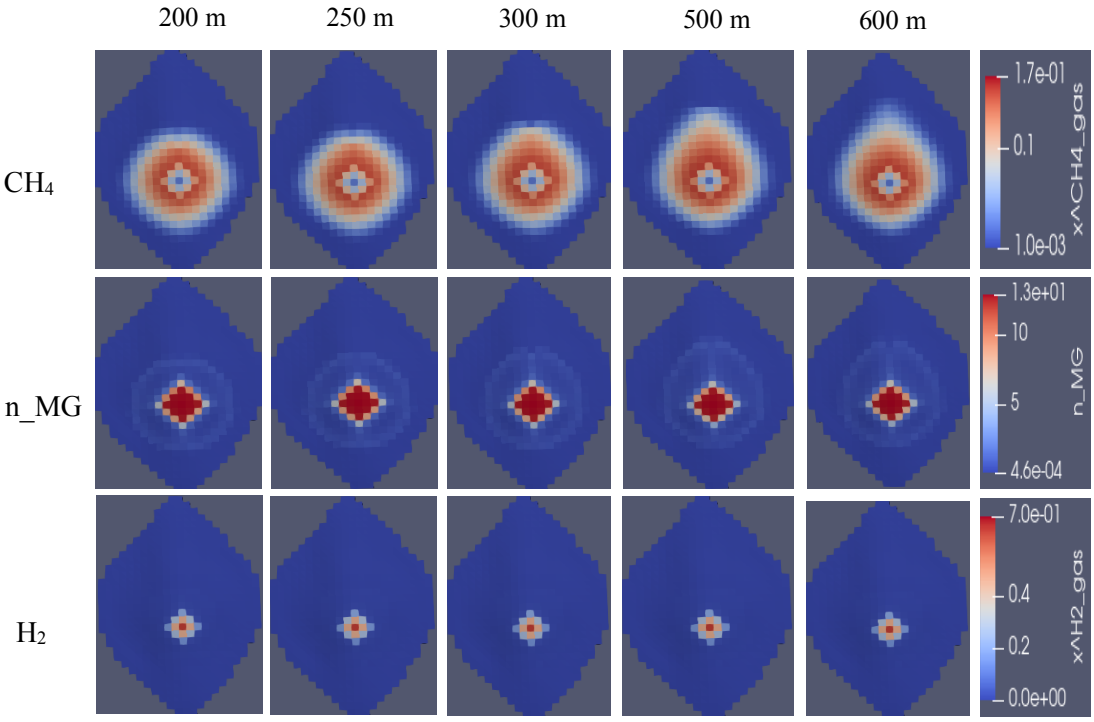

Figure 4-13 Concentration of generated gas as a function of well spacing

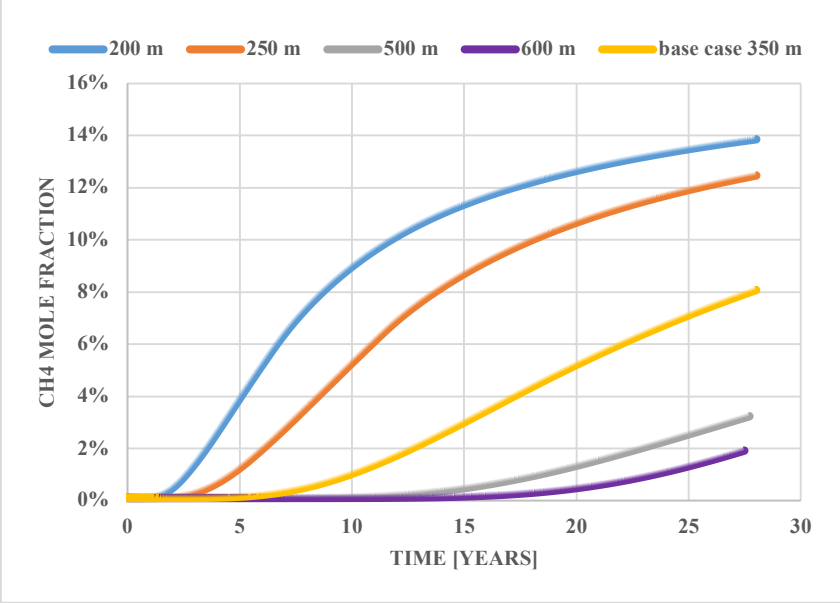

Figure 4-14 Concentration of generated methane over time as a function of well spacing

The objective in this part is to know which distance from the injection we can record the highest concentration of methane. It looks like the closer we are to the injector, the highest the methane concentration. This could be an indication that the reaction starts as soon as the gas is injected if the microbial concentration is high enough. A representation of the reaction that takes place and the gas front is shown in Figure 4-15

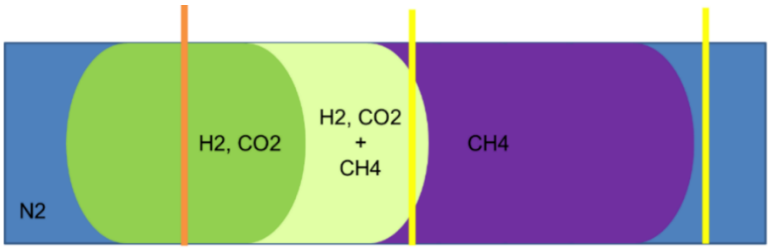

Figure 4-15 Design of underground methanation process, (Nikolaev, 2020)

4.1.8 Production Rate

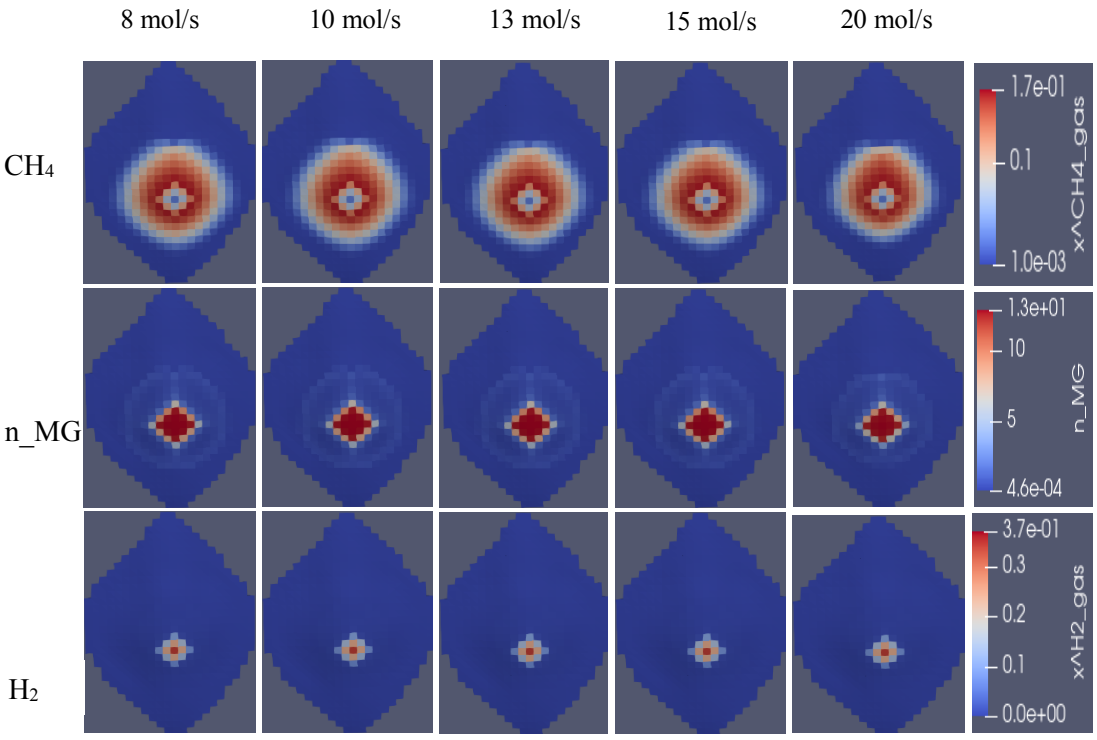

Figure 4-16 Concentration of generated gas as a function of production rate

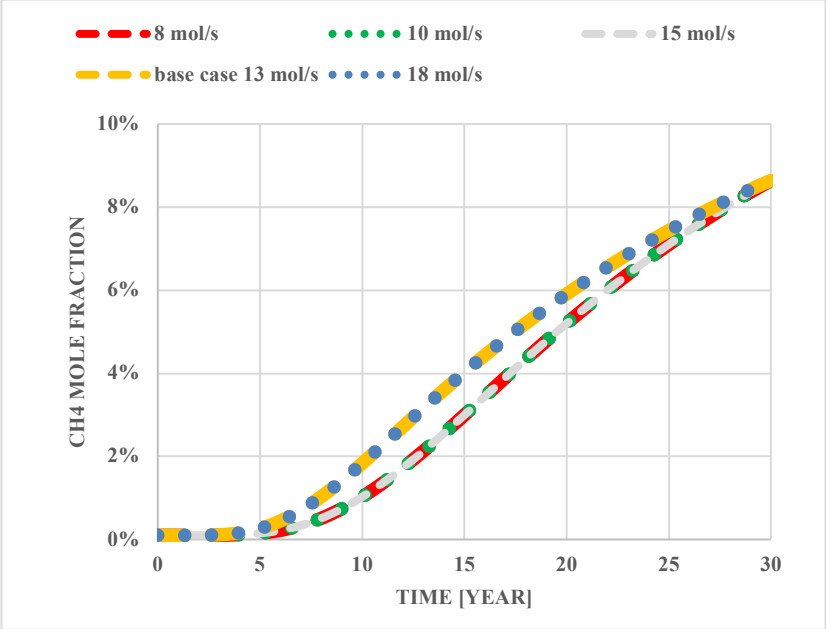

Figure 4-17 Concentration of the generated methane over time as a function of production rate

The production rate does not seem to play a big role in the concentration of methane recovered. We may expect a different outcome if we were to evaluate the cumulative amount of CH_4 but as we are only considering the methane concentration at the producer this result does not appear as surprising. Although there is a small gap in methane concentration in the middle of the simulation time, we observe that both production rates converge toward a methane concentration of 8% in the end.

4.1.9 Summary of the Sensitivity Analysis

A tornado plot is used to study the sensitivity of each parameter. A base case is considered with the parameters mentioned earlier:

- Microbial growth rate $\psi_m^{growth} = 3\times10^{-5}$ $[\frac{1}{s}]$
- Microbial yield = 2.5×10^{11} [/mol]
- Hydrogen half velocity constant = 1.1×10^{-7} [mol/mol]
- CO_2 half velocity constant = $3.2e\times10^{-4}$ [mol/mol]
- Distance between wells: 350 [m]
- Injection rate: 15 [moles/s]
- Hydrogen concentration in the injected gas: 40% H_2
- Production rate: 13 [moles/s]

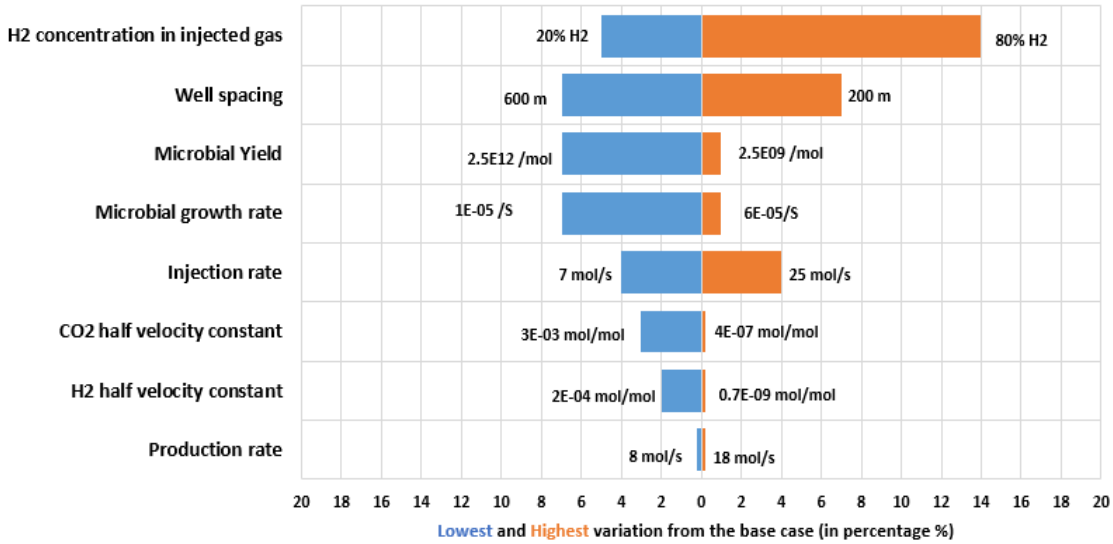

Figure 4-18 Tornado diagram summarizing the sensitivity analysis performed with different parameters

While evaluating each parameter, a sensitivity analysis is done by considering values, which are higher and lower than the ones in the base case. By doing so, we can find by how much the methanation rate differs from the one in the base case. Here in the x-axis, the zero values represent our base case, and the left and right values tell us how the methane concentration changes from the base case when a specific value for each parameter is considered.

From the tornado plot, it comes out that the concentration of hydrogen in the injected gas seems to be the parameter with a wider range of influence. This is logical, as H_2 is the main substrate in the chemical reaction leading to methanation. Up to 4 moles of H_2 and 1 mole of CO_2 are needed to produce 1 mole of methane, which means that the H_2 concentration is more determinant.

4.2 Hydrogen Plume Migration and Coupled Bio-reactive Transport

In an H_2 injection operation, a key knowledge that one would wish to have is the gas saturation over space and over time. Hydrogen will likely be injected in the presence of a cushion gas and we might ask ourselves if this could influence the hydrogen plume migration. Furthermore, when hydrogen is co-injected with varying amounts of CO_2 and depending on the microbial activity (growth rate) it would be very important to know the saturation profiles of each gas throughout the injection period. Having this information gives us insights into the speed of the

conversion rate, the concentration of the different components at different locations, and therefore the best location for the placement of a production well.

4.2.1 The Initial Conditions

The reservoir has the same structure and properties as seen at the beginning of the first chapter. It has an initial pressure of 90 bars and is filled with N_2 as cushion gas. The injection rate is 15 moles/s and the injected gas is mostly composed of hydrogen with varying amounts of CO_2.

It is important here to keep in mind those proportions such as 80% H_2, 20% CO_2 injected only represent the proportions of those components in the injected gas. The gas is then injected into a reservoir that is initially fully saturated (100%) by nitrogen, which is the cushion gas. Under such conditions, the proportions that are shown in the graphs are the concentration of each component in the total mixture.

Furthermore, the values of microbial growth rate that we use here are the minimum and maximum values that we were able to obtain based on our sensitivity analysis. These values are therefore adapted to our input parameters (injection rates, injected proportions, reservoir conditions). That means that under different conditions, the minimum and maximum values could be different. Our goal in the subsequent studies is to evaluate how the gas concentration in the reservoir could evolve when microbial parameters are changed.

4.2.2 Injection scenario with 80% H_2 and 20% CO_2

We can observe that without microbial activity, since no reaction is taking place, we observe a gradual increase of the hydrogen and CO_2 saturation over time and space. The values of H_2 and CO_2 concentrations remain almost constant between 20 and 30 years of injection, which might be indicative of a steady-state condition. The concentration of nitrogen is decreasing over space and over time simply because it is being displaced by the other injected gases. The same observation can be made when the microbial growth rate is increased to a minimum of 10^{-5} /s, which is not enough to produce a significant amount of CH_4 as shown in Figure 4-19.

When the microbial concentration is increased to 2×10^{-5}/s, the methanation process becomes visible around 10 years after the start of the injection and steadily increases to 20% at the end of the injection period. The formation of methane is logically associated with consumption of H_2 and CO_2 whose concentrations after 30 years are much lower than in the case where microbial activity is absent. The results of the simulations can be visualized in Figure 4-19 where the evolution of the gas saturation of each component is shown.

At the 3×10^{-5}/s growth rate, the methanation process can already be observed after 5 years and significantly increases over time. One particular thing associated with a high microbial concentration is the formation of the peak for methane concentration. In this case, the peak is at 40% after 30 years of injection. This methane peak is naturally associated with a minimum concentration of H_2 and CO_2. In physical terms, the peak is represented by a ring structure of the methane plume as can be seen in Appendix A.

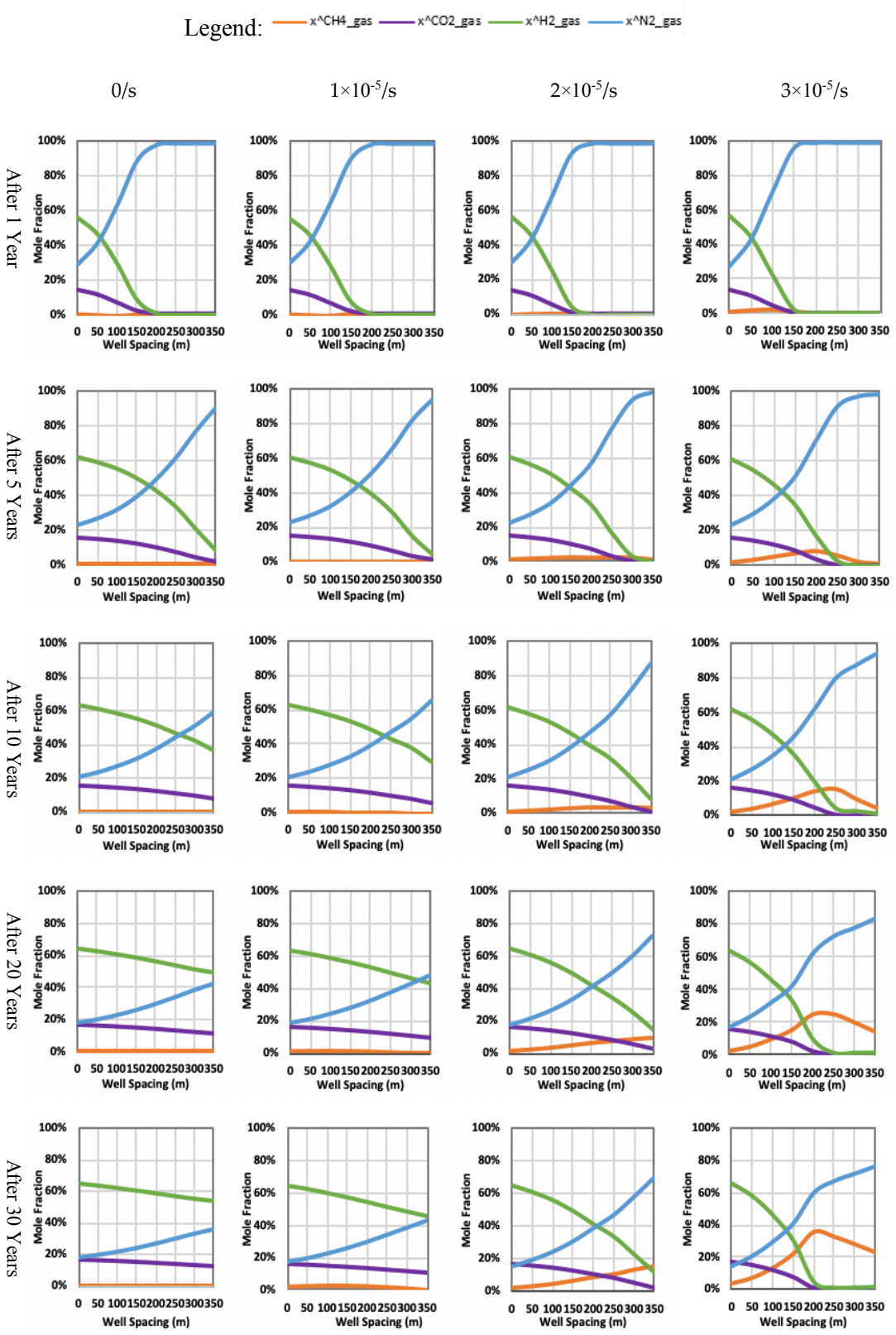

Figure 4-19 Gas concentration over space and time with 80% H2 and 20% CO2 injected

4.2.3 Injection Scenario with 95% H_2 and 5% CO_2

With only 5% CO_2 injected, it appears that the reaction takes place very slowly. The case without microbial activity is a simple injection scenario where the concentrations of H_2, CO_2 gradually increase over time, while N_2 is being displaced and therefore having its concentration increased over time. An almost steady-state condition is reached between 20 and 30 years of injection.

When the microbial growth rate is increased to 10^{-5}/s, we can see the reaction still does not take place and the case is similar to the one without microbial activity. This could be explained by the fact that the limited amount of CO_2 and the small growth rate hinders the methanation reaction.

Nonetheless, when we increase the microbial growth rate to 2×10^{-5}/s and 3×10^{-5}/s, some noticeable amount of CH_4 is visible after 20 years. This means that even with a limited amount of CO_2 when the microbial growth rate is high enough some reaction would take place. It is however important to mention that these rates are very low to pose a risk to the injected hydrogen. A global observation that we can make when 95% of H_2 is injected in combination with 5% of CO_2 is that a very limited amount of CH_4 can be expected.

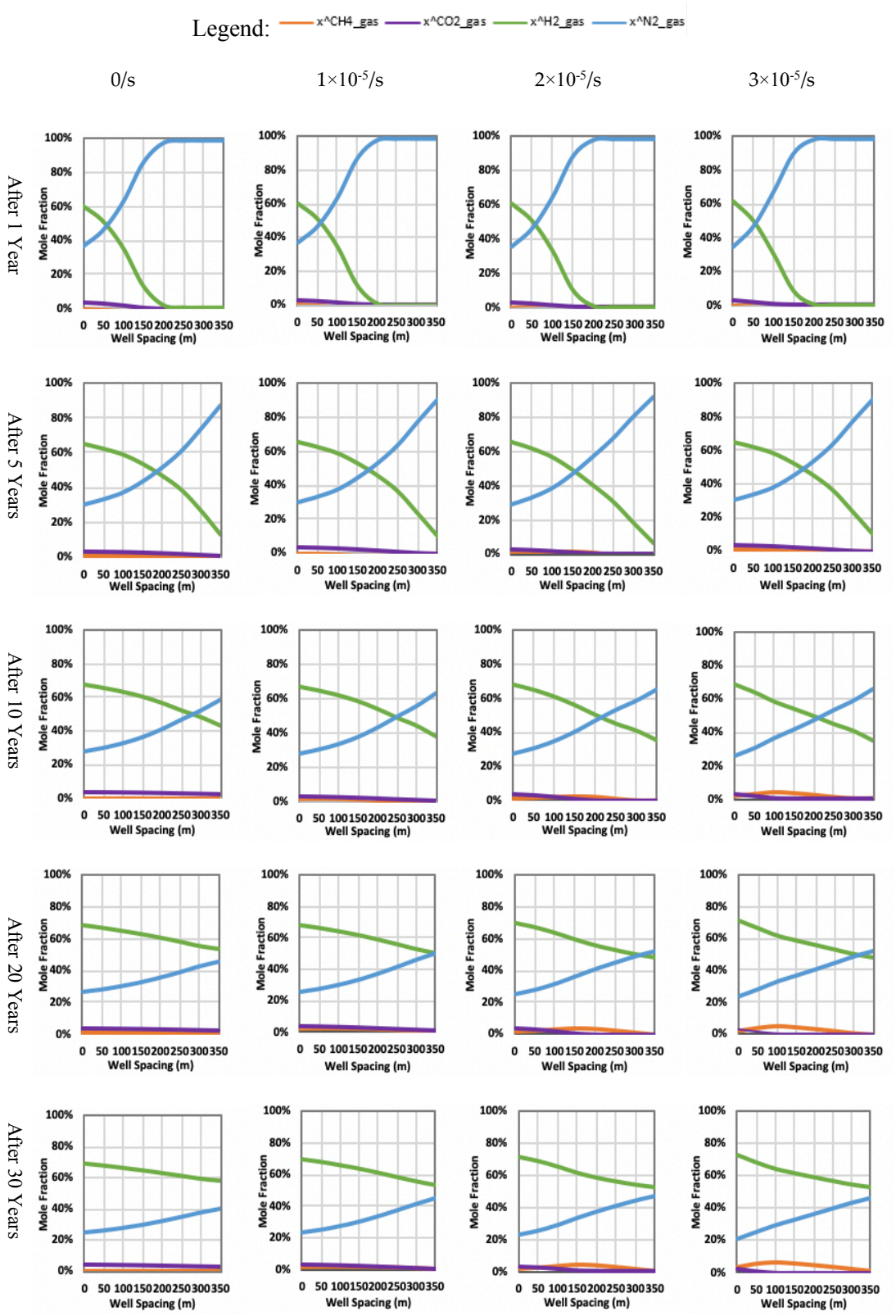

Figure 4-20 Gas concentration over space and time with 95% H2 and 5% CO2 injected

4.2.4 Injection Scenario with 75% H_2 and 25% CO_2

When the injected gas is composed of 75% H_2 and CO_2, as in the other cases no methanation occurs when the microbial growth rate is minimal. That situation can be accounted as a simple injection scenario with N_2 being displaced and H_2 and CO_2 having their concentration increased over time.

When the microbial growth rate is increased to 2×10^{-5}/s, we observe that the reaction takes place gradually and the methane concentration reaches almost 20% after 30 years. That is conjugated with a sharp decrease in the H_2 and CO_2 concentration.

When the microbial growth rate reaches a maximum of 3×10^{-5}/s, a peak of methane concentration is reached just as in the case with 80% H_2 injection. The peak is around 40% of methanation just like in the case with 80-20% scenario. This could be explained by the fact that the slightly smaller hydrogen mole fraction is compensated by the little increase in CO_2 amount, and therefore the proportions of generated methane are roughly similar. Because of the material balance, the peak of methane production is associated with a sharp fall in H_2 and CO_2 concentration.

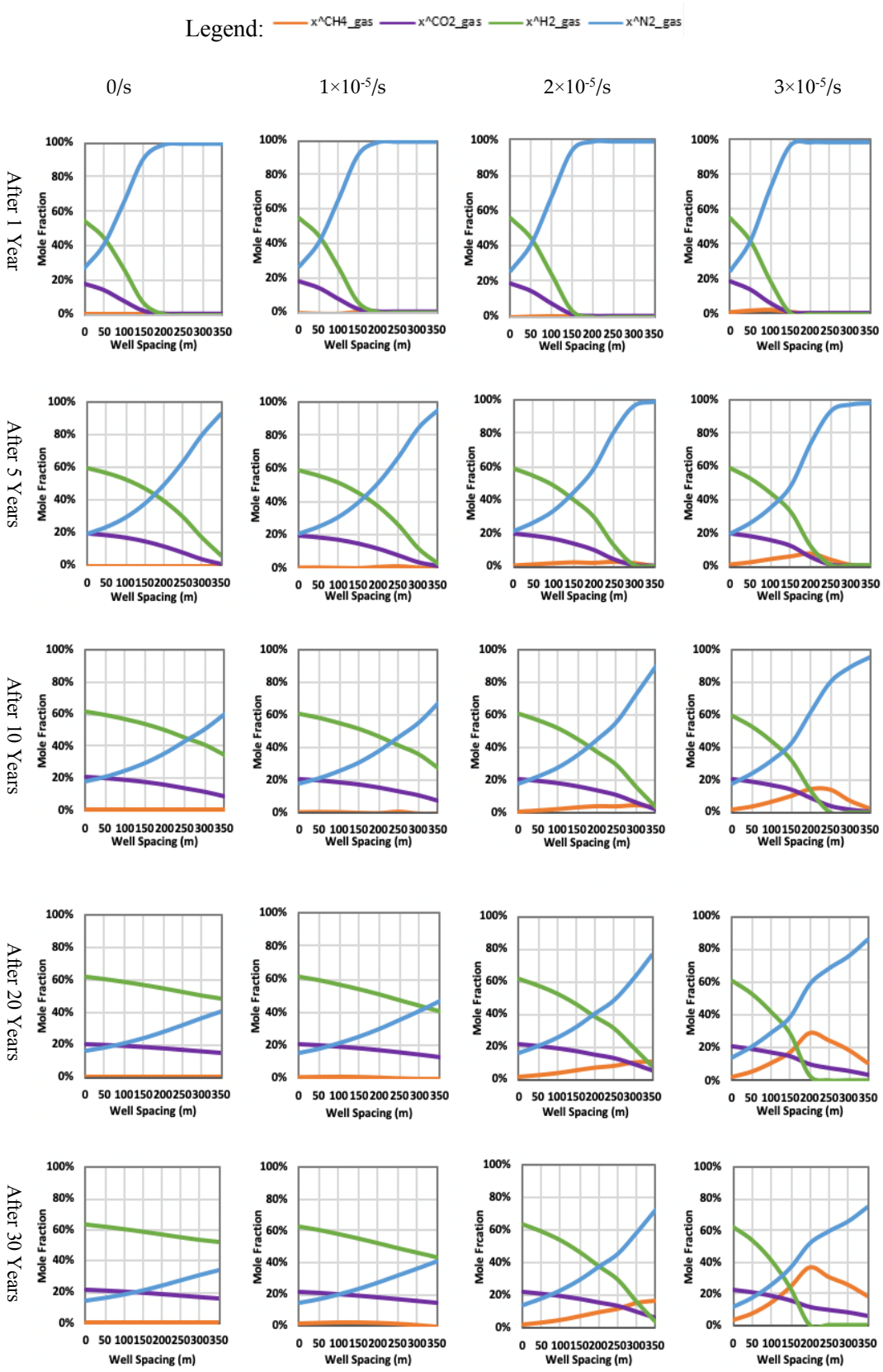

Figure 4-21 Gas concentration over space and time with 75% H2 and 25% CO2 injected

4.3 Estimation of Hydrogen Recovery based on Initial Conditions

In this section, we are considering 100% hydrogen with different cushion gases. The goal is to estimate the influence of the used cushion gas on the concentration of the gas recovered. This process was also studied under varying microbial growth. The combination of the 2 parameters which are microbial growth rate and employed cushion gas gave us an insight into which cushion gas provides the best recovery rates with hydrogen injection. The cushion gases that we considered in this section are nitrogen, carbon dioxide, and methane.

Nitrogen as we know has a higher density than hydrogen and can be used both in deep saline aquifers and in depleted oil and gas reservoirs as we have seen in (Felix Feldmann et al., 2016). The use of CO_2 as cushion gas sounds like an interesting prospect because it could become an opportunity to associate CO_2 and hydrogen underground storage. However, CO_2 is a substrate for methanogens as we know and we could ask ourselves whether an intense microbial activity combined with a large concentration of CO_2 would not cause a large-scale conversion of hydrogen. The results of our simulation shall enable us to bring an answer to such a question.

For the case of methane, we are trying to imitate a condition where the residual gas in the reservoir could serve as cushion gas. We know that depleted gas reservoirs can still possess high gas saturation. Although the density difference between hydrogen and methane is lower than the one between hydrogen and carbon dioxide or nitrogen, a stable displacement can be achieved if the injection rate is kept under control.

The initial conditions that we used in this section are shown in table 4-1

Table 4-1. Initial reservoir condition for hydrogen recovery estimation

Parameters	Value	Unit
Distance between wells	350	m
Total injection rate	15	moles/s
Injection gas composition	100% H_2	-
Total production rate	13	moles/s
Initial reservoir pressure	90	bars
Initial sulfate concentration in the water:	0.0018	-
Type of bacterial presence	Methanogens and sulfate reducing bacteria	
Cushion gas	N2 and CO2 and CH4	
Simulation time	30	Years

We varied the microbial growth rate between 0 and 3×10^{-5}/s to study the influence of microbial activity on the recovered gas concentrations. It is important to mention that in the cases where N_2 or CH_4 are used as cushion gases, we kept 5% of CO_2 in the reservoir to evaluate the potential for methane generation. It means N_2 or CH_4 represented 95% of the cushion gas. The microbial parameters are as follow:

- Microbial decay rate $\psi_m^{decay} = 2.3 \times10^{-6}$ $[\frac{1}{s}]$
- Microbial yield = 2.5×10^{11} [/mol]
- H_2 half velocity constant = 1.1×10^{-7} [mol/mol]
- CO_2 half velocity constant = 3.2×10^{-4} [mol/mol]

The results of our simulation are shown in Figure 4-22.

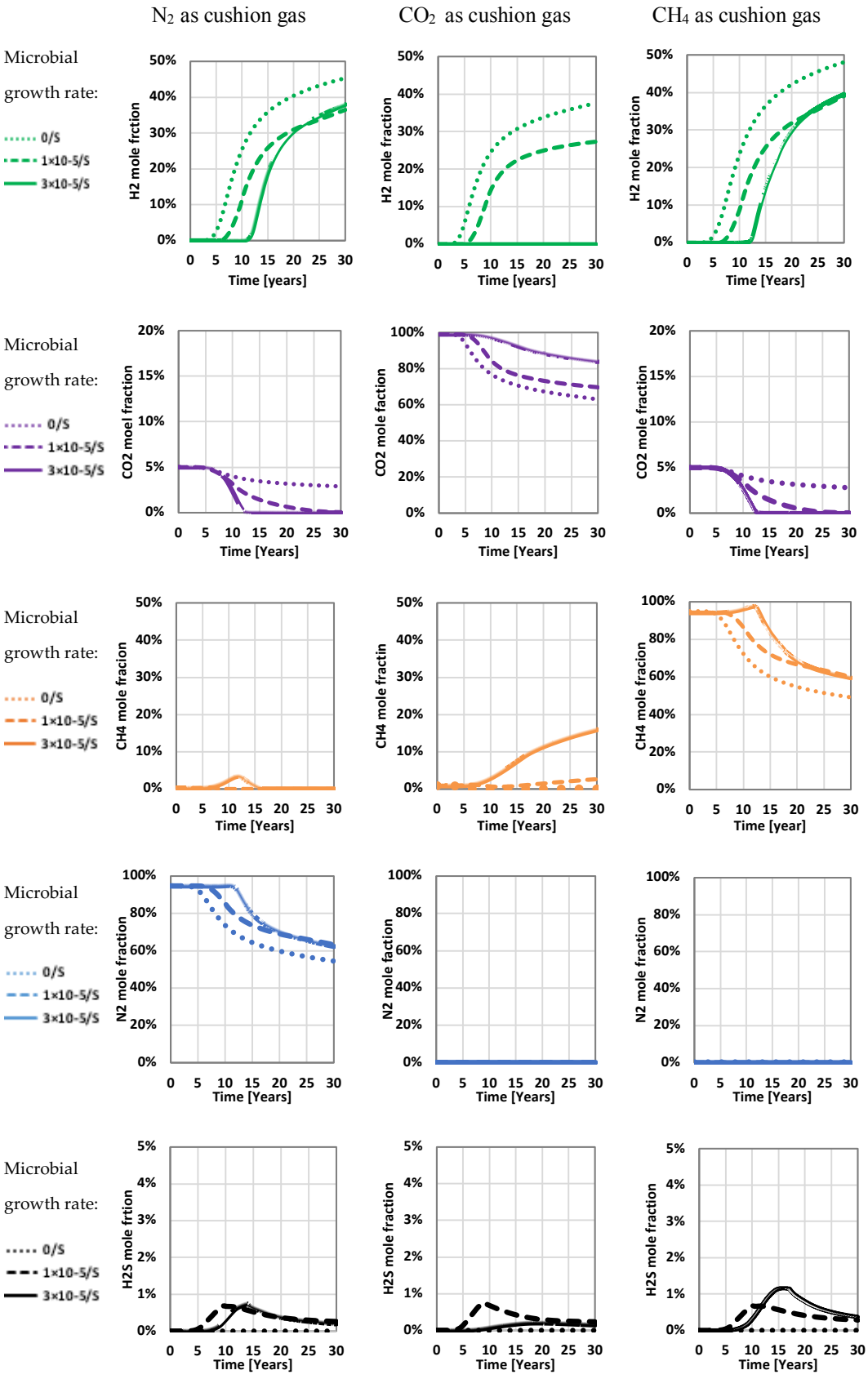

Figure 4-22 Gas mole fraction recovered

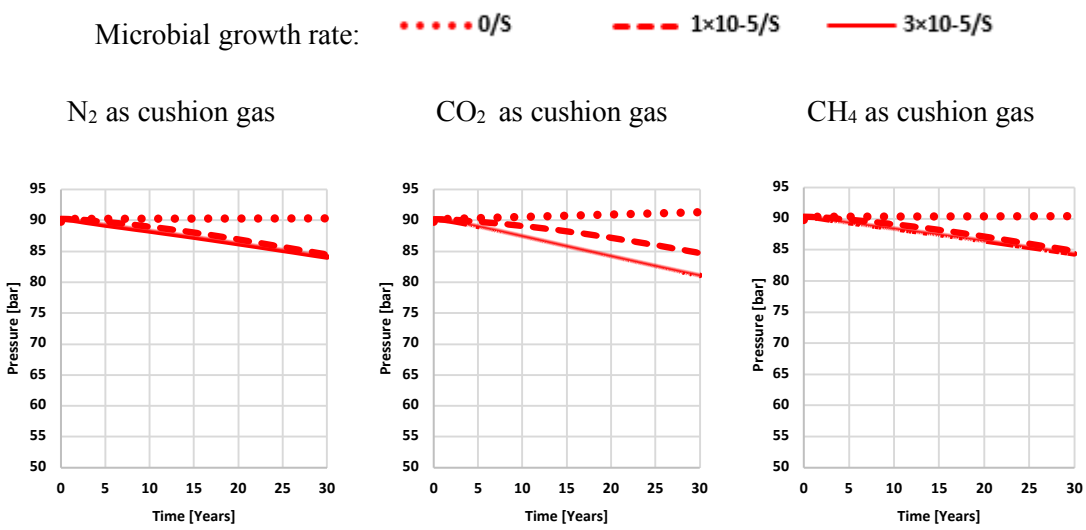

Figure 4-23 Pressure evolution with microbial growth rate with different cushion gases

When N_2 is used as cushion gas, we see that the microbial growth rate has a small influence on the mole fraction of gases recovered. Without microbial activity, the concentration of H_2 recovered at the production well is around 45% after 30 years of injection. Because no conversion is taking place, some of the CO_2 initially injected is still recovered (around 3% of the produced gas concentration). When the growth rate is increased to 1×10^{-5}/s, the concentration of H_2 falls to about 36% due to some of H_2 being converted into CH_4 and H_2S. When the microbial growth rate is increased to 3×10^{-5}/s, we see that although more methane is generated, the mole fraction of hydrogen recovered remains the same. This could be explained by the fact less H_2S is being generated as methanogenic bacteria could outperform sulfate-reducing bacteria under high microbial growth rate conditions. Another particular event is the delay of H_2 breakthrough at the production well. Indeed, without microbial activity, it takes about 3 years for H2 breakthrough to happen while it takes 6 years and 12 years for microbial growth rates of 1×10^{-5}/s and 3×10^{-5}/s respectively. As N_2 is continually pushed toward the production well and is not consumed, logically, its concentration increases with increasing microbial growth rate. The pressure remains constant in the case when no microbial activity takes place because no gas consumption takes place and the balance between injection (15 moles/s) and production (13 moles/s) could further explain this trend in pressure. However, in the presence of microbial activity, as hydrogen is being consumed and replaced by methane, which is a less mobile gas the pressure starts to decline over time.

When CO_2 is used at the cushion gas, we see that the amount of hydrogen recovered is drastically reducing over time with increasing microbial growth. From 38% molar fraction in the case without microbial activity, it falls to 28% with a 10^{-5}/s growth rate and it is consumed

when the microbial growth rate is raised to a maximum of 3×10^{-5}/s. This result does not come as a surprise because we know that H_2 and CO_2 are the required nutrients for methanation to occur and due to their abundant availability, it is logical that such consumption rates are observed. The conclusion that we can draw from this result is that the use of CO_2 as a cushion, although it may be an additional option for carbon storage depends on the microbial activity present in the subsurface as it poses a risk for the hydrogen injected. Without microbial activity, the pressure remains constant over time despite a slight increase, which could be explained by the fact that CO_2 has a high density compared to N_2 or CH_4. Nonetheless, as consumption occurs with increasing microbial activity and with the produced methane being less mobile than the injected hydrogen we see that the pressure starts to decline over time.

When CH_4 is used as the cushion gas, the concentration of CH_4 in the production well is naturally high. However, we observe that such concentration is increasing with increasing microbial growth rate, which is indicative of the occurrence of methanation. Indeed, the methane concentration in the production well goes from 50% without microbial to 60% with both 1×10^{-5}/s and 3×10^{-5}/s. We might be led to believe that the reason why the methane concentration remains constant from 1×10^{-5}/s and 3×10^{-5}/s is that since the concentration of methane (cushion gas) is already high in the reservoir the reaction rate will stabilize at some point from the kinetics point of view. The hydrogen concentration goes from 48% without considering microbial activity to 40% in cases with microbial activity. The CO_2 concentration goes to zero at the producer because its initial concentration is small and it is therefore totally consumed when microbial activity is taken into account. Again, the pressure trend remains globally constant without microbial reaction due to the balance between injection and production decline in the presence of microbial reaction as the hydrogen is being consumed.

Figure 4-24 represents the concentration of the dissolved components over time and with different values of microbial growth rate. One common observation for the dissolved mole fraction is that they are very small compared with the mole fraction of gases. We can observe that the concentration of dissolved components is related to the component density and its solubility in water. We know that CO_2 is the most soluble of all components here as it is the heaviest component, followed by H_2S, N_2, CH_4, H_2 in decreasing order of solubility.

The density difference could explain why the concentration of dissolved CO_2 is the highest a few years after the start of injection. For example, even in the case where N_2 and CH_4 are used as cushion gases, CO_2 remains the components with the highest dissolved concentration for many years after injection. Its concentration in the liquid phase falls to nearly zero after some time because it is a nutrient for the microbes. For methane, in the case where N_2 is used as a cushion gas, its dissolved concentration is globally small because of its low density but when CO_2 is used as cushion gas, the rate of methanation is increased to a level where the dissolved

concentration becomes more pronounced. For hydrogen, even though it is the lightest component, it starts being dissolved after some time as it is accumulating in the reservoir; this can be noticed in most cases. In cases where H_2S is generated, we can see that its dissolved concentration is noticeable as it reaches a peak in both cases. This noticeable concentration is explained by its higher solubility compared with components like H_2, CH_4, or N_2.

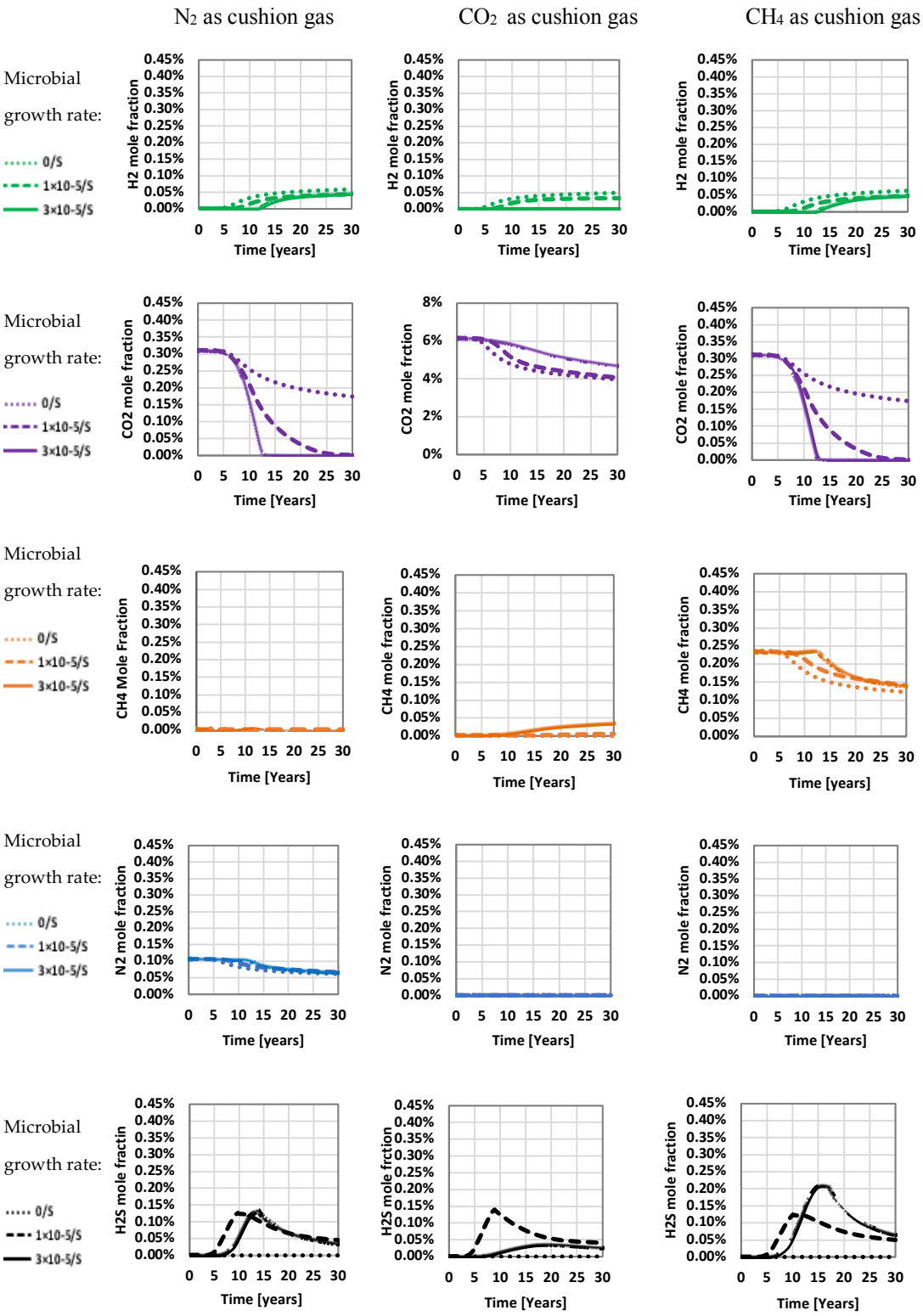

Figure 4-24 Dissolved mole fractions with microbial growth rate with different cushion gases

4.4 Effect of Microbial Growth on Porosity and Permeability

The microbial growth density is the parameter that determines the extent to which the rock physical parameters such as porosity and permeability could be impacted by biomass accumulation. To find out the discrepancy in microbial distribution and therefore in methanation rate between a heterogeneous and a homogeneous model, we simulated 2 different hydrogen injection scenarios by varying the injection rate and the injection composition and using both the homogeneous and heterogeneous models. The homogeneous model is the same as the one in the first chapter while the heterogeneous model has the properties shown in figures Figure 4-25 and Figure 4-26 :

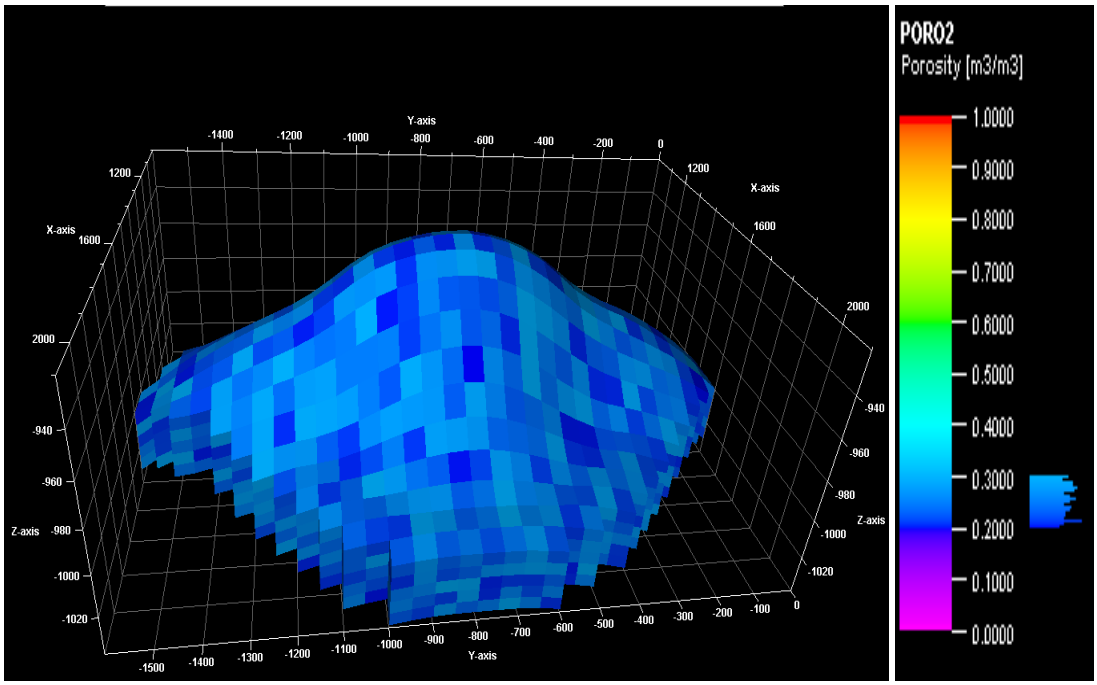

Figure 4-25 Porosity distribution of the heterogeneous model

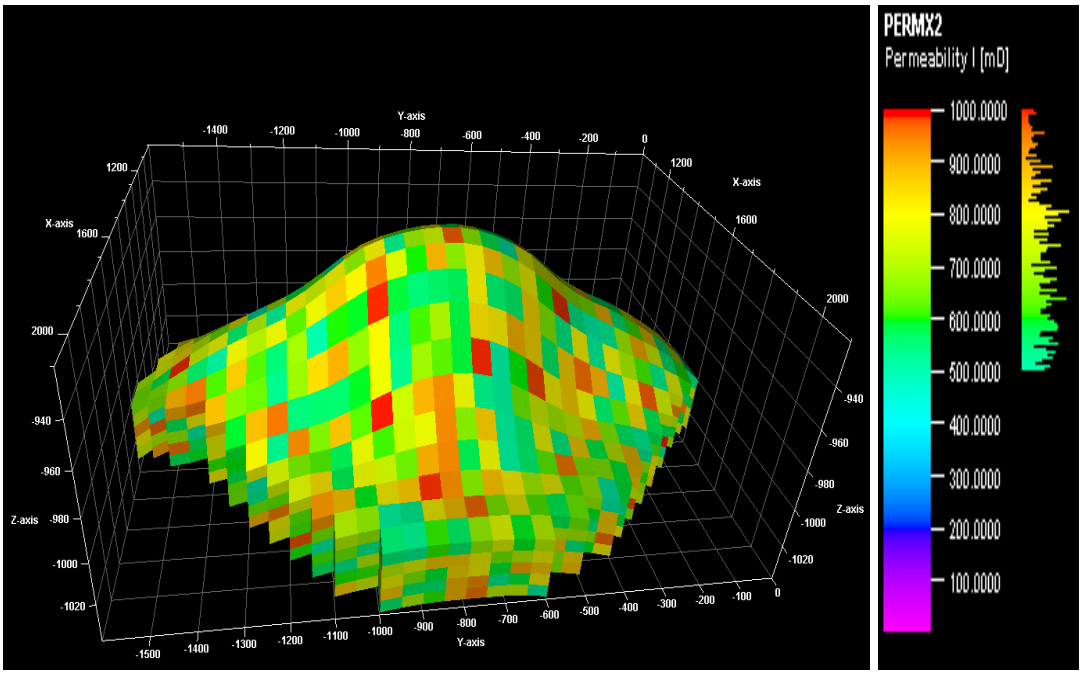

Figure 4-26 Porosity distribution of the homogeneous model

- Porosity range: 0.2-0.3
- Permeability range: 500-1000 mD

4.4.1 Effect of Heterogeneity on Biomass Distribution and Methanation based on Injection Rate

By varying the injection rate from 7 mol/s to 25 mol/s in both the homogeneous and heterogeneous models, the following results for the propagation of methane, microbial density, and hydrogen are obtained:

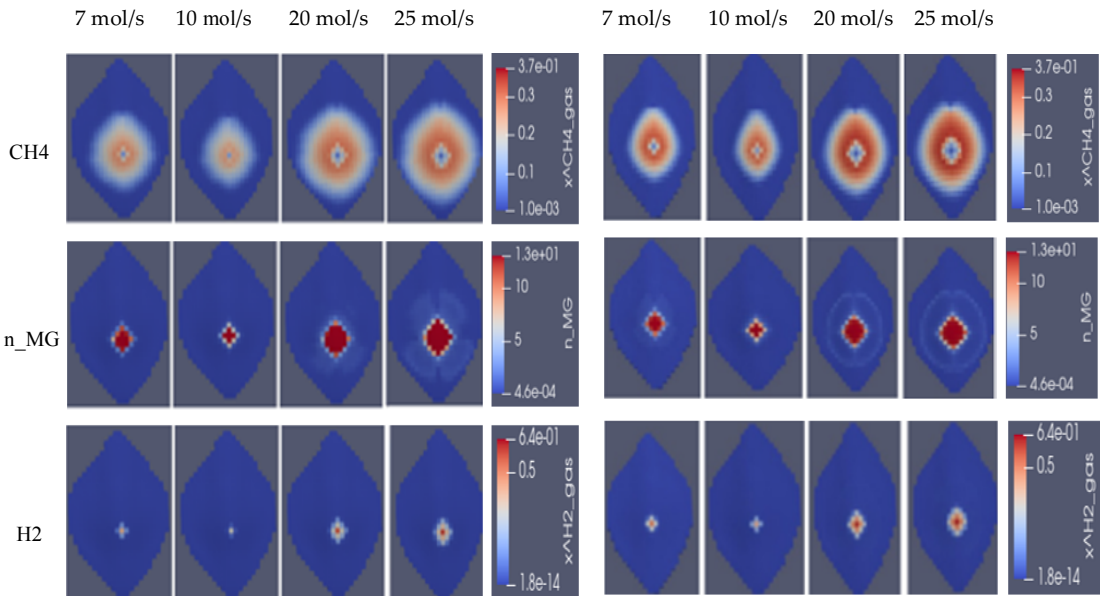

Figure 4-27 Concentration of generated gas based on injection rate in the heterogeneous model (Left) compared with the homogeneous model (Right)

4.4.2 Effect of Heterogeneity on Biomass Distribution and Methanation based on H_2 Injected Concentration

Using the same procedure we simulate the propagation of the different components by varying the hydrogen concentration in the injected gas

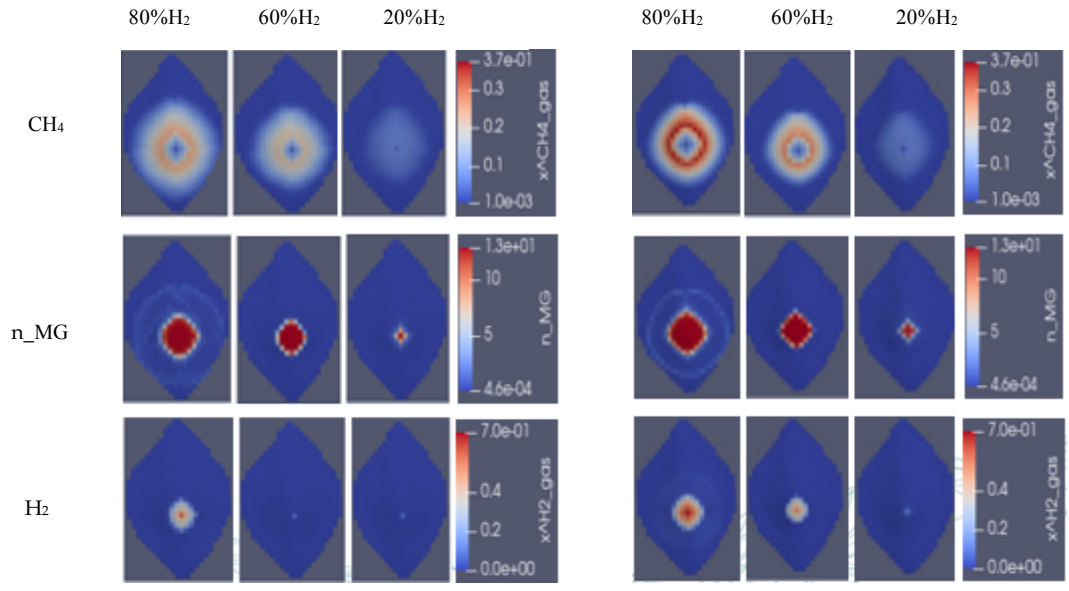

Figure 4-28 Concentration of generated gas based on H_2 concentration in the injected gas in the heterogeneous model (Left) compared with the homogeneous model (Right)

When analyzing the results obtained in both cases it appears to us that the homogeneous medium is more favourable for microbial growth. This is even more evident that the methane concentration is visibly higher in the homogeneous model when we analyze its propagation in both models. One explanation for this is that in the heterogeneous model, the cells will preferentially occupy the zone of higher porosity leaving other zones only partially occupied.

4.4.3 Average Microbial Density Evolution and Related Porosity and Permeability Reduction

The porosity reduction in Dumuxbio is defined by first considering an initial microbial density. In our case, the initial density is the n* as one of the parameters defined at the beginning of chapter 3. That value amounts to 6×10^{10} cells/m3 and was derived by averaging microbial density values obtained from the literature (Birger Hagemann, 2017). Over time with hydrogen injection, the microbial density increases, and that increase is shown by the dimensionless microbial density (n_MG). The dimensionless density shown on the scale is an indication of how many times the initial density has increased.

The volume of the biofilm was expressed in terms of porosity and the relation between the fraction of biomass volume and the porosity is given by :

$$V_{bfl} = 1 - \frac{\varphi}{\varphi_o} \quad \textit{(T. P. Clement et al., 1996)} \qquad \textit{(4-2)}$$

Where V_{bfl} is the pore volume fraction occupied by the biomass and $\frac{\varphi}{\varphi_o}$ is the ratio between the actual and the initial porosity.

The expression $\frac{\varphi}{\varphi_o}$ also represents the accessible porosity and can be written as:

$$\frac{\varphi}{\varphi_o} = 1 - V_{bfl} \qquad \textit{(4-3)}$$

As a result $Porosity\ reducion = 1 - \frac{\varphi}{\varphi_o}$ *(4-4)*

A simplified cell shape is assumed by considering a cell as a cylinder with a diameter and height of 1 µm plus two hemispheres with a diameter of 1 µm. Using these values the volume of a single cell is estimated to be around 7.85×10^{-19} m^3. This value can then be used to calculate the pore volume occupied by the microorganisms based on the evolution of microbial density. From the value of the volume occupied by microorganisms, a pore volume fraction is derived from which the porosity reduction can be determined.

The relationship between porosity and permeability is given by the Kozeny-Corman relationship (Martin Alberto Diaz-Viera & A. Moctezuma-Berthier, 2012):

$$K = C_k \frac{\varphi^3}{(1-\varphi)^2} \qquad (4\text{-}5)$$

Where C_K is a parameter related to the specific internal surface area of the pores in porous media.

The accessible permeability is the ratio between the actual permeability K and the initial permeability K_o and is therefore expressed as:

$$\frac{K}{K_o} = \frac{\varphi^3(1-\varphi_o)^2}{\varphi_o^3(1-\varphi)^2} \qquad (4\text{-}6)$$

Consequently $Permeability\ reduction = 1 - \frac{K}{K_o}$ (4-7)

At each time step in the simulation, the porosity and permeability values are updated and the porosity and permeability reduction can be calculated. The following graphs are the results obtained with an injection rate of 20 moles/s where hydrogen represents 40% of the gas injected along with CO_2 (10%) and nitrogen (50%). By selecting the cells around the injector, we can evaluate the average microbial density over time for both models and that can give us a numerical basis to evaluate the difference between the microbes' evolution in homogeneous and heterogeneous models. The values for porosity and permeability reduction are also obtained:

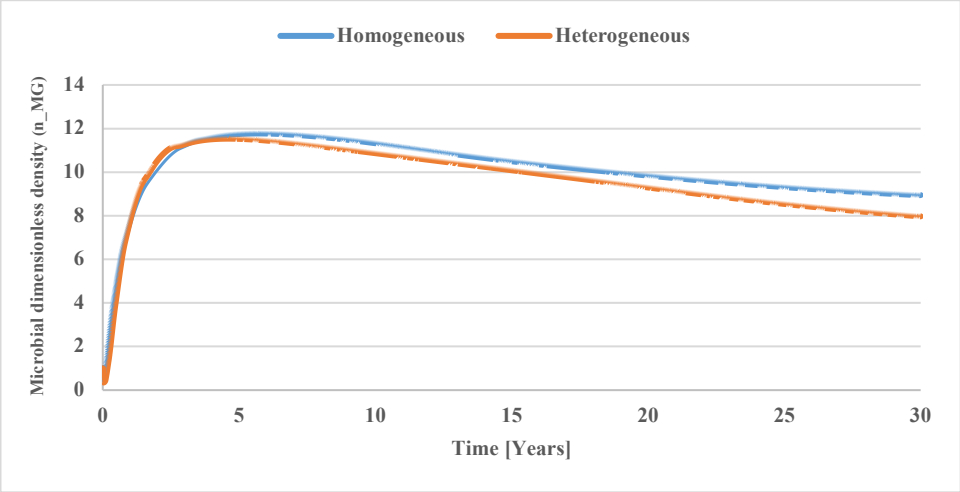

Figure 4-29 Evolution of microbial dimensionless density (the increase from the initial density) over time in the homogeneous and heterogeneous model

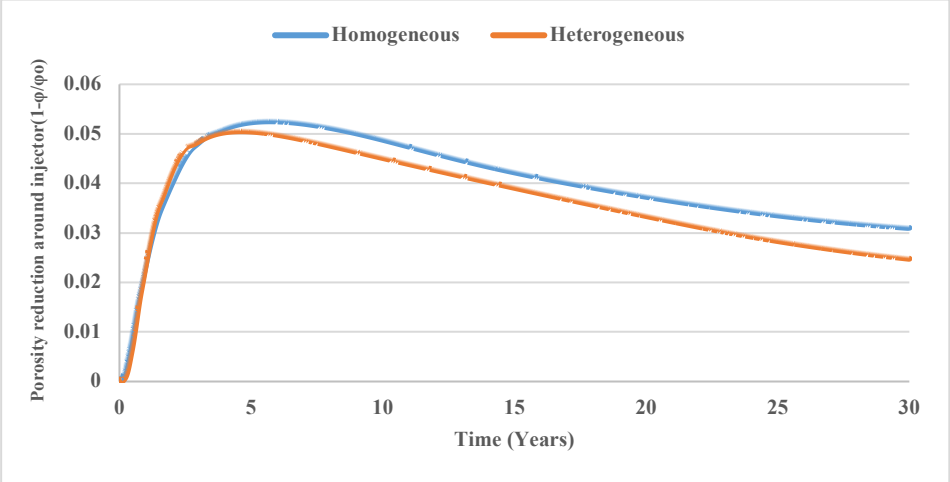

Figure 4-30 Porosity reduction over time in the homogeneous and heterogeneous model

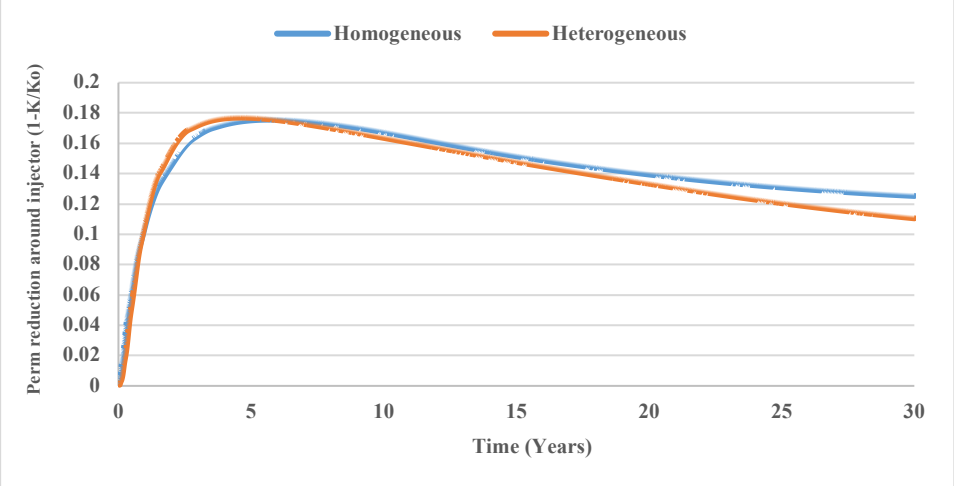

Figure 4-31 Permeability reduction over time in the homogeneous and heterogeneous model

We can observe from the graph that although the microbial densities are similar for the first few years following injection, the microbes grow faster in the homogeneous model because of the tendency of microorganisms to preferentially occupy the zones with high porosity. Consequently, the porosity and permeability reduction are on average more significant in the homogeneous model than in the heterogeneous model. The results above are from the cells around the injector which is the area where the microbial growth is more noticeable.

One particular observation that we elaborate on in the next point is the sharp increase in microbial density between 1 and 5 years followed by a slight decrease between 5 and 30 years. This translates into a sharp decline in porosity and permeability for 5 years followed by a small increase from 5 to 30 years as can be seen on the graphs above. To bring an explanation to this observation we evaluated the porosity and the permeability over space and over time and associate this with microbial dynamics.

4.4.4 Microbial Dynamics over Space and Time

In this section, since we want to compare the values of actual and initial porosity and permeability we would want to consider an initial value for both. For that reason, we would only consider the homogeneous porosity and permeability of 0.2 and 200 mD respectively. With an injection rate of 20 moles/s the following dynamics for microbial growth was observed :

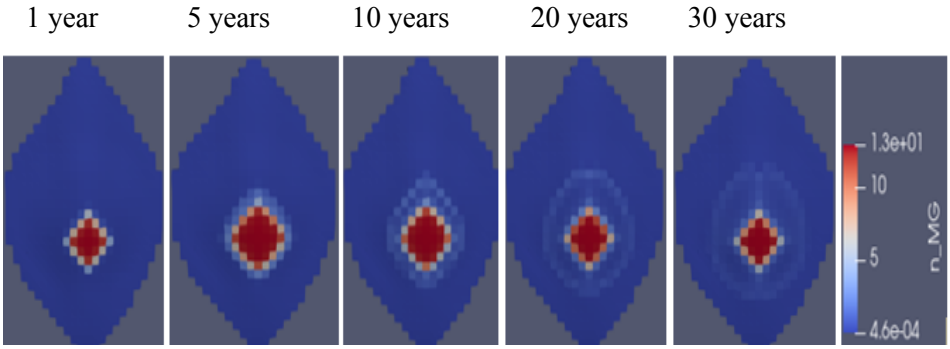

Figure 4-32 Temporal evolution of microbial density in the homogeneous model

From the figures above we can observe that the microbial density increases significantly after 5 years. From 5 to 30 years we observe a slight shrinkage of the microbial density back towards the injector at the centre of the grid. The reason why we believe that shrinkage occurs is that when we observe the profiles of porosity and permeability (Figure 4-33 and Figure 4-34) over space and time, especially in the interval between 100 m and 250 m, we notice that the values fall sharply between 1 and 5 years which is indicative of microbial growth phase. However,

when we consider the porosity and permeability profiles for 10, 20, and 30 years after injection we see that there is a continuous increase and the values are all higher than that of 5 years. The major explanation for this is the phenomenon of chemotaxis which states that microorganisms are attracted to zones where the concentration of nutrients is the highest. In order words as the microbial density increases competition for access to nutrients starts and a movement towards the injector where the concentration of nutrient is the highest is observed. That movement of microorganisms could explain why the porosity and permeability in some locations recover after a sharp decline. Consequently, that could explain why the lowest values for porosity and permeability are observed very close to the injector which in our case is the interval between 0 and 100 m.

Another phenomenon that could explain the recovery of porosity and permeability is the detachment of microorganisms from the solid phase. Indeed, with continuous injection, the pressure energy increases over time and such energy could lead to a forced movement of microbes towards the adjacent areas, reducing then the microbial density in the area around the injection well.

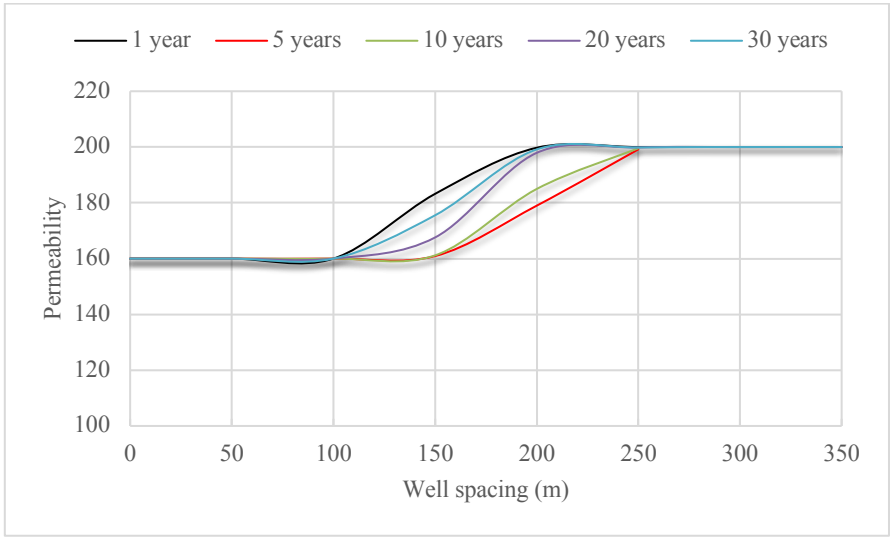

Figure 4-33 Temporal and spatial evolution of permeability

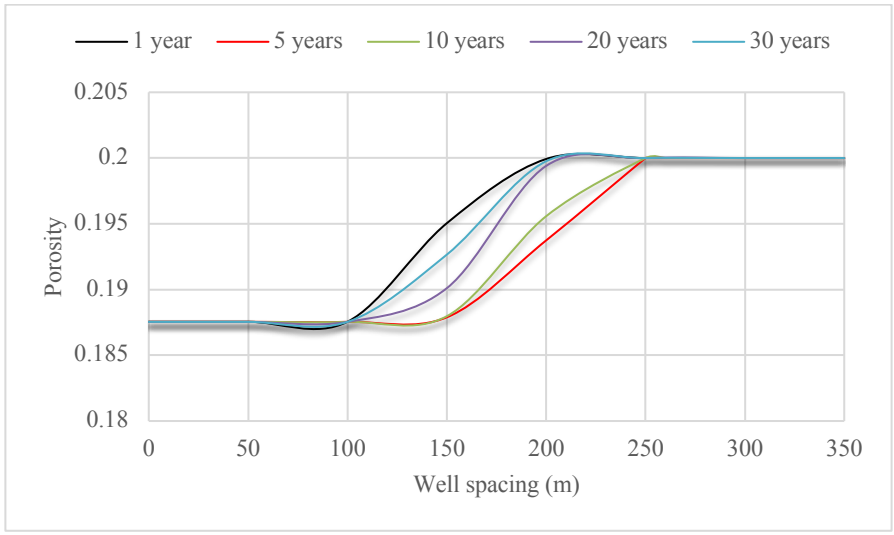

Figure 4-34 Temporal and spatial evolution of porosity

Chapter 5

Conclusion

5.1 Summary

Based on the sensitivity analysis that we conducted, it came out that the main parameter that determines the concentration of methane at the producer is the hydrogen concentration in the injected gas. This happens when the concentration of CO_2 co-injected or already present in the reservoir is enough to allow a reaction to take place. In most cases, we have investigated in this work and as can be seen in the second chapter, the CO_2 concentration should amount to at least a quarter of the hydrogen concentration. The second most influencing parameter is the well spacing. The sensitivity of the well spacing tells us the closer we are getting to the injector the highest the methane concentration; this could be an indication that the reaction takes place somehow shortly after the injection process.

When hydrogen is injected in combination with a varying concentration of CO_2, the extent to which microorganisms could disturb the hydrogen plume depends on the microbial growth rate. When the microbial growth rate is small, the saturation profiles for both hydrogen and CO_2 gradually increase until they reach almost steady-state between 20 and 30 years when the injected proportions are 80% H_2 – 20% CO_2 or 75% H_2 – 25% CO_2. The steady profile after 20 years is even more evident when the injected proportions are 95% H_2 – 5% CO_2. This is reflected in a constant profile of H_2 and CO_2 concentrations. However, when the microbial growth rate is raised to a certain level, the methanation reaction starts to take place and we can observe a significant drop in both H_2 and CO_2 concentrations. This is even more visible when the microbial growth rate is raised to a maximum value of 3×10^{-5}/s where a pick in methane concentration is observed at around 200 m from the injector.

The use of cushion gas especially for injection is important to avoid unstable displacement and ensure sufficient pressure is available in the reservoir for the reproduction stage. Nitrogen, CO_2,

and CH_4 can be used as cushion gases. It appears from our results that using methane as cushion gas provides the best hydrogen recovery at the producer probably because as it is the lightest of three, its capability to expand allows more mobility to take place in-situ. However, it has the lowest viscosity difference with hydrogen and we know that in a miscible displacement scenario, when the viscosity of the injected gas is a lot smaller than the displaced gas, viscous figuring may occur and the risk of unstable displacement will be higher. For the case of CO_2 as cushion gas, we have seen in this work that when the microbial growth rate is at a maximum value, most of the hydrogen injected might be converted into methane.

The concentration of the dissolved components in both cases reflects the difference in solubility levels in water between CO_2, hydrogen, methane, and H_2S. Indeed, when hydrogen and CO_2 are injected with the proportions 95% and 5% respectively, we noticed that the dissolved concentration of CO_2 remains the highest for many years because of its highest density compared to the other components. When it is used as a cushion gas, its dissolved concentration is even much higher than the other gases.

The microbial dynamics around the injector could cause a considerable reduction in porosity and permeability after many years of injection. The study of microbial dynamics teaches us that the first 5 years of injection are associated with an increase in microbial density around the injector. However, as the microorganisms are growing, there is an increasing competition for nutrients and a movement towards to injector where the nutrients are most abundant is interpreted. This causes a slight shrinkage of the microbial density, therefore a slight recovery of the previously lost porosity and permeability.

5.2 Future Work

It is known from (Heinemann et al., 2021) that geochemical in-situ reactions with minerals could consume part of the hydrogen injected. However, a quantitative assessment of the reaction products concentration is not well known.

The next thing we could investigate is the impact of the water produced during the methanation reaction by microorganisms on the rock hydraulic conductivity. We know that water is produced by methanogens along with methane during methanation, and one question we might ask ourselves is how the water influences the relative permeability of the gas phase (injected hydrogen).

Finally, concerning the hydrogen conversion rate, we could investigate scenarios of cyclic injection-production using a single well. In this work, we used two different wells, one as injector and the other as producer, so we could conduct another study with a single well and compare the conversion and recovery rates with what we have already.

Chapter 6

References

(n.d.).

Birger Hagemann. (2017). Numerical and Analytical Modelling of Gas Mixing and Bio-Reactive Transport during Underground Hydrogen Storage (PhD thesis).

C. Müller & T. Straube . (2016). How to do a Proper Cell Culture Quick Check.

Catarina R.Matos et al. (2019). Overview of Large-Scale Underground Energy Storage Technologies for Integration of Renewable Energies and Criteria for Reservoir Identification. *Journal of Energy Storage, 21*, 241-258. Retrieved from https://doi.org/10.1016/j.rser.2021.111481

Clement, W. P. (2008, February 2). *Writing and Thinking Well*. Retrieved July 13, 2016, from http://cgiss.boisestate.edu/~billc/Writing/writing.html

Curtis M. Oldenburg. (2003). Carbon sequestration in natural gas reservoirs: Enhanced gas recovery and natural gas storage.

Denis Nikolaev. (2020). Numerical simulation of Bio-reactive transport process (Master's thesis

E.M. Thaysen et al. (2021). Estimating microbial growth and hydrogen consumption in hydrogen storage in porous media. *Renewable and Sustainable Energy Reviews*, 111481. Retrieved from https://doi.org/10.1016/j.rser.2021.111481

F. Abe et al. (1999). Pressure-regulated metabolism in microorganisms. *Trends in Microbiology, 7*(11). Retrieved from https://doi.org/10.1016/S0966-842X(99)01608-X

Felix Feldmann et al. (2016). Numerical simulation of hydrodynamic and gas mixing processes in underground hydrogen storages. *Environmental Earth Sciences, 75*(16), 1165. doi:10.1007/s12665-016-5948-z

Heinemann et al. (2021). Hydrogen storage in saline aquifers: The role of cushion gas for injection and production. *International Journal of Hydrogen Energy*, 111481. Retrieved from https://doi.org/10.1016/j.ijhydene.2021.09.174

Holden JF et al. (2009). Abundances of hyperthermophilic autotrophic Fe(III) oxide reducers and heterotrophs in hydrothermal sulfide chimneys of the northeastern Pacific Ocean. *Appl Environ Microbiol*, 242-5. doi:10.1128/AEM.01462-08

Julien Mouli-Castillo et al.,. (2021). Mapping geological hydrogen storage capacity and regional heating demands: An applied UK case study. Applied Energy. *Applied Energy*, 116609. Retrieved from https://doi.org/10.1016/j.apenergy.2020.116348

Maier, Raina M. (2009). Soil, Water and Environmental Science. *Environmental Microbiology*, 37-54. Retrieved from https://doi.org/10.1016/B978-0-12-370519-8.00003-1

Martin Alberto Diaz-Viera & A. Moctezuma-Berthier. (2012). Dynamic porosity and permeability modification due to microbial growth using a coupled flow and transport model in porous media. *In book: Mathematical and Numerical Modeling in Porous Media: Applications in Geosciences*.

Neda Hassannayebi et al. (2021). Relationship between Microbial Growth and Hydraulic Properties at the Sub-Pore Scale. *Transport in Porous Media, 139(3)*. doi:10.1007/s11242-021-01680-5

Peter O Carden & L. Paterson. (1979). Physical, chemical and energy aspects of underground hydrogen storage. *International Journal of Hydrogen Energy, 4*(6), 559-569. doi:10.1016/0360-3199(79)90083-1

Sid Becker & Andrey Kuznetsov. (2014). *Heat Transfer and Fluid Flow in Biological Processes.*

Swiss Academic Software. (n.d.). *Citavi - Organize your knowledge. Reference management, knowledge organization, and task planning.* Retrieved May 24, 2016, from https://www.citavi.com/

T. P. Clement et al. (1996). Macroscopic Models for Predicting Changes in Saturated Porous Media Properties Caused by Microbial Growth. *NGWA. The Groundwater Association*. Retrieved from https://doi.org/10.1111/j.1745-6584.1996.tb02088.x

T.R.R Pintelon et al. (2012). The effect of biofilm permeability on bio-clogging of porous media. *Biotechnology and Bioengineering, 109*(4), 1031-42. doi:10.1002/bit.24381

Tek, M. R. (1989). Underground Storage of Natural Gas: Theory and Practice (N).

Waltraud Dilling & Heribet Cypionka. (1990). Aerobic respiration in sulfate-reducing bacteria. *FEMS Microbiology Letters, 71*(1-2), 123-127. Retrieved from https://doi.org/10.1111/j.1574-6968.1990.tb03809.x

Appendix A

Simulation results of gas plume migration

A.1 80% H2 and 20% CO2 injected

A.1.1 Microbial Growth Rate = 0/s

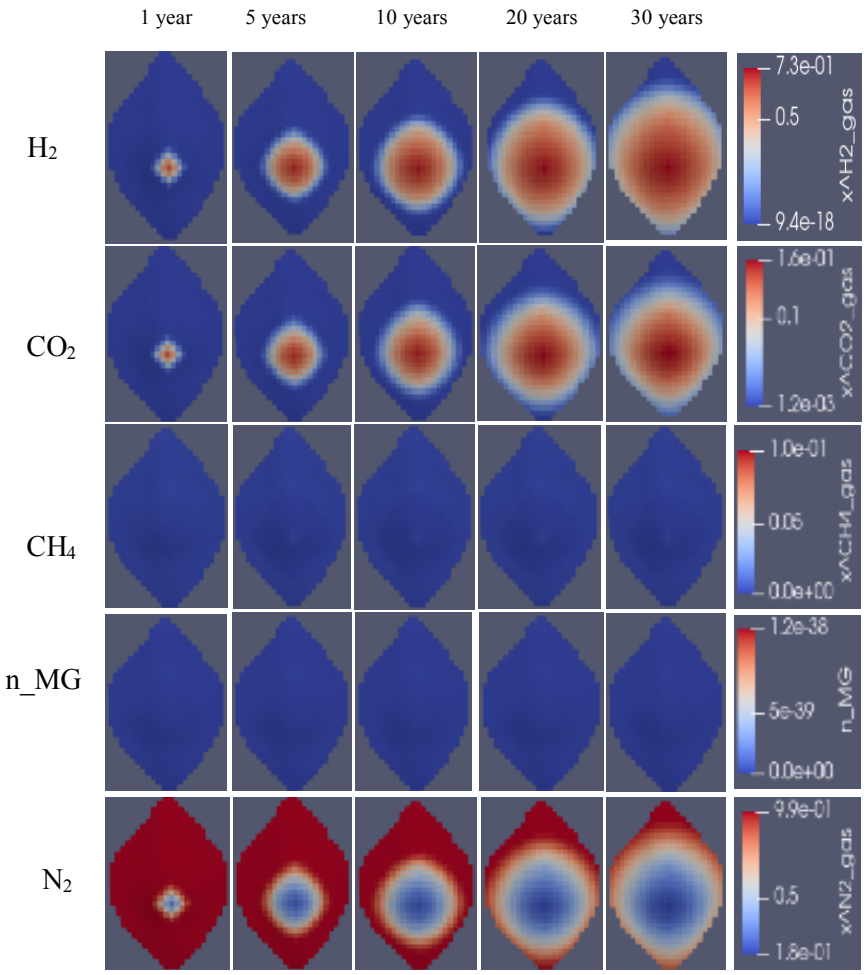

No reaction takes place when there is no microbial activity. The gas plumes expand largely.

A.1.2 Microbial Growth Rate = 1×10^{-5}/s

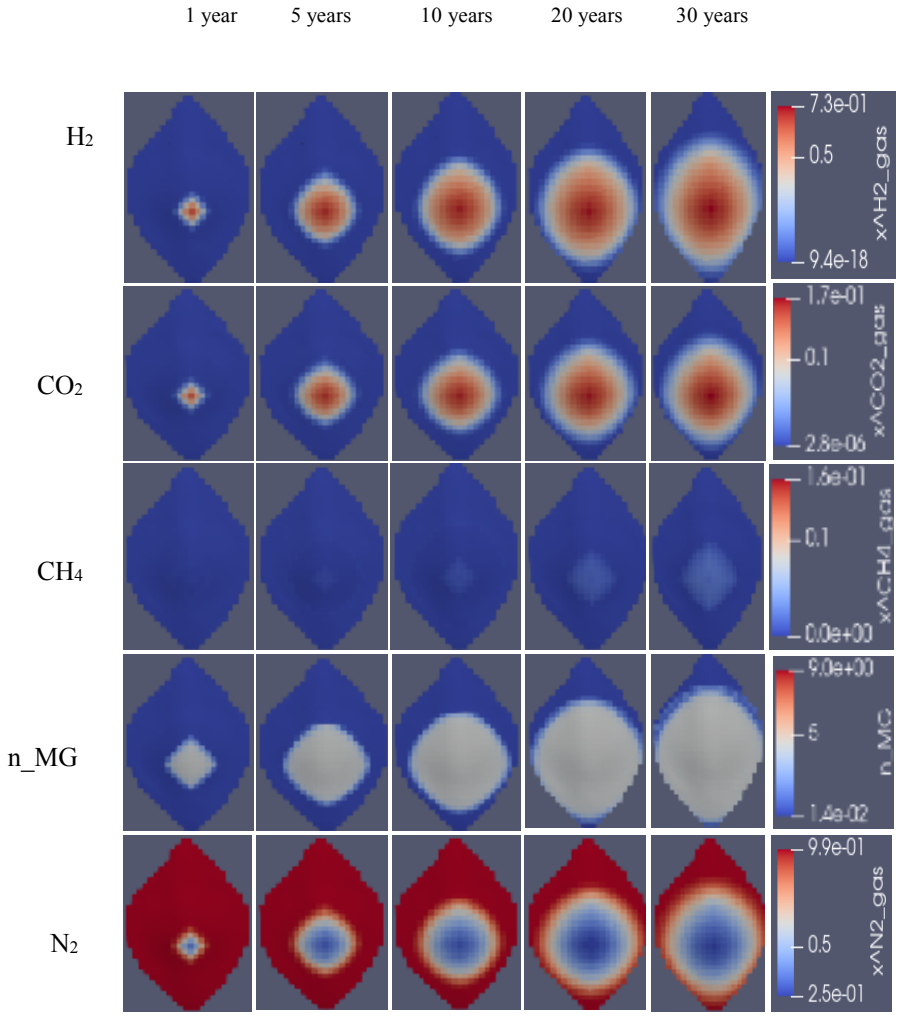

The minimal reaction takes place when the microbial growth rate is at a minimum value. In such a case, a little amount of methane is generated after several years of injection.

A.1.3 Microbial Growth Rate = 2×10^{-5}/s

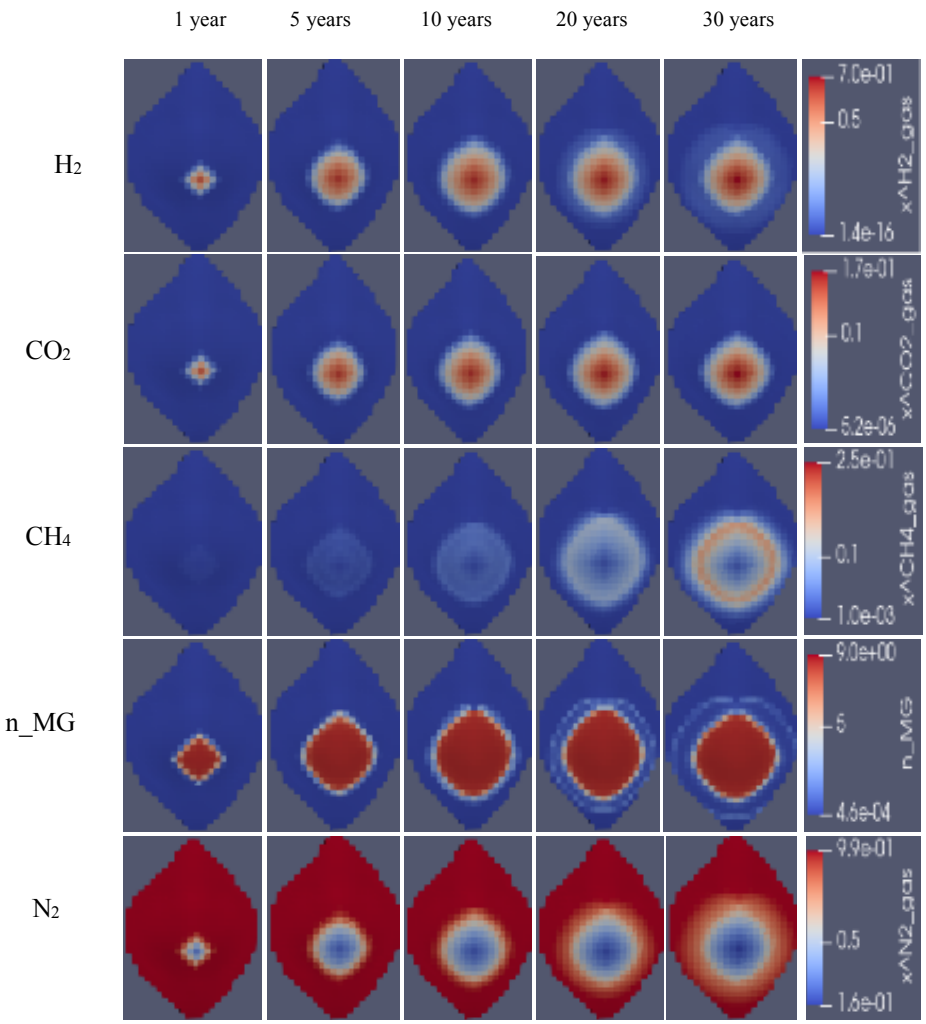

As the microbial growth rate increases, the conversion rate increases and methane generation becomes more evident. This is also reflected in a diminution of the hydrogen and CO_2 plumes propagation. With an increased growth rate, a high microbial density is observed as well.

A.1.4 Microbial Growth Rate = 3×10^{-5}/s

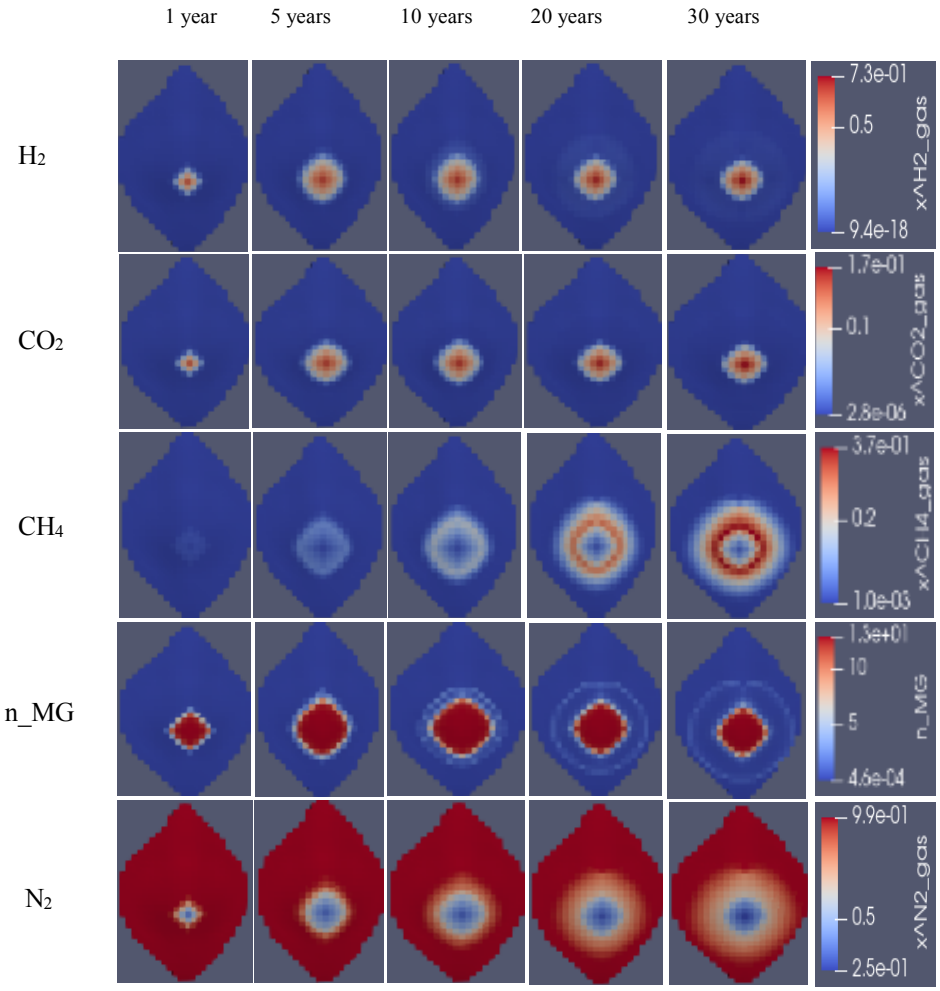

When the microbial growth rate is at a maximum value, most of the nutrients are consumed and the reaction rate is increased, which is reflected in a high concentration of methane after 20 years. As methane is a less volatile gas, the displacement of the cushion gas (N_2) occurs more slowly.

A.2 95% H2 and 5% CO2 Injected

A.2.1 Microbial Growth Rate = 0/s

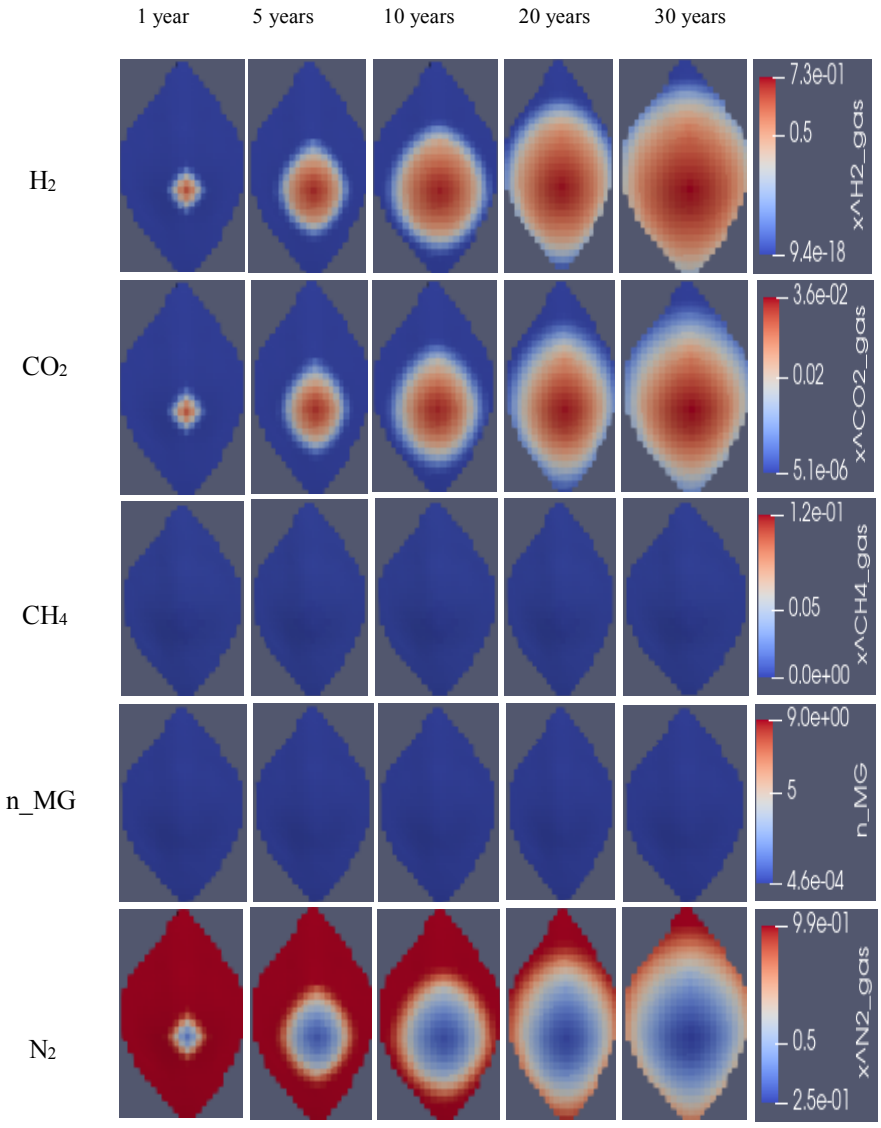

Without microbial activity, only an injection scenario is taking place. The cushion gas is effectively displaced by the injected gases which expand in the entire field.

A.2.2 Microbial Growth Rate = 1×10^{-5}/s

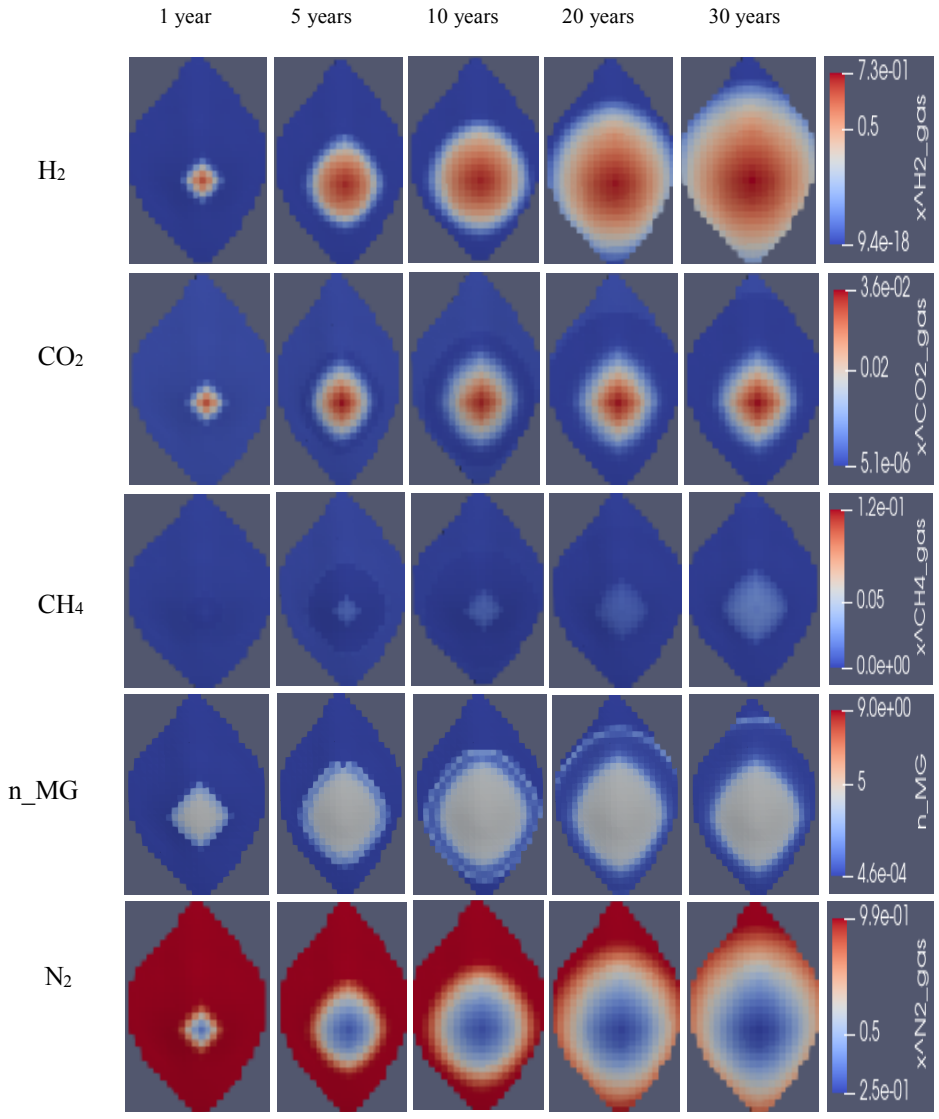

Only a little reaction takes place at a minimum growth rate. Although some methane is generated its concentration is very small and this is reflected both in the large expansion of the hydrogen plume and the small microbial density evolution.

A.2.3 Microbial Growth Rate = 2×10^{-5}/s

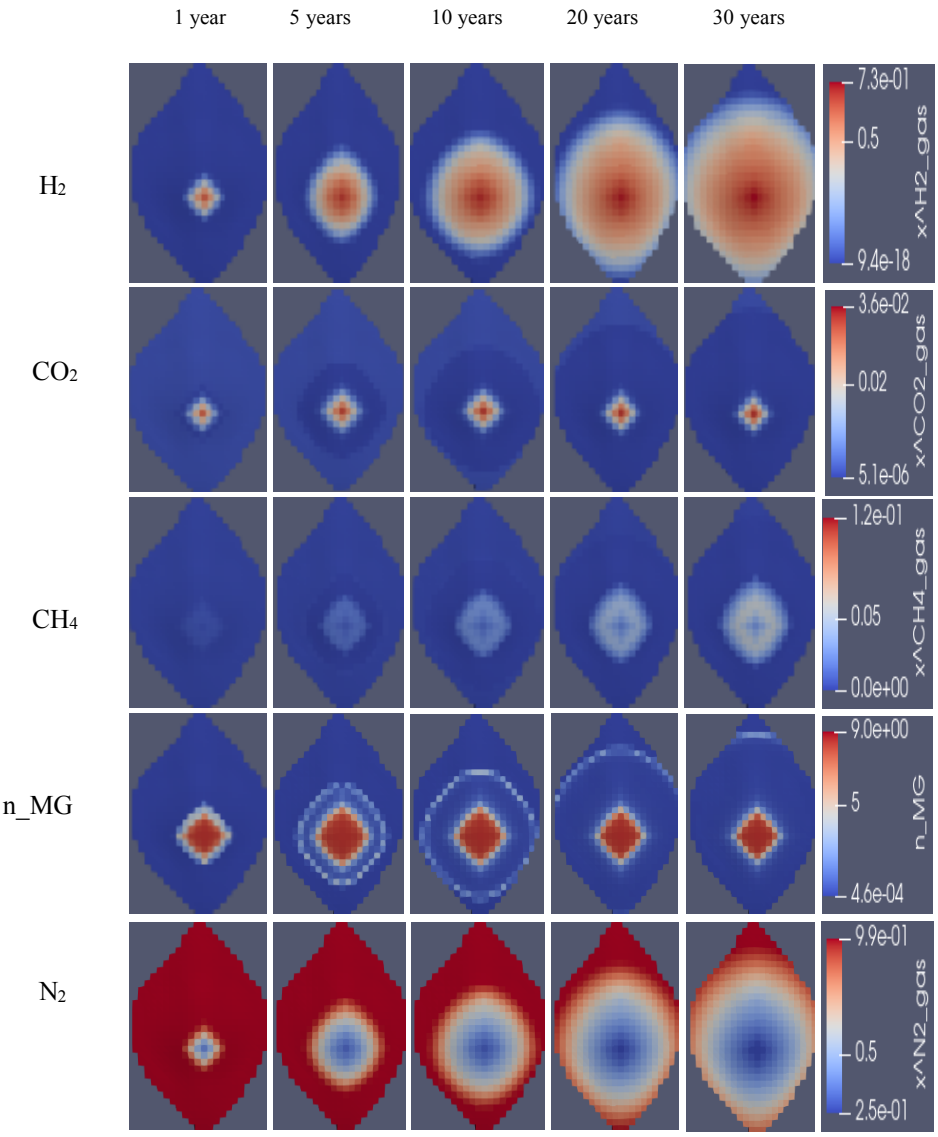

With an increased microbial growth rate, the reaction takes place but to a lesser extent in this case. The small concentration of the generated methane could be explained by the fact the amount of CO_2 is small as it amounts to only 5%.

A.2.4 Microbial Growth Rate = 3×10^{-5}/s

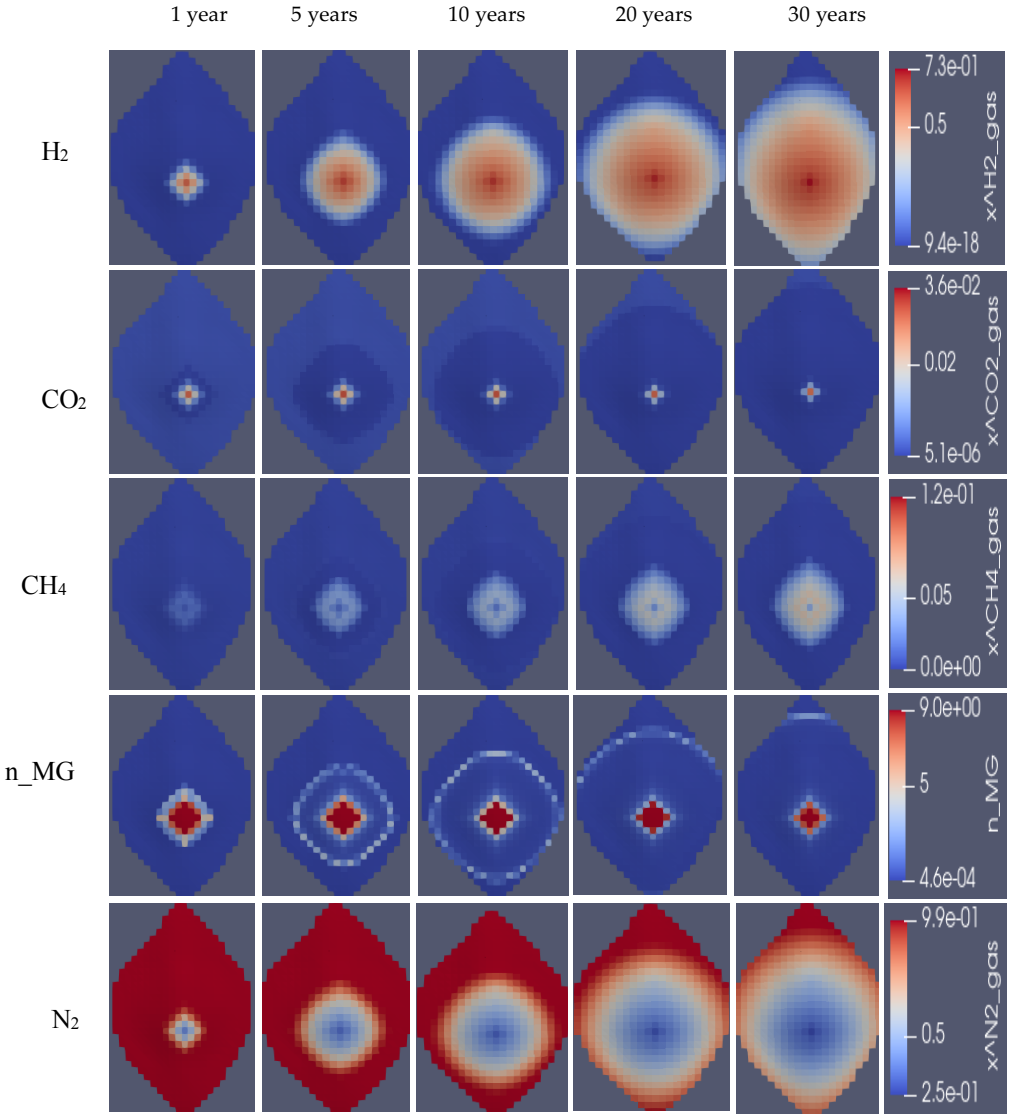

At a maximum value of the microbial growth rate, slightly more methane is generated but the concentration yet remains small since the amount of injected CO_2 is small.

A.3 75% H2 and 25% CO2 injected

A.3.1 Microbial Growth Rate = 0/s

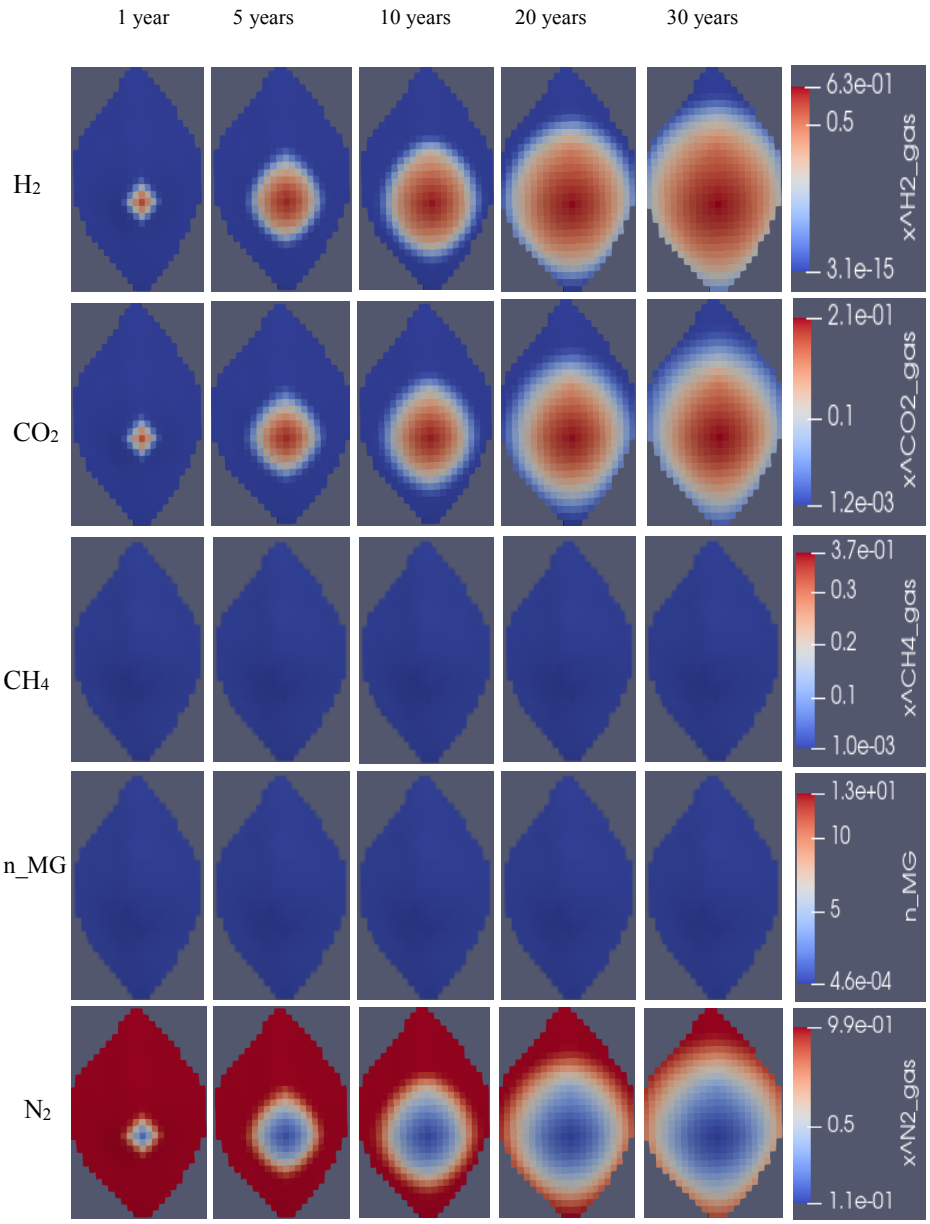

Unsurprisingly, no reaction takes place in the absence of microbial activity. The cushion gas is continuously displaced by the injected gases.

A.3.2 Microbial Growth Rate = 1×10^{-5}/s

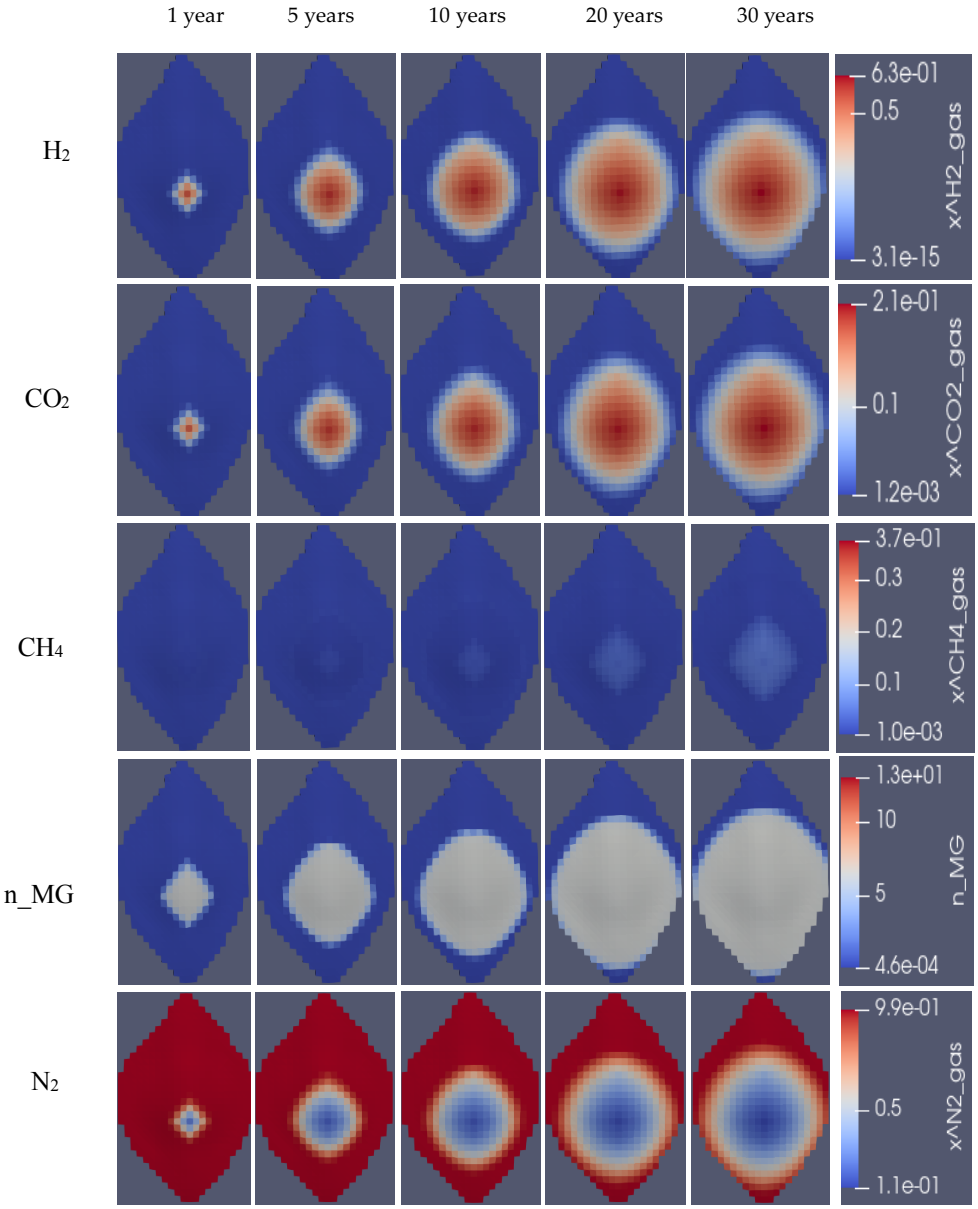

Like in the case with 80%H_2 - 20%CO_2, a little amount of methane is generated when the microbial growth is increased to a minimum level. Some nutrient consumption takes place, we notice it when we compare the gas plumes in this case with the ones without microbial activity (A.3.1).

A.3.3 Microbial Growth Rate = 2×10^{-5}/s

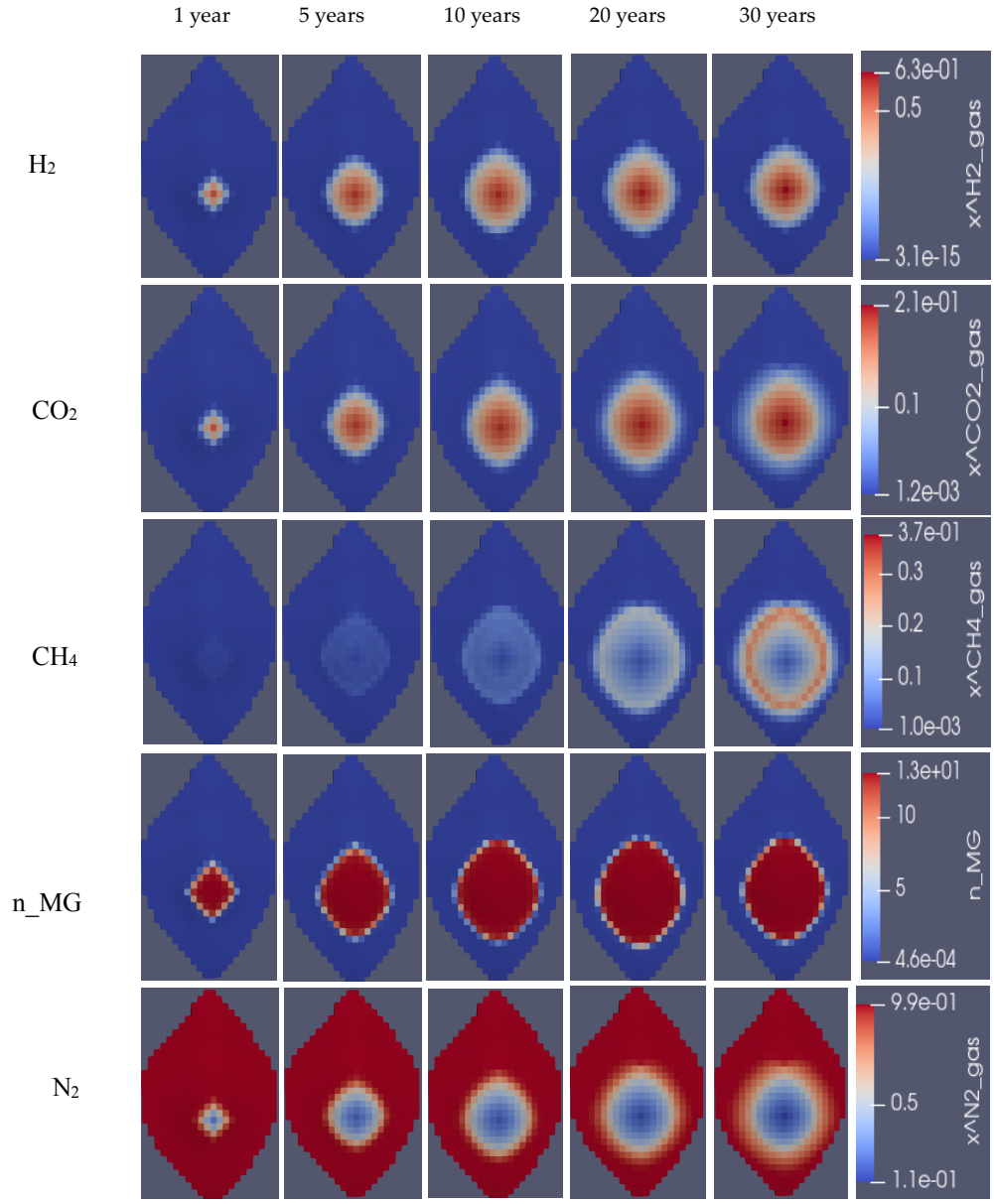

This case is again comparable to that of 80%H_2 - 20%CO_2. The reaction rate significantly increases with increasing microbial growth rate. The amounts of methane generated in both cases are indeed comparable (see A.1.3). The high amounts observed are explained by the large availability in both substrates (H_2 and CO_2).

A.3.4 Microbial Growth Rate = 3×10^{-5}/s

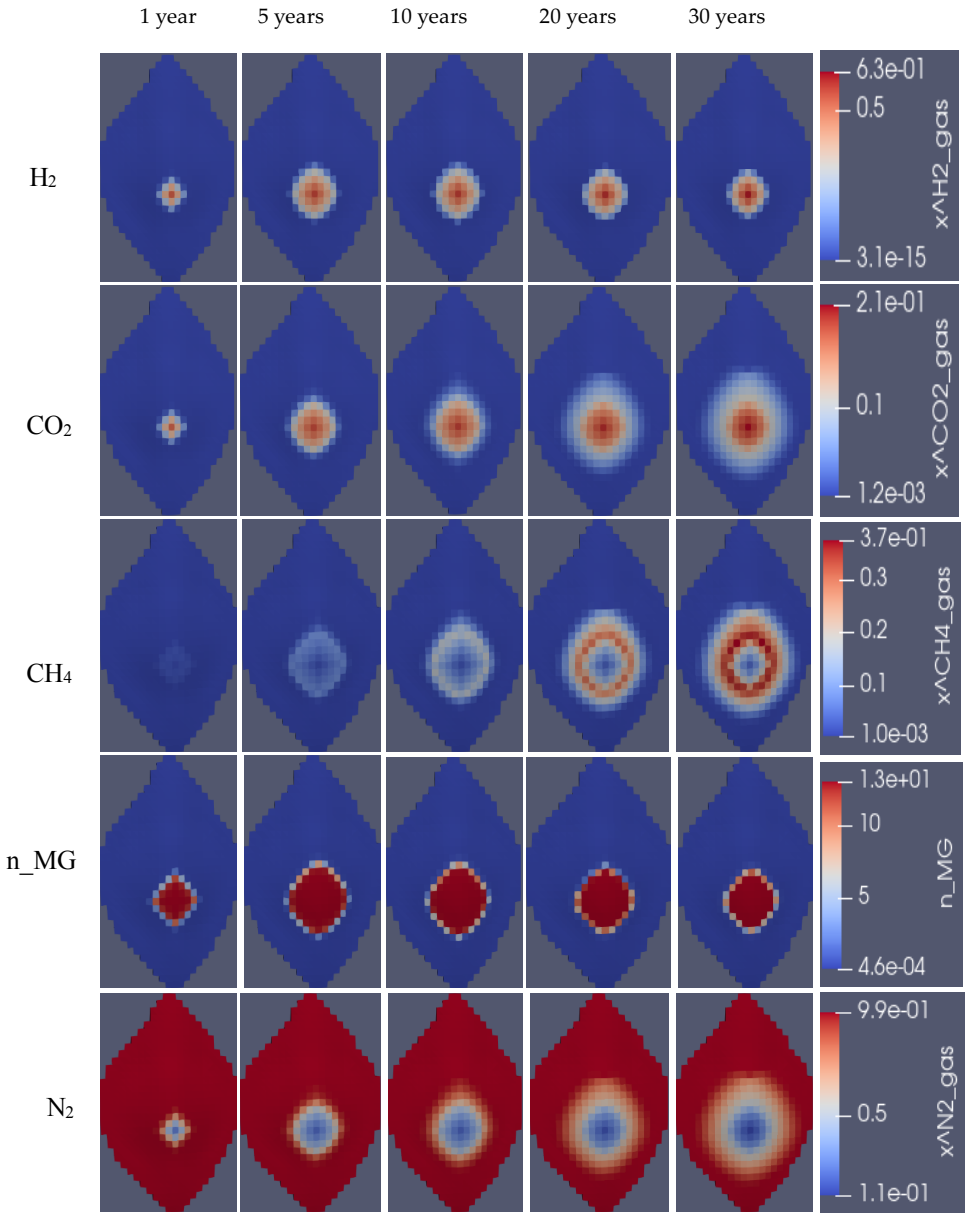

Our maximum conversion rate takes place with a microbial growth rate of 3×10-5/s. This is reflected in a high concentration of generated methane. The displacement of the cushion gas in such a case is slow.

Appendix B

Simulation results with 100% H2 injected

B.1. Nitrogen as cushion Gas (Results after 30 years of injection)

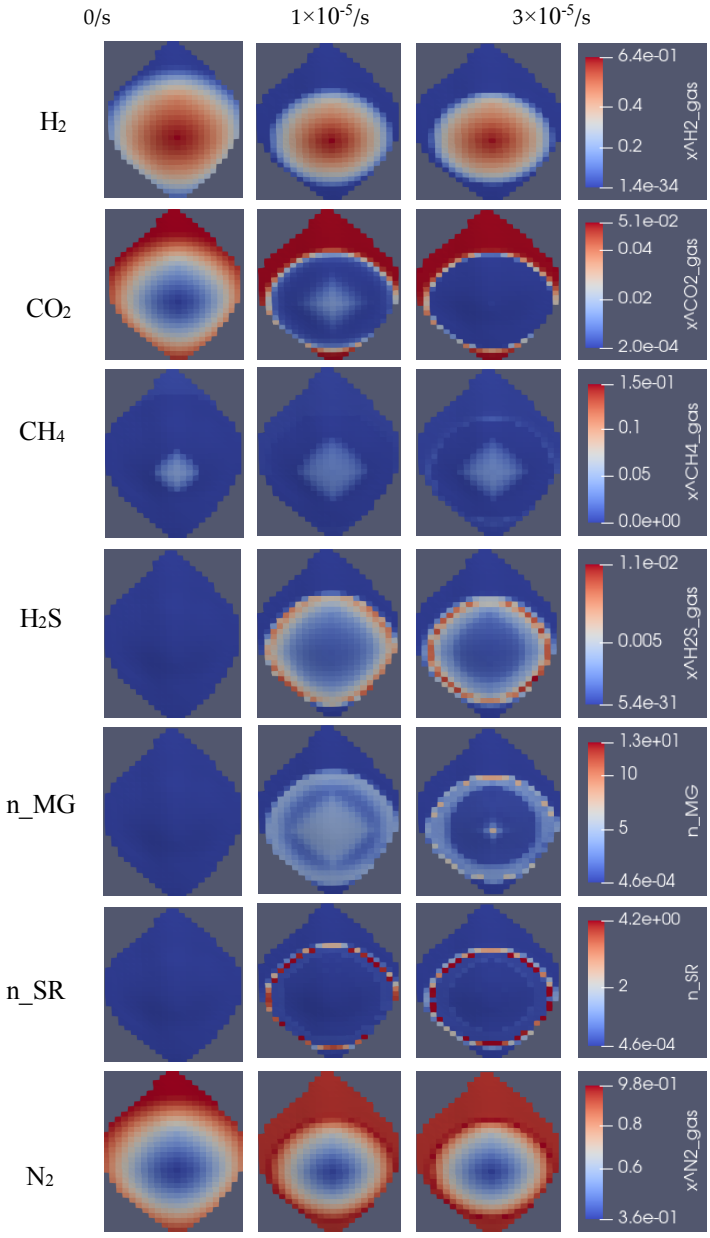

With 100% H_2 injected and 5% CO_2 initially present in the reservoir, the conversion rate is rather small. Even an increased microbial growth rate generates a small amount of methane.

B.2. CO2 as Cushion Gas (Results after 30 years of injection)

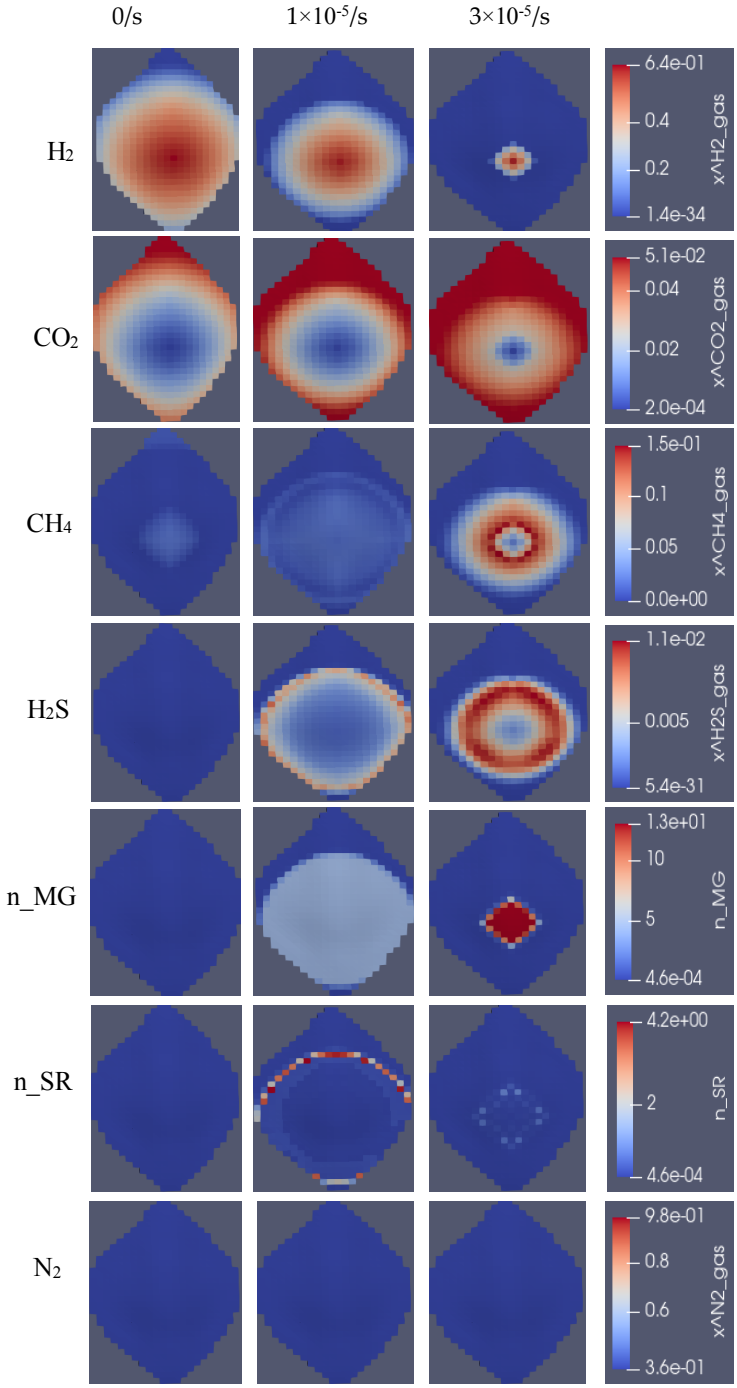

When CO_2 is used as cushion gas, a high microbial growth rate might lead to most of the injected hydrogen being consumed.

B.3. CH4 as Cushion Gas (Results after 30 years of injection)

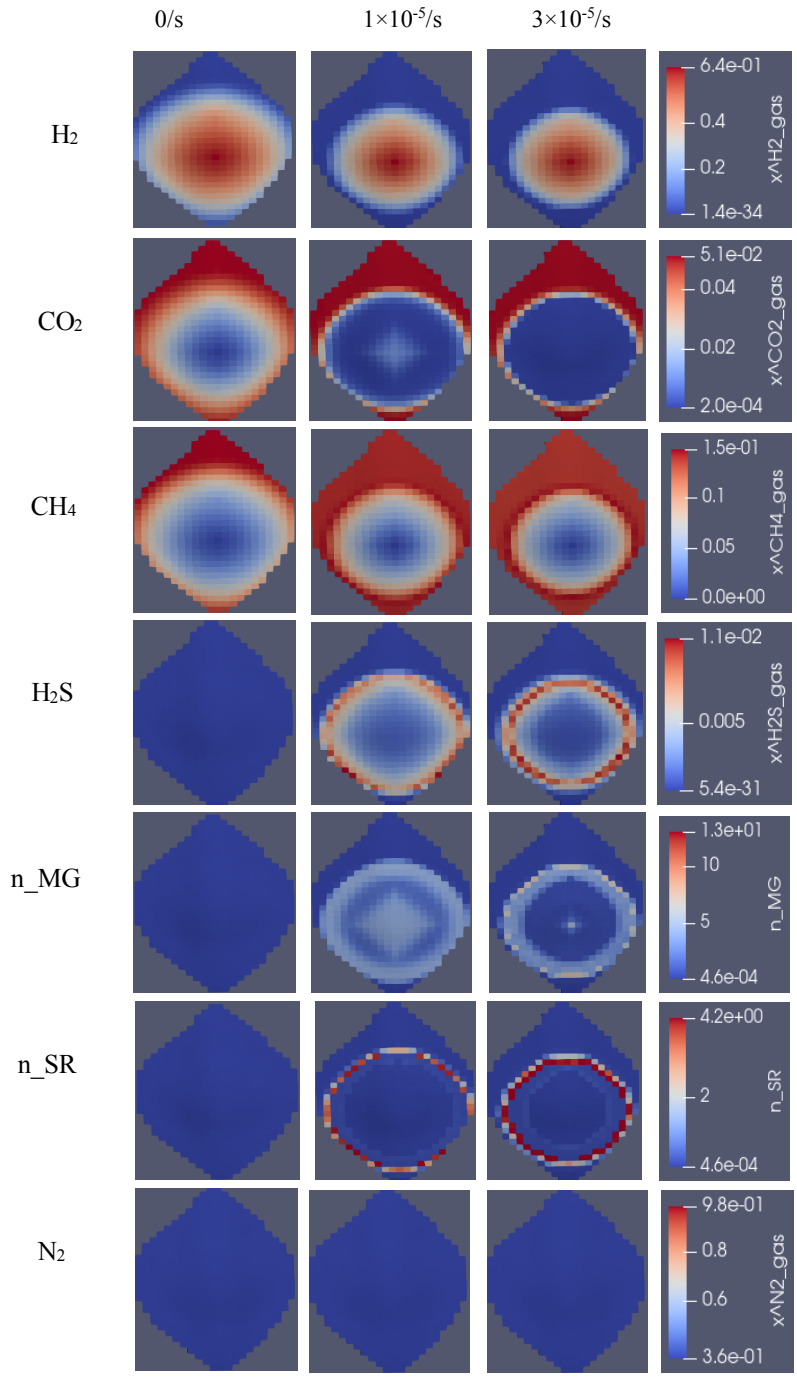

The reduction in hydrogen plume size is an indication that some reaction still takes place even when methane is used as cushion gas. However, as we have seen in Figure 4-22, the consumption rate is slightly smaller than in the case when N_2 is used as cushion gas. This could be explained by the fact that a large amount of methane already present in the reservoir slows down the reaction rate.